‘One medicine – one pathology’: Assessment and Validation of Animal Models of Orthopaedic Diseases

A DISSERTATION SUBMITTED TO THE FACULTY OF THE GRADUATE SCHOOL OF THE UNIVERSITY OF MINNESOTA

BY

Alexandra Armstrong

IN PARTIAL FULFILLMENT OF THE REQUIREMENTS FOR THE DEGREE OF DOCTOR OF PHILOSOPHY

Advised by
Cathy S. Carlson
Ferenc Tóth

JUNE 2022

Acknowledgements

I am filled with gratitude for the many people who assisted me in this process:

To my advisor, Cathy Carlson, for your unwavering support and believing in me at every turn. Your positive outlook helped keep me motivated and focused on my goals, and you knew exactly what I needed for success both in completing this work and entering the field as an anatomic pathologist researcher.

To my thesis committee, Tim O'Brien (chair), Casey Johnson, Ferenc Tóth, and Richard Loeser, for being generous with your time and kind but honest with your thoughtful comments. This work is better for your involvement, and I have been lucky to learn through the examples you have set. Extra thanks to Ferenc Tóth, my co-advisor, for keeping me laughing and keeping it real.

To Paula Overn and Katalin Kovacs, for patience with my many, many, many requests, troubleshooting, and the very careful handling of my precious samples.

To my husband, Joe, for supporting my passion for learning and my choice to stay in school for a solid 15 years of post-secondary education. Thank you for keeping me fed and warm!

To my son, Lochlan, whose arrival amid this work provided much-needed perspective on what is most important in life.

To my daughter, for adding to my motivation to finish this program and thesis so that I can focus on important tasks, like naming you and preparing for your arrival.

To my family, and especially my parents, Chris and Helen, and brother Gordon and sister Jacqueline, for being the best cheerleaders, day-in and day-out. You have done everything you can to make life easier and more fun for us, and there are no words for how grateful we are for the laughs and sunshine you have brought into our lives.

Last but certainly not least, to my loving pups, Wolfgang and Murphy, for reminding me why I went into veterinary medicine and for being the steadfast companions to many days and nights in the study and by the fire, working and writing.

Dedication

Dedicated to my paternal grandfather and avid Osler scholar, Dr. Charles Gordon Roland (1933-2009), and maternal grandmother, Dr. Mary Lomas Price Pougiales (1925-1985), who together imbued me with a natural appreciation for translational medicine, despite their lives being cut short prior to my entering the veterinary medical field. I am happy to carry on the family tradition of scholarship and life-long enthusiasm for learning and only wish they were here to bear witness. Thank you to my parents for helping pass on their legacies and passion for helping others through medicine.

Abstract

The projects presented here revolve around the utilization of three different animal models of developmental and degenerative orthopaedic diseases, with the work described in order of typical clinical onset in the relevant patient populations. These projects share an integral focus on characterization and validation of the chosen models by histological assessment. The objective of the first phase of this work was to histologically characterize the effects of surgically induced epiphyseal ischemia in a piglet model of Legg-Calvé-Perthes disease on the proximal femoral growth plate, with histomorphometry and immunohistochemical characterization. The objective of the second phase of this work was to determine the sensitivity and specificity of noninvasive quantitative MRI methods in detection of early naturally occurring osteochondrosis lesions *ex vivo* in the pig, with co-registration and characterization of lesions identified with advanced imaging and identified histologically. The objective of the third phase of this work was to determine the optimal approach for histological assessment of osteoarthritis in murine models, including comparison of two widely recognized murine-specific histological grading schemes and additional microscopic means of evaluation relevant to determination of osteoarthritis severity. Collectively, the results of this work highlight the need for careful evaluation and validation of animal models of orthopaedic diseases, with a focus on repeatability of the model, complete evaluation with reflection on how accurately the model mirrors the human disease, and statistical support for the approach to analysis.

Table of Contents

List of Figures

Chapter 2

Chapter 3

Chapter 4

Appendix 1

Appendix 2

List of Tables

Chapter 2

Chapter 3

Chapter 4

Appendix 2

Abbreviations

3D	Three-dimensional
AECC	Articular-epiphyseal cartilage complex
CI	Confidence interval (95%)
ECM	Extracellular matrix
H&E	Hematoxylin & eosin (staining technique)
JOCD	Juvenile osteochondritis dissecans
LCPD	Legg-Calvé-Perthes disease
OA	Osteoarthritis
OC	Osteochondrosis
OCD	Osteochondrosis dissecans
OCL	Osteochondrosis latens
OCM	Osteochondrosis manifesta
ONFH	Osteonecrosis of the femoral head
POC	Primary ossification center
ROI	Region of interest
SafO	Safranin O staining
SD	Standard deviation
SOC	Secondary ossification center
UMN	University of Minnesota

Chapter 1: Introduction – 'One medicine – one pathology'

Animal models of orthopedic diseases are common and provide a key foundation for much of our current understanding of the pathogenesis of these diseases in both humans and veterinary species. The field of anatomic pathology provides an ideal vantage point with which to explore the intersections of human and animal disease. Comparative pathology has long been celebrated by some of the fathers of modern medicine, including Rudolf Virchow and William Osler, who both practiced as pathologists and dramatically increased our understanding of anatomy, physiology, and pathology through their work.[1] While MD physicians by training, Virchow and Osler respected veterinary research and Osler, a Canadian physician, is credited with coining the phrase 'One Medicine'.[1] This approach holds central an appreciation for the close relationship of humans, animals, and public health. While this may be most appreciated in the realm of zoonotic diseases, the sentiment also has influenced the development of animal research and animal welfare guidelines and the approach to biomedical research in general. Research utilizing a 'one medicine' or 'one health' approach can provide mutual benefit to both human and veterinary medicine, leveraging models in veterinary species to increase our understanding of pathophysiology, disease development, progression, and effective interventions.[2]

Chronic, noncommunicable diseases are responsible for 7 in every 10 human deaths worldwide.[3, 4] Costs associated with management and mortality attributed to these diseases have been compounded by increasing inefficiency

and complexity in the development of therapies and medical devices for treatment.[3] The pathologist holds an essential role in the interpretation of normal anatomy and pathologic lesions within research species in the preclinical stage, ensuring appropriate interpretation of legitimate lesions while preventing cases of mistaken diagnosis.[1, 5] The gross and histological assessment of tissues provides key opportunities to 1) validate findings and 2) address research animal use through replacement, reduction, and refinement (3Rs).[2, 6] While there is a strong interest in embracing the principles of the 3Rs, concerns faced by researchers include the cost and time associated with implementation, loss of data, lack of adequate alternatives, and overall unrealistic expectations within the industry.[7] However, studies have shown reduction of animal numbers up to 50% or greater are achievable by improvements in study design and methods including optimizing control groups, reducing time points based on previous data, combining studies, adjusting dosing regimens, and other strategies.[7] These strategies, combined with the use of an appropriately characterized and validated model of disease, are essential to effective biomedical research that addresses the rising demand for effective medical interventions.[8, 9]

The objective of this work was to apply knowledge of human and animal disease to translational projects utilizing three established models of human orthopaedic diseases by using pathology analysis, including histopathology and immunohistochemistry, to ensure that the lesions were representative of the modeled diseases, that unusual or unique lesions were documented, and that the

methods of data analysis were appropriate to the questions at hand. This introduction will include a brief overview of the anatomy and development of the joints and a brief review of the available animal models for Legg-Calvé-Perthes disease, osteochondrosis, and osteoarthritis, including similarities and differences to humans and reasons for and against utilization of various species, followed by discussion of the specific models utilized in this thesis (piglets as a surgically-induced model of Legg-Calvé-Perthes disease, piglets as a natural model of osteochondrosis, and mice as models of osteoarthritis). The chapter will conclude with a summary of the aims of this work.

1.1 Anatomy and Development of Bone and Joints

The development of the skeleton occurs via a carefully orchestrated series of events that is well-conserved across species. Bones develop by either intramembranous or endochondral ossification. Intramembranous ossification is a process by which progenitor cells differentiate directly into bone-forming osteoblasts based on signals from the local microenvironment.[10] This process primarily occurs in the flat bones of the skull.[11] Endochondral ossification is the process by which most bones develop, via an embryonic cartilaginous anlage that is gradually replaced by bone.[12] This process includes an initial proliferation of chondrocytes, extracellular matrix production, hypertrophy of chondrocytes, matrix mineralization, and eventual chondrocyte death by apoptosis or transdifferentiation to osteoblasts.[13, 14] Capillary invasion accompanies

differentiation of progenitor cells into osteoblasts, osteoclasts, and bone marrow cells, which aid in the replacement of cartilage with bone.[12]

There are several types of joints present throughout the body, which are often characterized by the degree of joint movement. These include the synarthroses (no or minimal movement), the amphiarthroses (some but limited movement), and the diarthroses, which permit free movement and include the synovial joints in the appendicular skeleton, which are the focus of the disease processes described here.[15] The structure of the joints directly relates to their function. Synovial joints include a fibrous capsule (lined by synovium) that is continuous with adjacent tissues and the periosteum, a joint cavity containing synovial fluid, and the articular cartilage that lines the epiphyseal ends of the articulating bones. A variety of associated ligaments (e.g. the anterior cruciate ligament) and bones (e.g. the patella) provide additional support specific to each joint.[15] The collection of diverse tissues that make up the joint have contributed to today's acceptance of the joint as an organ.[16, 17]

Bone

Bone development is characterized by the initial formation of highly cellular woven bone, which is remodeled over time to form mature, stronger and slower-forming lamellar bone.[13] The outer compact cortex of the bone at maturity (cortical bone) is composed of cylindrical osteons and is covered by the periosteum, a connective tissue layer that provides nutrients via blood vessels.[13]

The inner portion of the bone consists of trabecular or cancellous bone that lacks osteons and is initially composed of woven bone with randomly arranged collagen fibrils that gradually organize into parallel collagen lamellae.[13] Bone is a dynamic tissue that undergoes remodeling throughout life in response to force. In the adult human, approximately 80% of the skeleton is composed of cortical bone (by weight) with 20% composed of trabecular bone.[18] Bone is composed of a core of hydroxyapatite mineral that gives bone its stiffness, associated with collagenous matrix predominated by type I collagen (90% of organic matrix).[19]

While the development of bone shares many features between humans and animal species, skeletal maturity occurs much earlier in most animal species, including large animals like the horse, dog, and pig, than it does in the human, providing unique challenges in performing translational research of developmental diseases across species.[20] Humans reach skeletal maturity between 14-22 years of age (earlier in females than males), while horses reach skeletal maturity by three years and pigs by 5-6 months of age.[18, 21-23] During development, bone repair responses occur more rapidly than after maturity has been reached.[18]

Growth Cartilage

Initially, avascular cartilaginous tissue is present where bone will later develop and provides a template for the future bones that will form through endochondral ossification. As chondrocytes hypertrophy, they express type X

collagen, a key step in initiation of calcification or mineralization of the matrix, and vascular endothelial growth factor (VEGF), which stimulates vascular growth from the periosteum at the diaphysis (central region of bone) following the development of a bone cuff around the mid-portion of the cartilage anlage.[13] This vascular in-growth leads to a cascade of events including development of the primary ossification center (POC). Following development of the POC, a secondary ossification center (SOC) develops within the epiphysis through a similar process initiated by vascular invasion, with an additional important step of cartilage canal development within the epiphysis and what will become the epiphyseal cartilage of the articular-epiphyseal cartilage complex (AECC).[13, 24, 25] The cartilage canals serve to provide nutrients to and remove waste from the developing cartilage and to provide osteogenic cells to the SOC.[24] During development and as the epiphyseal cartilage thins, the cartilage canals are either incorporated into the endochondral ossification front or undergo chondrification (filling in with chondrocytes and matrix).[25, 26] Failures of these processes have been implicated in the development of osteochondrosis.[27, 28] Transphyseal vessels pass through the growth plate from the metaphysis to the epiphysis in the neonatal and infant period, but the growth plate is thought to lack transphyseal vessels in children by two years of age.[29]

As hyaline cartilage matures and the centers of ossification develop, there are two types of growth cartilage that are largely responsible for the growth and development of both the bone (via endochondral ossification) and the articular

surfaces. These are termed the epiphyseal growth plates, situated between the POC and SOC, and the AECCs, located at the epiphysis, respectively. These regions of growth cartilage have characteristic zonal organization and morphology that reflect their specialized roles in growth.[30] The epiphyseal growth plate contributes to expansion of the POC and the AECC is responsible for expansion of the SOC.[12, 30-32] This work specifically investigates the effects of Legg-Calvé-Perthes disease on the epiphyseal growth plate, although it is characterized by involvement of both the epiphyseal growth plate and AECC. Osteochondrosis (OC) can affect both types of growth cartilage as well, though the focus of this work is on articular OC, which involves the AECC.[32, 33]

Cartilage is populated by chondrocytes, which originate from chondroprogenitors produced by multipotent mesenchymal stem cells under the influence of SOX9.[34] SOX9 is a transcription factor that binds to enhancer regions in the promoters of extracellular matrix proteins present in cartilage, including aggrecan and several collagen types.[34, 35] The type of collagen subsequently expressed by chondrocytes depends upon the tissue location and does not undergo significant variation throughout development, with type II collagen expressed more ubiquitously (and predominating in adult articular cartilage), type III collagen expressed pericellularly, and type X collagen expressed during establishment of the tidemark (junction between mineralized and unmineralized cartilage) and in conjunction with mineralization of the matrix.[16, 36] In adulthood, any need for chondroprogenitors is filled by progenitor

cells originating from the inner layer of the perichondrium, a connective tissue layer that covers bone and some cartilage (excluding the epiphysis and articular surfaces).[13]

The epiphyseal growth plate is composed of a disc of cartilage that separates the primary spongiosa (cartilage matrix scaffold where bone matrix is initially laid down within the metaphysis) and the SOC (bony epiphysis located at the ends of long bones).[24, 37] Within the growth plate, the resting or reserve zone borders the bony epiphysis and is characterized by small round chondro-progenitor cells scattered individually within matrix.[38] These chondrocytes are thought to function as a source of chondro-progenitors to the growth plate. The proliferative zone is characterized by somewhat flattened cells arranged in columns oriented parallel to the long axis of the bone. Within the AECC, columns are shorter and less distinct.[30] In the proliferative zone, chondrocytes divide rapidly and produce matrix. Chondrocytes then proceed to differentiate to a hypertrophic phenotype, characterized by large round cells that remodel and calcify the cartilage matrix surrounding them.[30, 39] Together, these steps characterize the process of endochondral ossification.[32] Much of the longitudinal growth of the bone is attributed not to cell proliferation in the growth plate but to chondrocyte hypertrophy and accumulation of matrix.[40] Disruptions of this process, as may occur in LCPD or other diseases involving the growth plate, can lead to altered bone growth and premature growth plate closure.

At the articular surface, the cartilage is not replaced by bone but instead consists of the articular epiphyseal cartilage complex, which has similar but less distinct zones to those observed in the growth plate.[24] At maturity, the epiphyseal cartilage is replaced by bone and the adult zonal organization of the articular cartilage includes a thin superficial zone, a thick intermediate/deep zone with columnar organization of the chondrocytes, and a mineralized zone below a tidemark with large chondrocytes bordered by subchondral bone.[41] The articular cartilage that lines the articular surface is avascular throughout life. Many diseases that either affect the articular cartilage directly, such as osteoarthritis, or indirectly, such as late-stage OC (osteochondritis dissecans), are characterized by irreversible damage to the articular cartilage. Conversely, the vascularized growth cartilage displays repair capabilities that are absent in mature articular cartilage, which is especially evident when considering OC. For example, while many studies have found large variation in the prevalence of OC lesions in horses, much of this variation is attributed to differences in the age of evaluation, given the high propensity of early lesions to undergo complete healing.[42] Confusion regarding the origin of OC in humans has persisted, likely due in large part to the limited access to pediatric joint specimens that have only recently allowed identification of these early OC lesions in humans.[43]

Signaling in Cartilage

The proliferation and maturation of the growth cartilage chondrocytes is regulated by complex molecular mechanisms that include a central role for parathyroid-related protein (PTHrP) and Indian hedgehog (Ihh), which regulate the progression of chondrocytes to the hypertrophic zone.[39] New bone formation is actively occurring in the hypertrophic zone and the primary spongiosa, where osteoblasts and osteoclasts replace the calcified cartilage with trabecular bone and remodel the bone.[39] Cell proliferation in the growth cartilage is dependent on cross-talk involving several signaling molecules. Indian hedgehog (Ihh) is secreted by pre-hypertrophic chondrocytes in the growth plate. Ihh expression stimulates production of TGF-β, which inhibits chondrocyte hypertrophy by inducing expression of PTHrP by perichondrial and juxtaarticular cells.[37] PTHrP binds to its receptor on proliferating and pre-hypertrophic zone cells, delaying their differentiation to hypertrophic cells. While previous studies of LCPD have often failed to include detailed assessment of the effects on the growth plate of the proximal femur, these pathways may be relevant to the growth disruption reported in roughly one third of patients with LCPD.[44, 45]

Articular Cartilage Structure and Function

Articular cartilage is avascular and lacks innervation.[46] The metabolic needs of the chondrocytes and matrix are satisfied through either diffusion from the articular surface or the subjacent marrow. Reparative capacity is very low, with reduction in the ability of chondrocytes to maintain and restore articular

cartilage with increasing age, despite the presence of a chondroprogenitor cell population in both immature and mature hyaline cartilage.[36, 46, 47] Chondrocytes have low resting energy requirements that are largely addressed by glycolysis, and are thought to persist for decades based on the lack of cell division in articular cartilage.[48] Given the low cellularity of the cartilage (approximately 1% of the cartilage volume in adult human articular cartilage), the matrix is a subject of great interest.[36] The matrix in adulthood is sparsely populated by chondrocytes and is composed of water (up to 80% of wet weight of articular cartilage), collagen, and proteoglycans, with small amounts of noncollagenous proteins and glycoproteins.[36, 46] Proteoglycans, predominated by aggrecan, are composed of a protein core with one or more glycosaminoglycan chains, with a negative charge that helps in attracting water.[36, 40] The glycosaminoglycans found in cartilage include hyaluronic acid, chondroitin sulfate, keratan sulfate, and dermatan sulfate. Chondrocytes are responsible for both synthesis of matrix components and assembly and organization of matrix, typically in response to biomechanical stimuli.[36] The articular cartilage has integral roles in both protecting the surfaces from loads up to 10 times the body weight and producing various macromolecules that help lubricate the joint, reduce friction, and contribute to the synovial fluid.[15, 16, 41] Over time, there is a decrease in the hydration of the matrix that corresponds with an increase in stiffness to compressive forces.[46] Newly developed quantitative MRI techniques for assessing cartilage injuries are informative due to their sensitivity to changes in the composition of cartilage,

including water content, collagen orientation, and proteoglycan content, amongst others.[49-52]

Several excellent reviews exist that summarize many of the general anatomical and biomechanical differences affecting the musculoskeletal system in various species of interest.[2, 20, 53, 54]

1.2 Animal Models of Legg-Calvé-Perthes disease

Legg-Calvé-Perthes disease (LCPD) is a childhood disease characterized by osteonecrosis of the femoral head. Many different theories related to the inciting factor in development of LCPD have been considered, including trauma, disorders of thrombosis, inflammation, abnormalities of growth factor signaling or collagen structure, and exposure to cigarette smoke.[55] Although the underlying cause of LCPD remains to be determined, the result is ischemia to the femoral head, leading to variable incongruence of the hip joint due to collapse of the femoral head that can lead to long-term deformity and osteoarthritis.[56, 57] In some patients, effects extend beyond the bony epiphysis to the growth plate and metaphysis.[56] LCPD is typically diagnosed in children ages 4 to 6 years old, though patients may present between 2 and 14 years of age.[58] LCPD is difficult to treat, with success rates varying from 27-69% following various approaches including both medical management (activity restriction) and surgical management (Scottish Rite orthosis, femoral osteotomy, or Salter innominate osteotomy).[59]

LCPD represents the rarest condition of the three studied in this work, and this is reflected in the limited animal model options that recapitulate the human condition, with small numbers of studies in goats, rabbits, mice, dogs, and piglets providing insight to the disease pathogenesis and treatment options.[60] LCPD occurs spontaneously in young, small-breed dogs, but its relative rarity makes it difficult to study. A surgically induced model in the piglet is the most widely used and was utilized in this work (described in detail below). While models specific to LCPD are limited, there are a wide variety of animal models that have been used to study osteonecrosis of the femoral head (ONFH), the adult-onset disease characterized by femoral head necrosis and collapse. A previous review categorized the available animal models of osteonecrosis into traumatic models (surgical vascular occlusion, physical insult, chemical insult), non-traumatic osteonecrosis models (chemically-induced, steroid-induced, alcohol-induced, LPS-induced, dysbaric, and spontaneous), and combinations of these models.[61] Several surgical models, including in the adult dog, immature goat, and the rat, failed to develop joint collapse as seen in ONFH or LCPD.[60, 62, 63] Rabbits develop osteonecrosis following systemic administration of glucocorticoids, similar to humans who are susceptible to steroid-induced osteonecrosis. Unfortunately, the distribution of lesions in rabbits is often random and not limited to the femoral head. Indeed, some studies have failed to confirm the induction of osteonecrosis following glucocorticoid treatment or have not disclosed details relating to the size and distribution of the induced lesions, leaving unresolved

questions about how well this lagomorph model replicates human disease.[64-66] Most rabbit studies utilize adult rabbits, likely recapitulating ONFH more closely than LCPD. A steroid-induced mouse model of osteonecrosis has been developed associated with an arteriopathy characterized by transmural necrosis and thickening of arterioles, but lesions tend to affect the distal femoral epiphysis rather than the femoral head.[67]

Models specifically looking at the role of ischemic injury in growth plate disruption are extremely limited. While early studies utilizing an ablation procedure at the proximal femoral growth plate in the goat induced growth disturbance in the operated femur similar to that observed in some LCPD patients, the regions of the growth plate affected and the degree of femoral head deformity fell short of an ideal model.[60] While the skeletal system, and cartilage in particular, is well-conserved in development and structure among species, it is worth noting that porcine growth plates have been reported to include a thicker resting/reserve zone compared to rats and adolescent humans.[68] Much of the past work comparing various animal model anatomy and physiology to that of humans has focused on adults, particularly in large animal models. Uniquely, rats and mice do not undergo growth plate closure; the rate of growth slows with age but the cells remain active.[9]

Porcine Models of LCPD

A common model of LCPD thought to closely recapitulate the clinical, imaging, and pathophysiological mechanisms of disease utilizes a surgical technique to induce femoral head ischemia in Yorkshire or Yorkshire cross piglets at six to eight weeks of age. Ischemia is induced by placement of a circumferential ligature at the femoral neck, coupled with transection of the ligamentum teres to cause complete ischemia to the femoral epiphysis.[69, 70]. Within the first two weeks following surgery, the femoral head becomes necrotic and remains avascular (avascular stage).[55] At three to four weeks following ischemia induction, the vascular repair stage begins with revascularization and resorption of necrotic epiphyseal tissue by osteoclasts coupled with delayed bone formation.[55, 70] Femoral head deformity may be observed by eight weeks after ischemia induction.[70] Studies using this model have contributed both to the understanding of the pathogenesis of the disease and to the evaluation of novel diagnostic and treatment strategies.[55, 71-75] Abnormalities of the physis and metaphysis have been previously reported in this model, with morphological changes to the proximal femoral growth plate and metaphyseal radiolucent changes (due to retained cartilage, cyst formation, or fibrovascular tissue) reported in a subset of piglets by four to eight weeks following ischemia induction.[44, 45] While there are some facets of the model that may not replicate the human disease, such as the invasive nature of the surgical procedure required to induce ischemia, over two decades of utilization demonstrate the

many shared radiographic, MRI, gross, and histological features that support the use of this model to study LCPD in children.[44, 45, 69-73, 76-79]

1.3 Animal Models of Osteochondrosis (OC)

Osteochondrosis (OC) is a developmental disorder affecting the articular-epiphyseal cartilage complex. While the name osteochondrosis is widely accepted in the veterinary literature, osteochondritis dissecans (OCD), or juvenile osteochondritis dissecans (JOCD) in patients with open growth plates, is more commonly used in the human medical literature. A host of specific names based on the affected site also exist in the human literature, but it is highly likely that these represent a similar pathogenesis and single disease manifesting at different joints.[20] OC causes pain and swelling of joints, secondary to development of a region of epiphyseal cartilage necrosis and subsequent delayed endochondral ossification.[28, 32] In the end-stage, this may lead to fracture of the overlying articular cartilage and clefting through the diseased epiphyseal cartilage that can progress to development of a loose cartilaginous or chondrosseous intraarticular fragment. While the underlying cause of disease remains unclear, animal studies have shown that predilection sites correlate with areas of low vascularity and vascular regression. The inciting factor is focal failure of blood supply to the epiphyseal cartilage of the articular-epiphyseal cartilage complex. This is supported by studies in pigs, goats, and horses that demonstrate the relationship between vascular supply to predilection sites and

the ability to induce lesions by targeted surgical transection.[80-83] The epiphyseal cartilage lesions may progress with involvement of the articular cartilage and/or the subchondral bone in the later stages of disease.[28, 32, 84] This understanding of the pathogenesis has been accepted in veterinary medicine and has gained significant traction in human medicine in recent years as the earlier stages of the disease have increasingly become recognized.[85-87]

OC has been characterized in several large animal species, given its natural occurrence in dogs, horses, pigs, chickens, and more. Much of the insight into the disease pathogenesis in both humans and animals has come from studies of veterinary species, due to the ready availability of postmortem samples for histological study at different stages of disease.[20, 33, 84, 88-90] Due to economic impact and a high prevalence, much of what we know comes from studies of commercially bred pigs, where lameness is an important welfare issue that can lead to increased culling[91, 92], and horses, which often undergo orthopedic screening at a young age.[20, 89] Studies in pigs and horses have allowed development of the etiologic understanding that OC develops due to disruption of the blood supply to the growth cartilage during development.[28, 32, 89, 93] There are clinical similarities in the presentation between humans and animal species. The rates of OC have been increasing in parallel with an increase in enrollment in youth sports, suggesting athletic involvement contributes to development of clinical disease, similar to the increased rates of the disease in horses involved in athletic activities.[94]

Predilection sites are often conserved among species, with a few notable exceptions, and characteristic stages of disease have been described histologically with conservation of features across species. The earliest stage of disease, consisting of a well-defined region of chondrocyte cell death with associated matrix pallor, is termed *osteochondrosis latens*. The intermediate stage of the disease is characterized by chondrocyte cell death and associated delay of endochondral ossification termed *osteochondrosis manifesta.*[32] These early stages both have the potential to heal without long-lasting damage to the joint; in a small portion of cases, *osteochondrosis manifesta* lesions progress and develop clefting to the overlying articular surface, entering the end-stage termed *osteochondrosis dissecans.*[32] These clefts may ultimately lead to separation of an osteochondral fragment that becomes a loose body in the joint, causing pain and necessitating surgical removal.[95, 96] In humans, if lesions are detected prior to major clefting and/or separation, they may be stabilized surgically.

Horses are a popular choice for the study of OC, given the high disease prevalence in this species and the economic incentive to reduce disease occurrence through selective breeding. Advantages to the use of horses to study OC include the frequency of imaging studies prior to intervention, the size of the joints, and the high frequency of surgical intervention to assess and treat disease, providing opportunities to evaluate new treatment methods.[20] Disadvantages include their large size and associated implications for imaging and surgical management and the limited availability to study horses in a

research setting, given the costs involved in upkeep, management, and ethical concerns.[20] Other large animal models of OC include small ruminants, which do not develop OC naturally but provide the opportunity to study surgically-induced lesions that may provide some additional insights into factors related to healing or progression.[80, 81, 97]

Pigs have gained acceptance in preclinical research as one of the best models regarding similarities to human anatomy and physiology.[98] Both conventional pigs and minipigs are frequently utilized in biomedical research, with minipigs providing advantages for extended studies (duration of months to years) due to their slower growth rates, given that conventional pigs can reach a weight of several hundred pounds by 6 months of age.[82] While the lamellar bone structure closely resembles that of humans, the trabecular network in adult minipigs is more dense than in humans.[99] The rate of bone regeneration in pigs is closer to that in humans than the rate in dogs (human, 1.0-1.5 mm/day; pig, 1.2-1.5 mm/day; dog, 1.5-2.0mm/day).[100] The composition of bone is similar between pigs and humans, as are the bone remodeling processes and accompanying mechanical parameters.[18, 100] These features further justify the use of pigs as animal models of OC.

Conventional Pigs as Models for OC

Specifically regarding OC, pigs provide many advantages over other existing models. The incidence of early lesions of naturally occurring OC is nearly

100% in domestic pigs at predilection sites, providing ample opportunities for studying the progression or resolution of lesions and risk factors for development of clinical disease.[20, 101] In humans, the sites most often affected by OC are the knee (medial femoral condyle), elbow (humeral capitellum), and ankle joints.[20] Similarly, OC in pigs most often occurs at the medial femoral condyle within the knee/stifle joint and also affects the elbow (humeral condyle). Genetic risk factors are thought to be involved in development of OC in both humans and animals, though the sporadic occurrence of most human cases suggests a polygenic and more complex genetic component in most cases. Heritability estimates in the pig range from 0.14-0.52 depending on the site affected and the definition of disease.[102, 103] The application of susceptibility weighted imaging (SWI) and quantitative susceptibility mapping (QSM) approaches have allowed visualization of the cartilage canals in piglets and human cadaver samples, revealing nearly identical vascular architecture at the shared predilection sites in the distal femoral condyles of pigs and humans.[26, 97, 104, 105] These findings have both supported the hypothesis that vascular failure is central to the pathogenesis of OC and that domestic pigs are an ideal naturally occurring model based on anatomic similarities key to the underlying pathogenesis of the disease.[97]

1.4 Animal Models of Osteoarthritis

Osteoarthritis (OA) is the most common form of arthritis and a major cause of joint pain and disability in older adults. There are many risk factors for OA, which include age (by far the most important risk factor), joint injury, gender,

obesity, genetic factors, and structural abnormalities.[106, 107] The characteristic lesions include degeneration and loss of the articular cartilage, formation of osteophytes at the joint margins, subchondral bone thickening, degeneration of the menisci and ligaments, hypertrophy of the joint capsule, and variable synovitis.[17] OA can lead to remodeling of the subchondral bone and thickening and alterations to the calcified cartilage that can cause duplication of the tidemark that separates the articular and calcified cartilage histologically.[17] While the features of OA are generally well-defined and accepted, several phenotypes have been defined based on differences in clinical presentation, progression, and response to treatment that complicate the study of the disease and add to the importance of selecting of an appropriate animal model.[107, 108]

Numerous naturally occurring and induced animal models have been utilized to study OA, with a continued predominance of small animal models dominated by mice, rats, and the Dunkin Hartley guinea pig, particularly as gene-editing techniques and genetically modified strains of mice have become more widely available. The literature is complicated by the increasingly complex understanding of osteoarthritis as a disease process in humans, as several different phenotypes with varying clinical features, rates of progression, and response to treatment have been defined that preclude a single model from accurately representing all facets of OA as we currently understand it.[2, 107]

Of the small animal models, Dunkin Hartley guinea pigs are one of the more commonly utilized due to the high rate of spontaneous disease.[109] Male

Dunkin Hartley guinea pigs develop histologic lesions of OA by three months of age, with progression by six months to lesions that are morphologically similar to human OA.[18] While this provides an efficient model, the propensity of relatively young animals to develop OA suggests there may be underlying differences in pathogenesis from that of human OA. Mice are small and readily available, provide many options for evaluation, particularly extensive histological evaluation, and are inexpensive to manage in a research setting. Spontaneous OA in mice is considered representative of human disease from a pathogenetic standpoint, though it requires a long study duration (a year or more) to onset.[110] A myriad of surgical models have been developed in mice, including partial or total meniscectomy, destabilization of the medial meniscus (DMM), anterior or posterior cruciate ligament transection, medial and/or lateral collateral ligament transection, meniscal tears, and transarticular impact-induced OA.[53] While the advantages of small animal models for the study of OA are the same as for the study of many disorders, there are several skeletal-system-specific disadvantages to the use of mice. First, the articular cartilage is much thinner than that in people, averaging just 0.03 mm thick as compared to 2.2-2.5 mm thick, respectively.[53] In addition, the animal age, sex, and strain all can have major effects on the resulting OA lesions observed, the progression of disease, and the molecular pathophysiology.[107]

Studies utilizing large animal models of OA are less common but are important in the modeling of human disease and determining efficacy of

interventions. This is especially true given the frequency of development of spontaneous OA with age in many species (dogs, cats, horses, non-human primates, etc.).[53] Dogs have similar bone composition to humans and are similarly able to undergo rehabilitation. They naturally develop spontaneous OA with age and are prone to post-traumatic OA, particularly following cruciate ligament rupture.[111] Dogs have higher rates of trabecular bone turnover than humans (averaging 94-100% per year vs. 10-55% per year in adult humans).[112, 113] Despite the abundance of both spontaneous and surgically-induced small and large animal models of disease, there has been an ongoing failure of drugs tested in animal models to translate to effective disease-modifying osteoarthritis drugs in humans.[114] This failure appears multifactorial, with possible contributors including the variability in the methods and experimental design of OA studies, inadequate large animal studies to determine translatability of results, and the selection of animal models.[9, 115] For example, many preclinical studies are performed in young male animals without comorbidities, which fail to replicate the disease as observed in older adult humans, the target of clinical trials evaluating disease-modifying OA treatments.[107, 116, 117]

Mouse Models of OA

While there are some notable disadvantages to using mice to study OA,[9] the wide variety of available murine models of OA provides a unique opportunity to align the features of the model to best represent the patient population and

disease phenotype one hopes to study, assuming the features of disease in that model have been well-defined. Two models were utilized in this work: one utilizing OA induced by destabilization of the medial meniscus (DMM) (surgically induced) and one spontaneous (aged). These models are highly complementary, with the DMM model providing an opportunity to study post-traumatic OA that develops more rapidly and at a younger age in humans, while spontaneous murine models of OA mirror human disease developing with advancing age, a major risk factor for human OA development.[114] Importantly, both models have been extensively studied and the histological features have been well-defined.[118-121] The DMM model has a slower rate of progression than surgically induced models that utilize anterior cruciate ligament transection and has been shown to be highly reproducible.[114] Certain strains of mice have higher incidences of spontaneously occurring OA, including the Balb/c and C57Bl/6 strains and STA/1N and STR/ort substrains.[122-124] Several studies have been published demonstrating the features of age-related OA in C57Bl/6 mice, the strain that was utilized in this work. These studies demonstrated more severe medial tibial plateau OA than lateral tibial plateau OA, similar to humans and most veterinary species, with a correlation of articular cartilage thickness and area with increasing severity of OA based on scoring using a published and validated histological grading scheme.[120, 121, 123] Together, the young DMM C57Bl/6 mice and aged C57Bl/6 mice provide both a post-traumatic and spontaneous model of

disease, representing complementary and potentially differing mechanisms of OA pathogenesis.

1.5 Objectives of Thesis Work

The general aim of this thesis was to use a combination of orthopaedic small and large animal models of human diseases to both advance the understanding of the human conditions and to validate the use of the models in achieving the specific study objectives. These projects included the use of surgically induced lesions in the piglet to investigate the pathogenesis of the growth disturbances occurring in LCPD, the use of early-stage naturally occurring lesions of OC in the pig to validate MRI methods for identification as a step towards applying the methods to *in vivo* diagnosis in humans, and the comparison and validation of commonly used histological grading schemes and techniques for assessment of murine models of OA. This constellation of projects met two important objectives: 1) develop expertise in the use of a diverse group of animal models of orthopedic diseases and 2) further our understanding of how these models mirror human disease and address the needs of translational research.

The specific objectives are to:

I Determine the effects of acute femoral head ischemia (surgically induced) on the proximal femoral growth plate in a piglet model of Legg-Calvé-Perthes disease (Chapter 2)

II Determine the capability of quantitative MRI techniques (T2, T1ρ) at ultrahigh magnetic fields (10.5T) for identification of naturally occurring early osteochondrosis lesions in the pig at predilection sites in the distal humerus and distal femur (Chapter 3)

III Compare two published histological grading schemes for murine osteoarthritis (the Osteoarthritis Research Society International (OARSI) and Articular Cartilage Structure (ACS) grading schemes) when applied to multiple and single sections, along with additional histologic measures, in two mouse models of osteoarthritis (Chapter 4)

Chapter 2: Effects of acute femoral head ischemia on the proximal femoral growth plate and metaphysis in a piglet model of Legg-Calvé-Perthes Disease

2.1 Introduction

Legg-Calvé-Perthes disease (LCPD) is an idiopathic form of osteonecrosis of the femoral head that affects children between the ages of 2 and 14 years old.[125, 126] LCPD can lead to permanent deformity of the femoral head and premature osteoarthritis.[56] While its underlying cause has not been determined, the disease is characterized by a period of disruption to the blood supply (ischemia) of the femoral head, with subsequent development of necrosis of the tissues of the femoral head.[56, 127] Controversy exists regarding the optimal treatment protocols for LCPD because its underlying etiology, the ideal method for monitoring its progression, and the efficacy of different treatment options have not been determined. [56, 57, 128, 129] Prospective studies have found unsatisfactory outcomes with both conservative and surgical treatment of LCPD, with patients having persistent deformation of the femoral head in 49-64% of cases and growth disturbance of the affected hip in approximately 30% of cases.[59, 129] These poor outcomes indicate a complex pathogenesis involving not only ischemic injury to the bony epiphysis but also to the growth cartilage surrounding the developing femoral head.

While the major site of ischemic injury in LCPD is the bony proximal femoral epiphysis, there is evidence that the epiphyseal growth plate is also injured. The structure of the proximal femur in growing individuals includes the

epiphysis (where the secondary center of ossification is located), overlying layers of epiphyseal and articular cartilage, and the proximal femoral growth plate (i.e., physis), which separates the epiphysis from the metaphysis of the femur.[29] This growth plate is responsible for the longitudinal growth of the femoral neck, and injury can lead to proximal femoral growth disturbance in the form of angular and shortening deformities.[44] The occurrence of growth disruption in a third of LCPD patients implicates damage to the proximal femoral growth plate in the course of disease.[130, 131] This is supported by the histological identification of growth plate lesions in patients with LCPD.[132] Up to 90% of patients with LCPD also have metaphyseal radiolucent changes, which is evidence that injury extends into the femoral neck.[45, 133] Interestingly, increased diffusion in the metaphysis as detected by diffusion MRI has also been shown to be predictive of radiographic outcomes including femoral head deformation.[134-136] Collectively, these findings support that the effects of ischemia on the growth plate and metaphysis are important contributors to clinical outcomes for patients with LCPD.

Given the scarcity of samples for histological assessment from patients with LCPD, animal model studies have been critical to advance the understanding of this disorder and evaluate diagnostics and treatments. The most established model of LCPD involves surgical induction of femoral epiphyseal ischemia in piglets, with the contralateral hip acting as an unoperated control.[137] Previous studies using the piglet model of LCPD have found effects of ischemia on the growth plate to vary from mild (thickening of the growth plate) to

severe (complete disruption of the growth plate) by 4 to 8 weeks following induction of ischemia.[45, 69, 137] However, morphologic changes to the growth plate have not been reported in the two weeks following induction of ischemia.[44, 45, 69] Furthermore, prior studies did not include histological assessment of the metaphysis (which includes the primary spongiosa, where endochondral ossification is occurring) at acute time points (<2 weeks following induction of ischemia).[45, 69] By assessing both the growth plate and the metaphysis together in the initial period following ischemic injury, there is an opportunity to develop a more complete understanding of the effects of epiphyseal ischemia on growth in the early phases of LCPD, potentially leading to identification of lesions relevant to pathogenesis, prognosis, and treatment selection.

The objective of this study was to conduct histological assessment of the proximal femoral growth plate and metaphysis in the LCPD piglet model at three early time points (2 days, 7 days, and 28 days) following onset of ischemia. Evaluation included both qualitative and quantitative histological assessment of the growth plate zones and primary spongiosa using histomorphometry and immunohistochemical characterization.

2.2 Methods

Animals

This work was approved by the Institutional Animal Care and Use Committee at the University of Minnesota and Scottish Rite for Children. 28

Yorkshire piglets (22 male and 6 female) were sourced from a commercial provider (either Change of Pace, Aubrey, TX or Manthei Hog Farm, Elk River, MN). Piglets were assigned to one of three post-operative time-points: 2 days (n=8), 7 days (n=6), or 28 days (n=14). Group sizes were chosen based on the needs of prior studies evaluating quantitative MRI methods.[76, 78, 79, 138] At six weeks of age, piglets underwent unilateral surgical induction of ischemia to the whole proximal femoral epiphysis by placement of a ligature around the femoral neck and transection of the ligamentum teres, as previously described.[69, 70] Piglets were operated on by one of two surgeons (HKWK or FT). Two 2-day animals and five 28-day animals (all male) underwent surgery at Scottish Rite for Children, and the remaining 21 animals (15 male, 6 female) underwent surgery at the University of Minnesota. The contralateral hip was unoperated and served as a control. Piglets were euthanized with an intravenous injection of potassium chloride (75-150 mg/kg) or sodium pentobarbital (100 mg/kg) to allow for collection and histological assessment of the femoral heads. The 2-day samples (n=8) and a subset of the 28-day samples (n=5) underwent a freeze/thaw cycle prior to preparation for histology.

Overview of Histological Methods

Harvested ischemic and control femoral heads from the piglets were bisected in the coronal plane and fixed in 10% neutral buffered formalin. Tissues were decalcified using 10% ethylenediaminetetraacetic acid, and 3.0 mm thick

mid-coronal slabs were routinely processed. Consecutive 5-μm thick sections were collected and were stained with hematoxylin and eosin (H&E), safranin O, and toluidine blue. Histological sections (operated and control femoral heads), special stains, and immunohistochemical results were assessed in a blinded fashion by a board-certified veterinary pathologist (ARA) with four years of experience in musculoskeletal pathology with secondary review by a board-certified veterinary pathologist with over 30 years of musculoskeletal pathology experience (CSC). Several techniques were chosen to provide insight into morphological changes affecting the growth plate and primary spongiosa. First, histomorphometry was used to quantify the thicknesses of the growth plate, growth plate zones, and primary spongiosa and the size and number of cells within the hypertrophic zone (largest cells and most distinct zone based on morphologic features; H&E-stained sections). Second, special stains were used to determine the relative proteoglycan content of the chondroid matrix (toluidine blue and safranin O staining) and the number of osteoclasts (i.e., the cells responsible for bone resorption) within the primary spongiosa (tartrate-resistant acid phosphatase [TRAP] staining). Third, immunohistochemistry was performed to further assess the mechanism of alteration in growth plate morphology.

Histomorphometry

Exclusion criteria for histomorphometry were complete full-thickness disruption of the growth plate by fibrosis and/or fibrovascular tissue or the

presence of a secondary or superimposed disease process (e.g. inflammation). Based on these criteria, seven animals did not undergo further assessment: for the 2-day time-point, one animal was excluded due to a focal full-thickness disruption of the physis; for the 7-day time-point, one animal was excluded due to the presence of bacterial osteomyelitis; and for the 28-day time-point, five animals were excluded due to full-thickness physeal disruption, which precluded meaningful evaluation of the growth plate zones (Appendix 1 - Supplementary Figure 1). Thus, in total, 7/8, 5/6, and 9/14 pigs were included in the histomorphometry assessment at the 2-, 7-, and 28-day time points, respectively.

All measurements were performed using ImageJ (version 1.53a; imagej.nih.gov/ij)[139] with photomicroscopy images collected with NIS Elements D (version 5.20.00) using a light microscope (ECLIPSE Ci; Nikon Instruments; Melville, NY). The growth plate zones were defined by morphological criteria.[31, 39] To measure the full thickness (i.e., height) of the growth plate and the thicknesses of the three physeal zones (resting zone, proliferative zone, and hypertrophic zone) and primary spongiosa, three adjacent non-overlapping 4× fields were evaluated that included the central portion (approximately 75%) of the width of the growth plate, excluding the margins of the sections. Within each field, the total growth plate thickness and that of each physeal zone were measured five times, including a central measurement, one at either margin of the visible field, and measurements at the midpoints between the central measurement and the marginal measurement (i.e., the field divided into

quarters). Means were generated from the 15 total measurements taken per region per sample. Care was taken to avoid vascular profiles or areas of distortion of the growth plate zones, with measurements taken from the described regions in areas with the most even columnar arrangement of cells.

Hypertrophic Cell Number and Size

Additional assessment was performed on H&E-stained sections from the 7- and 28-day samples to measure the number and size of hypertrophic cells. Samples that underwent a freeze-thaw cycle were excluded due to confounding artifacts for these measurements, including loss of small to moderate numbers of hypertrophic chondrocytes, changes in cell morphology (shrinkage), and accumulation of eosinophilic material within marrow spaces of the primary spongiosa. This left n=4 samples at 7 days (one excluded due to extent of chondrocyte cell death and disorganization within the growth plate) and n=4 samples at 28 days (five excluded due to freeze-thaw cycle). To evaluate the number and size of the hypertrophic chondrocytes, five adjacent nonoverlapping 20× fields were assessed. The widest diameter of 10 randomly selected hypertrophic chondrocytes within the 1-2 cell rows nearest the metaphysis were measured and the mean was calculated. To determine the mean number of hypertrophic chondrocytes, these cells were counted in 10 linear columns per 20× field, using the same images for assessment as those used to assess hypertrophic cell size.

Special Stains

Tartrate-resistant acid phosphatase (TRAP) staining was performed on one section per femoral head for piglets at 7 days (n=4) and 28 days (n=4) post-ischemia to evaluate the number of osteoclasts within the primary spongiosa in control and ischemic samples (same animals that were assessed with cell counting/measuring as described above). Deparaffinized sections were hydrated with water, treated with acetate buffer (0.2M; 20 min), and placed in TRAP stain for 1-4 hours (37ºC) until osteoclasts were bright red. To evaluate the number of osteoclasts within the primary spongiosa, three adjacent non-overlapping 10× fields were evaluated in TRAP-stained sections. All multinucleated cells with strong red staining were counted using ImageJ and a mean TRAP-positive cell count per 10× field was generated for each femoral head. Additional sections were stained with safranin-O and Toluidine blue.

Immunohistochemistry

Immunohistochemical protocols for TGFβ1 (regulator of chondrocyte proliferation and differentiation[140]) and Indian hedgehog (Ihh; inhibits chondrocyte hypertrophy[141]) were performed on consecutive sections from 7-day (n=4) and 28-day (n=4) post-ischemia femoral heads and their contralateral controls (the same pigs as described for the hypertrophic cell and TRAP measurements). The TGFβ1 antibody was purchased from Invitrogen (#PA1-29032) and applied at a dilution of 1:100 following trypsin (Biocare) digestion. For Ihh, a polyclonal Ihh

antibody from Novus Biologicals (NBP1-59443) was applied at a dilution of 1:100 following pepsin (Biocare) digestion. Both protocols utilized the Dako Rabbit Envision detection system with 3,3'-diaminobenzidine (DAB, brown staining) as chromogen and Harris hematoxylin as the counterstain. The distribution and immunoreactivity pattern (cytoplasmic, nuclear, membranous) were evaluated for both TGFβ1 and Ihh.

Statistical Analysis

Statistical analyses were performed using GraphPad Prism (version 9.2.0 for macOS; GraphPad Software; San Diego, CA). Within each time-point, control and ischemic femoral head histomorphometry values (total physis thickness, mean zonal thicknesses, and mean primary spongiosa thickness) were compared with two-tailed paired *t*-tests. To determine the difference in overall growth plate thickness between the three time points, one-way analysis of variance was used. For all tests, $p<0.05$ was considered statistically significant.

2.3 Results

Histological Findings

Two days following ischemia (n=7), histological evaluation of the growth plate identified minimal changes in the H&E-stained sections. Chondrocyte cell death was not observed in the growth plate and there was no fibrosis,

microfracture, inflammatory infiltrate, or osteolysis observed at the growth plate or within the epiphysis. The primary spongiosa was present.

By 7 days post-ischemia (n=5), morphological alterations to the growth plate were readily apparent in H&E-stained sections. Chondrocyte cell death was frequent and widespread, with multifocal areas of chondrocyte cell death in the physis in 4/5 samples (Figure 2-1A, 2-1B). Loss of intensity of safranin O and toluidine blue staining from the growth plate matrix directly corresponded with areas of chondrocyte cell death. The primary spongiosa was markedly thinned to absent in all the examined ischemic samples (n=5), with an abrupt transition from the hypertrophic zone to the bone and bone marrow of the metaphysis (Figures 2-2, 2-3).

By 28 days post-ischemia (n=9), morphologic changes were more variable between individual samples. Chondrocyte cell death was seen in 8/9 samples but varied in extent, with some samples demonstrating chondrocyte cell death confined to the resting zone while others had widespread chondrocyte cell death or focal areas of full-thickness chondrocyte cell death additional zones (Figure 2-1C). Changes to the primary spongiosa were similar to those observed in the 7 day samples, with thinning to absence of the primary spongiosa and abrupt transition from the growth plate to subchondral bone and marrow spaces.

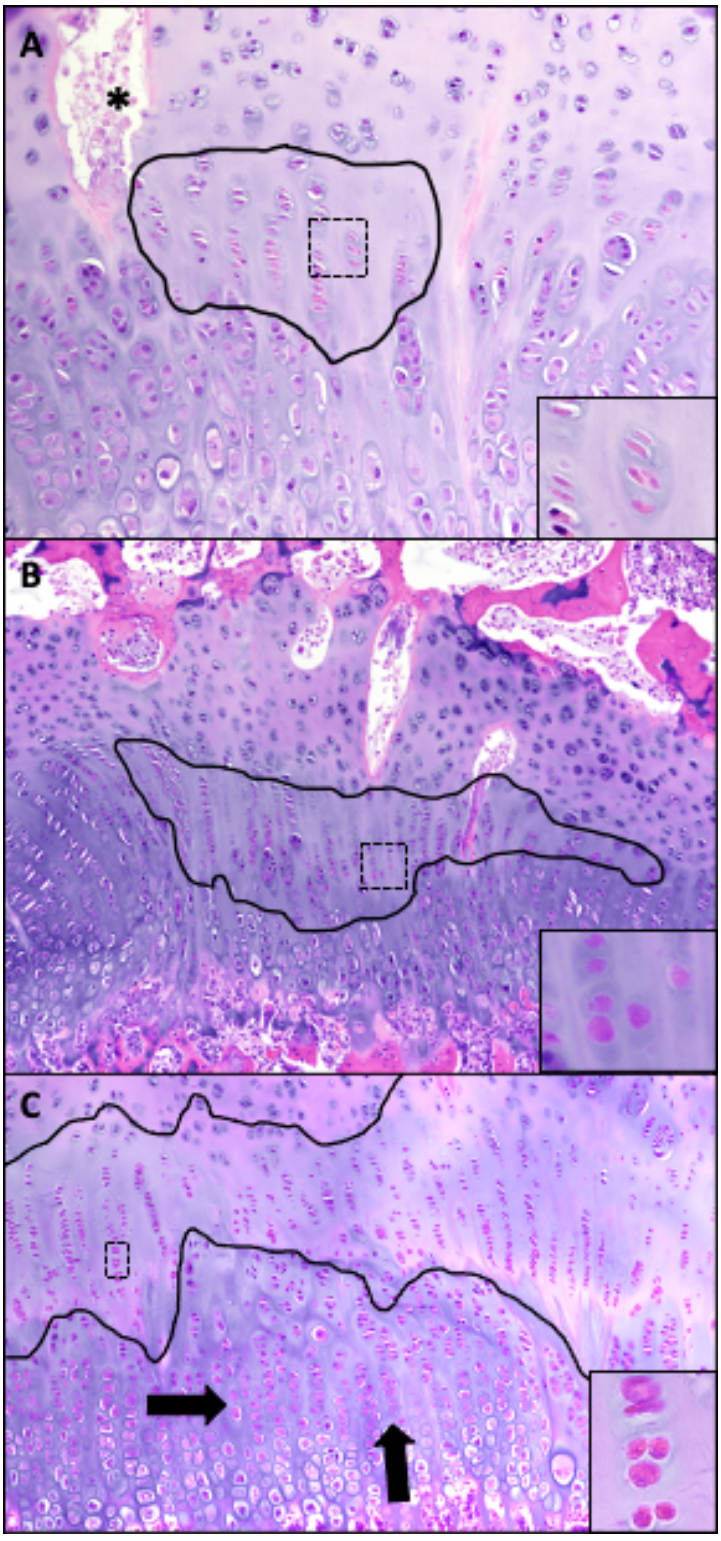

Figure 2-1. Histological lesions within the proximal femoral growth plate at 7 days and 28 days post-ischemia. (A) *Focal region of chondrocyte cell death affecting the*

*resting and proliferative zones at 7 days post-ischemia outlined in black. Inset (40×) shows chondrocyte cell death within area indicated by box, characterized by condensation and eosinophilia of chondrocytes with loss of nuclear detail. * = necrotic vascular profile containing cellular debris. H&E, 10×.* ***(B)*** *A large variably well-defined region of chondrocyte cell death affecting the proliferative zone at 7 days post-ischemia (within black outline); inset shows 40× magnification of chondrocyte cell death indicated by box. H&E, 4×.* ***(C)*** *At 28 days post-ischemia, there is a large area of chondrocyte cell death (outlined in black) affecting the proliferative zone (inset shows detail from area in box at 40×), with smaller numbers of dead chondrocytes in the resting zone. Several columns of chondrocytes in the hypertrophic zone also appear to be undergoing necrosis, with fading nuclear detail and increased cytoplasmic eosinophilia (arrows). H&E, 10×.*

Histomorphometry Findings

The resting zone, bordering the bony epiphysis, was of similar thickness in ischemic and control samples until 28 days following induction of ischemia, when it was significantly thickened in ischemic samples ($p=0.009$; Table 2-1). The mean thickness of the proliferative zone was consistently reduced (thinned) in the ischemic growth plates by 2 days following ischemia ($p=0.009$; Figure 2-2A, B). This thinning persisted at 7 days ($p=0.041$) and 28 days ($p=0.049$) days following induction of ischemia. Similarly, the hypertrophic zone was thinned by 2 days ($p=0.015$) with thinning persisting at 7 days ($p=0.026$) and 28 days ($p=0.0003$) following induction of ischemia (Figure 2-2A-F). Interestingly, the primary spongiosa was thickened in all (7/7) of the ischemic samples at 2 days following induction of ischemia ($p=0.041$) but was thinned as compared to the control primary spongiosa at 7 days ($p=0.020$) and 28 days ($p=0.003$) following induction of ischemia (Figure 2-2A-F; Figure 2-3). This thinning of the primary spongiosa affected all animals at 7 days (5/5) and most animals at 28 days (8/9). The total growth plate thickness (including resting zone, proliferative zone, and hypertrophic zone) was not significantly different between ischemic and control growth plates at any time point (Table 2-1). There was no significant difference in the total growth plate thickness between time points within either the control ($p=0.440$) or ischemic ($p=0.103$) growth plates.

Table 2-1. **Histomorphometry of the proximal femoral growth plate.**

Timepoint	Mean thickness, physis (μm)	Mean thickness, resting zone (μm)	Mean thickness, proliferative zone (μm)	Mean thickness, hypertrophic zone (μm)	Mean thickness, primary spongiosa (μm)
2 days (n=7)					
Control	767.0 (90)	285 (66)	330 (78)	108 (11)	404 (116)
Ischemic	697 (105)	305 (63)	267 (66)	89 (15)	458 (150)
p-value	0.086	0.155	**0.009**	**0.015**	**0.041**
7 days (n=5)					
Control	845 (161)	262 (37)	421 (104)	181 (33)	453 (179)
Ischemic	711 (71)	271 (22)	311 (44)	100 (23)	141 (62)
p-value	0.142	0.518	**0.041**	**0.026**	**0.020**
28 days (n=9)					
Control	799 (68)	243 (62)	377 (65)	168 (46)	345 (96)
Ischemic	799 (100)	314 (114)	325 (78)	119 (36)	296 (80)
p-value	0.998	**0.009**	**0.049**	**<0.001**	**0.003**

Values reported = mean (SD).

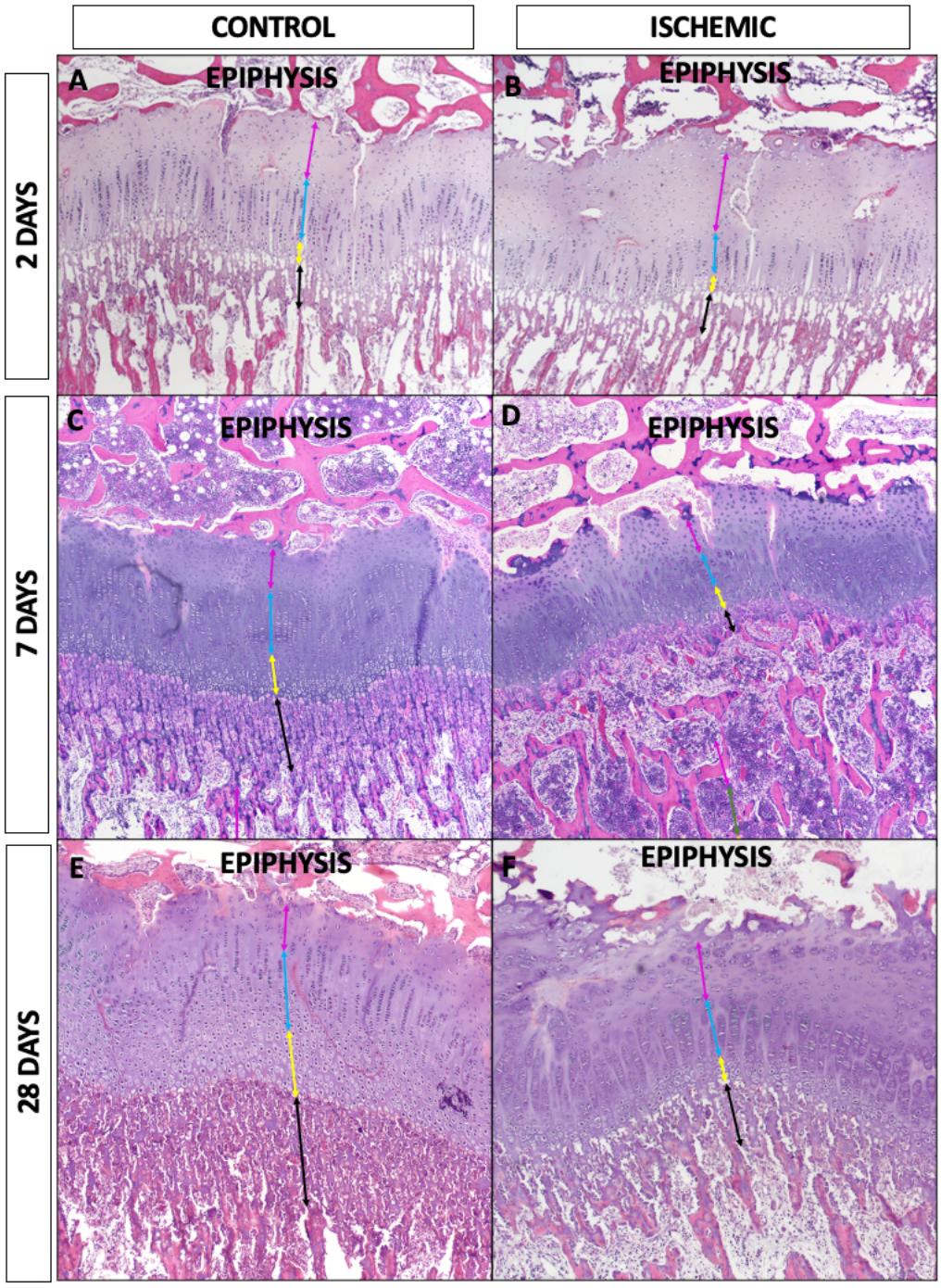

Figure 2-2. Thinning of the proliferative zone, hypertrophic zone, and primary spongiosa at 2-, 7-, and 28-days post-ischemia. (A) *and* ***(B)*** *By 2-days post-induction of ischemia, the mean thickness of the proliferative zone and hypertrophic zone were thinned in ischemic femoral heads (right), with thickening of the primary spongiosa.* ***(C)***

*and **(D)** By 7-days post-induction of ischemia, the mean thickness of the proliferative zone, hypertrophic zone, and primary spongiosa were thinned in ischemic femoral heads as compared to controls. **(E)** and **(F)** By 28-days post-induction of ischemia, the mean thickness of the proliferative zone, hypertrophic zone, and primary spongiosa were thinned in ischemic femoral heads as compared to controls, with thickening of the resting zone of the ischemic growth plates (right) as compared to the control growth plates (left). H&E, 4×. Magenta arrows = resting zone; light blue arrows = proliferative zone; yellow arrows = hypertrophic zone; black arrows = primary spongiosa.*

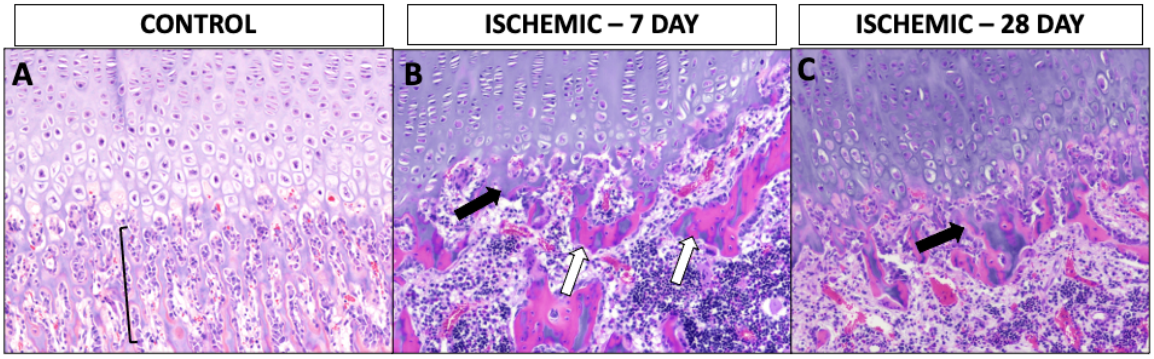

Figure 2-3. Abrupt transition with loss of primary spongiosa at 7 days and 28 days following induction of ischemia. (A) *Control growth plate (left) in a piglet 7 days following induction of ischemia at the contralateral hip demonstrating distinct primary spongiosa characterized by trabeculae of mineralized chondroid matrix (purple trabeculae within bracketed zone), extending down from the hypertrophic zone, which is populated by several layers of loosely columnar hypertrophic chondrocytes that are approximately equal in width and height.* ***(B)*** *Abrupt transition in a representative example at 7 days following induction of ischemia with nearly complete absence of primary spongiosa. Scant chondroid matrix forms short, irregular trabeculations (black arrow) that abruptly transition to marrow contents and remodeled bone (eosinophilic trabeculae; white arrow).* ***(C)*** *At 28 days following induction of ischemia, there is an absence of distinct primary spongiosa with abrupt transition to broad, blunted and anastomosing trabeculae composed of a mix of chondroid and osseous matrix. H&E, 10×.*

Hypertrophic Cell Number and Size

By 7 days post-ischemia, the mean cell diameter of chondrocytes in the hypertrophic zone of the ischemic femoral head was significantly less than that of control hypertrophic chondrocytes ($p=0.011$; Table 2-2). The mean cell number per column within the hypertrophic zone was also reduced in the ischemic samples as compared to the controls ($p=0.007$), and this difference persisted at 28 days post-ischemia ($p=0.007$).

Osteoclast Cell Number

The mean number of osteoclasts within the primary spongiosa based on TRAP staining did not vary significantly between ischemic and control growth plates at either time point (Table 2-2).

Table 2-2. **Hypertrophic zone histomorphometry.**

	Mean cell diameter (μm)	Mean cell number* per 10 columns of hypertrophic cells (20× field)	Mean osteoclast number, primary spongiosa (10× field)
7 days (n=4)			
Control	29.5 (2.0)	61.8 (6.9)	47.8 (9.6)
Ischemic	23.2 (1.5)	41.4 (6.9)	41.0 (5.4)
p-value	**0.011**	**0.007**	0.427
28 days (n=4)			
Control	28.2 (1.8)	62.0 (4.3)	55.8 (17.5)
Ischemic	25.9 (1.2)	46.0 (1.6)	39.4 (17.9)
p-value	0.095	**0.007**	0.262

*Cell count = mean number of hypertrophic chondrocytes in 10 adjacent columns within the hypertrophic zone (SD).

Immunohistochemistry Findings

TGF-β1 expression was uniformly strong in the resting zone chondrocytes at all time points and in both ischemic and control growth plates. At 7 days post-ischemia, the hypertrophic zone chondrocytes in the ischemic growth plates had moderate to strong cytoplasmic expression of TGF-β1, which was absent in the control growth plates (Figure 2-4). At 28 days post-ischemia, this pattern of immunoreactivity was not observed in the hypertrophic zone, with expression only within the resting zone in both the control and ischemic growth plates. This suggests that TGF-β1 plays a role in cessation of endochondral ossification in the more acute phase following induction of ischemia, but this effect did not persist to 28 days following induction of ischemia.

Indian hedgehog (Ihh) was expressed ubiquitously throughout the growth plate zones at all time points, without significant variation in expression between ischemic and control growth plates, suggesting that Ihh expression by growth plate chondrocytes is not altered during the acute period following induction of ischemia.

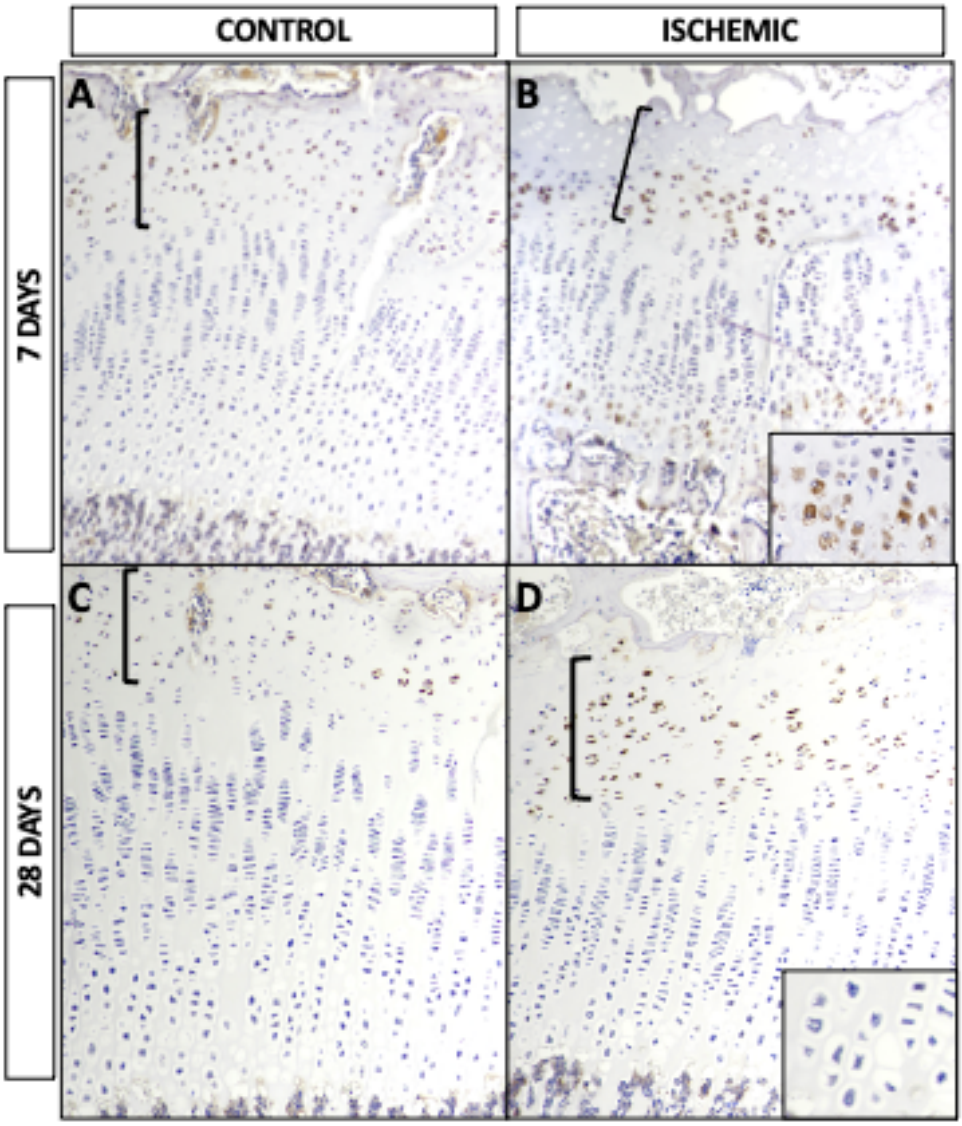

Figure 2-4. Expression of TGF-β1 by the hypertrophic zone chondrocytes at 7 days post-ischemia but not at 28 days post-ischemia. (A) *Control (left) and* ***(B)*** *growth plates from ischemic samples (right) at 7 days following induction of ischemia. Control and ischemic samples have strong cytoplasmic immunoreactivity (brown) within most resting zone chondrocytes (indicated by black brackets), with strong cytoplasmic immunoreactivity within hypertrophic zone chondrocytes in the ischemic sample only (inset, brown). Some of the resting zone chondrocytes lack counterstain in the ischemic sample due to chondrocyte cell death. 4×. Inset, 20×.* ***(C)*** *Control and* ***(D)*** *ischemic*

growth plates at 28 days following induction of ischemia have strong cytoplasmic immunoreactivity within most resting zone chondrocytes (brown), without expression in the other growth plate zones. 4×. Inset shows higher magnification (20×) of chondrocytes without TGF-β1 expression within the hypertrophic zone.

2.4 Discussion

Our results indicate that the proximal femoral growth plate and primary spongiosa are impacted within 2 days of onset of epiphyseal ischemia in piglets, with persistence of abnormal morphology at 28 days post-ischemia. We found that the proliferative and hypertrophic zones of the growth plate were persistently thinned at 2, 7, and 28 days following ischemic injury. This finding was accompanied by profound thinning of the primary spongiosa at 7 and 28 days without concurrent increases in osteoclast activity, indicating a disruption of endochondral ossification. We also observed TGF-β1 expression within the hypertrophic zone of the ischemic femoral heads at 7 days following induction of ischemia, but expression was absent in the hypertrophic zone by 28 days. Our findings suggest growth at the proximal femur may be disrupted at an earlier timepoint than previously reported.

By assessing the growth plate and primary spongiosa together, we were able to appreciate the effects of ischemia on multiple unique types of tissue involved in the process of endochondral ossification. The thinning of the proliferative and hypertrophic zones at 2, 7, and 28 days following induction of ischemia suggest that growth disruption may occur earlier than previously thought. The longitudinal growth of bones depends largely upon the rates of proliferation and hypertrophy of the growth plate chondrocytes.[142, 143] In our study, we found that both the zone of proliferation and zone of hypertrophy were thinned in response to epiphyseal ischemia and that this thinning was already

evident at 2 days following induction of ischemia. Early studies in a rabbit model of osteonecrosis found similar reduction in the layers of chondrocytes within the growth plate to those reported here[144] and determined that disruption of the resting zone of the growth plate had major impacts on endochondral ossification, suggesting this zone was most important regarding growth potential.[145] In contrast, while there may be biochemical effects on the resting zone secondary to ischemia prior to 28 days following ischemic injury, in our study the thickness of the resting zone was not significantly altered until 28 days following ischemia. The growth plate zones have different functions and may respond differently to injury, with varying impacts on endochondral ossification.[145] These findings suggest early (<28 days) assessment of the thickness of the zones of proliferation and hypertrophy might demonstrate the extent of ischemic injury prior to these types of injury becoming apparent at the resting zone, despite its closer proximity to the bony epiphysis.

In contrast to a previous study that did not identify metaphyseal changes prior to 28 days following ischemic injury, we observed significant variation in the primary spongiosa thickness at all time points.[45] Interestingly, the primary spongiosa was thickened at 2 days following induction of ischemia in all (7/7) of the examined ischemic femoral heads as compared to the controls. This suggests the effects of epiphyseal ischemia, including thinning of the proliferative and hypertrophic zones, precedes the interruption of endochondral ossification at the primary spongiosa. We also found the effects on the primary spongiosa to be

highly uniform at the examined timepoints, with the primary spongiosa thinned in eight of nine animals in our study and altered in just one of fourteen animals at 28 days post-ischemia.[45] Histologically, lesions in the primary spongiosa were limited to cessation of endochondral ossification with thinning of the primary spongiosa, without any animals developing retained tongues of growth plate cartilage or diffuse resorption of the growth plate cartilage.[45] The frequency of primary spongiosa disruption and the variability in histological appearance between studies using this model reinforces the importance of including examination of the metaphysis in studies of growth disturbance in LCPD that use this model.

Our findings suggest that TGF-β1 expression is temporally regulated in response to ischemia. TGF-β1 has important roles in maturation of chondrocytes within the proliferative and hypertrophic zones, and the roles in different zones are thought to vary in the mechanisms of action.[146] The increased expression of TGF-β1 by hypertrophic chondrocytes at 7 days post-ischemia but not at 28 days post-ischemia suggests some temporal specificity of TGF-β1 regulation related to the acute stage of ischemia. Transforming growth factor βs (TGFβs) are secreted proteins that bind to a variety of receptors to trigger kinase activities, and past studies have found treating chondrocytes with TGF-β1 decreases Ihh.[147] Ihh stimulates chondrocyte proliferation through by promoting synthesis of parathyroid related protein.[148] Despite the relationship between these factors, we did not identify decreases in Ihh expression in ischemic samples at either 7- or

28-days following ischemia. There are several possible reasons for the lack of an observed effect on Ihh expression, including 1) the magnitude of increase in TGF-β1 within the hypertrophic zone was not great enough to cause a noticeable alteration on Ihh expression, 2) Ihh expression was not altered at the time points examined, or 3) a different mechanism is responsible for the observed decrease in proliferation by growth plate chondrocytes.

Our study has several limitations. First, immunohistochemistry was not conducted on 2-day specimens, with only four piglets per time point assessed at 7 and 28 days. However, the findings in this subset of animals were quite uniform and suggest a strong effect, given the consistency of the results. Second, immunohistochemical evaluation was limited to two antibodies. Additional antibodies relevant to growth plate biology (RUNX2, osteocalcin, SOX9, type II and X collagen, VEGF) underwent evaluation and were not selected for further work-up due to lack of specificity and/or poor immunoreactivity or artifactual loss of cartilage from decalcified porcine tissues. The developmental biology of the growth plate is complex and there are many markers of chondrocyte differentiation and signaling that have high potential for future investigations. Given the unique structural arrangement of the growth plate with distinct morphological zones, novel spatial transcriptomic techniques may provide a better opportunity to shed light on the mechanistic role of ischemia in growth plate injury.[149] Lastly, this study was limited to histological assessment. The addition of MRI assessment of the growth plate and metaphysis could extend

findings to three dimensions and create a direct link to imaging techniques that can be utilized in children with LCPD, highlighting possible clinical applications as we develop an increased understanding of injury to the growth plate and metaphysis secondary to epiphyseal ischemia.[76, 79]

In conclusion, femoral epiphyseal ischemia has a significant impact on the proximal femoral growth plate morphology and function as early as 2 days following induction of ischemia. These acute effects of ischemia lead to disruption of endochondral ossification and persist to 28 days post-ischemia. Given the frequency with which children with LCPD may experience disruptions in growth of the proximal femur, these alterations in the piglet model may provide the opportunity to study growth disturbances and evaluate the efficacy of interventions in affected individuals.

2.5 Acknowledgements

We thank Kathleen Stuebner, Kelly Bergsrud, Andrea Chehadeh, Sara Pracht, and Amber Winter in the University of Minnesota Veterinary Clinical Investigation Center for their assistance with the animal model studies. We also thank Katalin Kovacs and Paula Overn from the University of Minnesota Masonic Cancer Center Comparative Pathology Shared Resource Laboratory for their careful preparation of the histologic and immunohistochemical sections assessed in this study.

2.6 Role of the Funding Source

This project was supported by grants from several institutes at the National Institutes of Health, including the National Institute of Arthritis and Musculoskeletal and Skin Diseases (R56AR078315, K01AR070894, and T32AR050938), National Center for Advancing Translational Sciences (UL1TR002494), and Office of the Director (K01OD021293 and T32OD010993). The study sponsors had no role in the study design, collection, analysis and interpretation of data, the writing of the manuscript, or the decision to submit the manuscript for publication. The content is solely the responsibility of the authors and does not necessarily represent the official views of the National Institutes of Health.

Chapter 3: Naturally occurring *osteochondrosis latens* lesions identified by quantitative and morphological 10.5T MRI in pigs

3.1 Introduction

Juvenile osteochondritis dissecans (JOCD) is a pediatric orthopaedic disorder affecting the articular-epiphyseal cartilage complex and the underlying subchondral bone. Clinically apparent disease is characterized by pain and gait deficits that are associated with a focal delay of endochondral ossification and, in a subset of patients, development of chondrosseous flaps and fragments. Lesions are most commonly diagnosed in the knee (distal femur), elbow (distal humerus), and ankle joints of young athletes and, if left untreated, they may progress to early-onset osteoarthritis.[86] Although the exact pathogenesis of JOCD in people remains incompletely understood, the ischemic theory, implicating disruption of endochondral ossification secondary to ischemic necrosis of the epiphyseal cartilage, has recently been gaining traction.[85, 97]

Much of the current understanding of JOCD in humans stems from extrapolating findings from osteochondrosis (OC) in animals, a disorder that shares the imaging, histologic and clinical features of JOCD.[20, 150] Histological sentinel studies conducted at JOCD predilection sites in asymptomatic juvenile pigs and horses have identified two early stages of OC that precede the formation of the osteochondral clefts and fragments that are characteristic

features of the late stage of disease, termed *osteochondrosis dissecans* (OCD).[84, 150] The earliest lesions, termed *osteochondrosis latens* (OCL), are confined to the epiphyseal cartilage and consist of areas of chondrocyte necrosis associated with necrotic cartilage canals, often accompanied by matrix degeneration. Delayed ossification of these necrotic areas of epiphyseal cartilage is known to result in radiographically apparent focal failure of endochondral ossification, consistent with progression to the next stage of the disease, termed *osteochondrosis manifesta* (OCM).[32, 84, 151, 152] Exposure of OCM lesions to biomechanical trauma is believed to trigger formation of osteochondral flaps and fragments, characteristic of OCD. Importantly, regions of epiphyseal cartilage necrosis consistent with OCL and OCM recently have been identified in biopsy specimens obtained from predilection sites in cadavers of children, bolstering support for the theory of a shared pathogenesis between JOCD and OC.[87] Identification of a characteristic, avascular region in the epiphyseal cartilage at the distal femoral JOCD/OC predilection sites using specialized MRI techniques in juvenile humans and pigs also supports the notion of shared pathophysiology across species.[97, 105] Indeed, this avascular region was absent in juvenile goats, a species that does not naturally develop OC, further supporting the role of vascular failure in the pathogenesis of JOCD/OC.[97]

Due to limited access to cadaveric specimens of children for histological evaluation, further understanding of the pathophysiology of JOCD requires the development of a non-invasive approach that can identify and monitor the

progression and/or resolution of OCL and OCM lesions *in vivo*. Implementation of quantitative and morphologic MRI techniques in animal models of orthopaedic disorders that are characterized by ischemic necrosis of the epiphyseal cartilage (OC and Legg-Calvé-Perthes Disease) demonstrated the sensitivity of T2 and T1ρ relaxation time maps to acute ischemic injury, suggesting that these are suitable methods to further examine the pathophysiology of JOCD.[76, 78, 81] These quantitative cartilage mapping methods have been used to identify surgically induced OCL and OCM lesions in a goat model of OC by focusing on specific areas that were rendered ischemic after transection of cartilage canal vessels.[81, 153] The use of these imaging methods to identify naturally occurring OCL and OCM lesions at predilection sites has not previously been accomplished. Doing so would demonstrate their value as research tools and diagnostic methods for children suspected of developing OCL or OCM lesions.

The objective of the current study was to demonstrate the utility of non-invasive MRI methods in identifying naturally occurring OCL and OCM lesions in the distal femoral and humeral predilection sites in cadaveric specimens of intact knee and elbow joints obtained from juvenile pigs. The nearly 100% prevalence of OCL and OCM lesions in both the distal femur and distal humerus in 12-week-old pigs, along with a joint size that is small enough to allow exhaustive histological evaluation for validation of the accuracy of the MRI techniques, supported the selection of these animals for the proposed study. Performing these studies at 10.5T provided the highest sensitivity for identifying and

characterizing these lesions with future studies planned to investigate the translatability of these techniques to *in vivo* studies at lower, clinical field strengths (≤7T).

3.2 Methods

Animals

Unilateral elbows (n=3) and knees (stifles) (n=3) were harvested immediately after euthanasia from three male Yorkshire-cross piglets aged 4, 8 and 12 weeks. These ages were chosen to include: 1) an age prior to that when OCL and OCM lesions at these sites have been reported (4 weeks); and 2) ages in which OCL and OCM lesions would likely be present (8 and 12 weeks, respectively).[33, 154] The University of Minnesota Institutional Animal Care and Use Committee approved the reported experiments (IACUC # 2004-38082A).

Imaging

Intact joint specimens were scanned in a whole-body 10.5-T MRI scanner[155] using an 8-channel dipole transceiver head coil.[156, 157] Morphological images were acquired with a 3D DESS (repetition time/echo time (TR/TE)= 21/6.2 ms, resolution= 0.3×0.3×0.3 mm^3) using a 19-minute scanning time. T2-weighted images were acquired with a 2D multiecho spin echo sequence with fat suppression (TR= 5800 ms, 13 TEs= 10.4-135.2 ms, resolution= 0.3×0.3×1.5 mm^3) and a 37-minute scanning time. T1ρ-weighted images were acquired using an adiabatic T1ρ-prepared 3D turbo spin echo sequence (TR = 6000 ms, 6 spin-lock times = 0-80 ms, spin-lock frequency = 500Hz, resolution = 0.45×0.45×2.0

mm^3) and a scanning time of 25 min. Imaging parameters are listed in Table 3-1. T2 and T1ρ maps were calculated by fitting a mono-exponential function to MR signal decay using a non-linear least-square fitting routine in MATLAB (v2019b; MathWords; Natick, MA). Clearly demarcated areas of increased signal intensity in 3D DESS, T2- and T1ρ-weighted images within the articular-epiphyseal cartilage complex were considered suspicious for the presence of OCL and/or OCM lesions.

Table 3-1. **10.5T MRI imaging parameters.**

Acquisition Parameters	**3D-DESS**	**T2 FS**	**T1ρ**
Sequence	Double Echo Steady State	2D Multi Echo Spin Echo	3D Turbo Spin Echo
Repetition time (ms)	21	5800	6000
Echo time (TE)/ Spin lock (SL) time (ms)	6.2	13 TEs: 10.4-135.2 ms	6 SL times: 0-80 ms
Echo train length	2	13	280
Number of averages	1	1	1
Field of View (mm)	128×128	128×128	173×173
Matrix size	384×384	384×384	384×384
Resolution (mm)	0.33×0.33	0.33×0.33	0.45×0.45
Slices / Thickness (mm)	/0.33	/1.5	/2
Flip Angle (degrees)	60	180	180
Pixel bandwidth (Hz/px)	128	250	766
Spin-Lock Frequency (Hz)	n/a	n/a	500
Scan Time (min)	18:42	37:30	24:36

Histology

At the conclusion of the MRI sessions, the joints were disarticulated, and distal humeri and femora were fixed in 10% neutral buffered formalin, decalcified in 10% ethylenediaminetetracetic acid, and serially sectioned in the sagital plane into 2.0 mm thick slabs that spanned the total thickness of the epiphysis. Individual slabs (approximately 7-9/site) were processed into paraffin blocks for histological evaluation. At least two 5-µm-thick sections were collected from the surface of each slab and stained with hematoxylin & eosin (H&E). Additional serial sections at 50-*µ*m intervals were obtained and stained with H&E to confirm all OCL and OCM lesions identified in the evaluated specimens (approximately 4-10 sections per suspected lesion). Histological sections were assessed by a board-certified veterinary pathologist with experience in musculoskeletal pathology (ARA). OCL lesions were defined as areas of chondronecrosis associated with necrotic vascular profiles that were confined to the epiphyseal cartilage.[32] OCM lesions were defined as areas of chondronecrosis in the epiphyseal cartilage that were accompanied by a delay in endochondral ossification.[32]

MRI Data Analysis

First, 3D DESS, T2- and T1ρ- weighted images were qualitatively evaluated by a blinded investigator for the presence of discrete areas of increased signal intensity (ROIs) suggestive of the presence of OCL and OCM

lesions and compared to the location and size of histologically identified OCL (areas of chondronecrosis) and OCM (areas of chondronecrosis with delay of endochondral ossification) lesions. Subsequent quantitative evaluation of the lesion region was performed by transferring the ROIs onto the corresponding T2 and T1ρ maps. For precise delineation of the ROIs, the position (i.e., distance from articular cartilage surface) and size of the lesions were first measured in ImageJ (Version 1.53a) in the histological sections by a board-certified veterinary pathologist before co-registration to the corresponding MR images. In samples with multiple discrete lesions, the largest lesion was used for MRI assessment and statistical analysis. Control ROIs were designated in comparably sized, histologically unaffected areas. Average T2 and T1ρ relaxation times were calculated from the ROIs comprising each OCL and OCM lesion and control regions.

Statistical analysis

To determine the difference between the lesion and adjacent control ROIs, the mean T2 and T1ρ relaxation times from ROIs were compared using paired t-tests. First, the comparison was performed separately for the OCL and for the OCM lesions and their respective control ROIs. Then, comparisons were made across all lesions (OCL and OCM) and control ROIs. Statistical analyses were performed using GraphPad Prism (version 9.2.0 for macOS, GraphPad Software, San Diego, CA). For all tests, $p<0.05$ was considered statistically significant.

3.3 Results

Gross and Histological Assessment

On gross examination, a focal region accompanied by delay of endochondral ossification was present in the 12-week-old humeral specimen at the trochlea. The other specimens were grossly normal. Histological analysis of sections corresponding with MRI slices containing suspected OCL and/or OCM lesions confirmed their presence in all suspected MRI locations (Table 3-2), which included all distal humeri (3/3) and one distal femur (1/3; 12-week-old) (Figures 3-1, 3-2, 3-3, and 3-4). Comprehensive histological evaluation of all distal humeri and femora failed to identify any additional OCL or OCM lesions that were not identified by MRI. Thus, the MRI techniques used in this study allowed detection of all lesions present in the evaluated joints.

Solitary OCL lesions were identified in one humeral (4-week-old) and one femoral (12-week-old) specimen, while the 8-week-old humeral specimen had three distinct OCL lesions, the largest of which was used for the quantitative comparisons (Figure 3-2). All humeral lesions were located at the trochlea of the distal humerus, whereas the distal femoral lesion was located at the medial condyle. The OCL lesions (n=5) were discrete areas within the epiphyseal cartilage characterized by loss of staining (pallor) of the matrix surrounding a central arboriform vascular profile with necrotic endothelium and necrosis of the adjacent chondrocytes. The OCM lesions (n=2) were identified in the 12-week-old pig, one in the distal humeral trochlea and one in the medial femoral condyle.

The OCM lesion (Figure 3-3) in the distal humerus was accompanied by an additional, separate, and discrete area of epiphyseal cartilage necrosis that was diagnosed as a small OCL lesion. The OCM lesion at this site included a localized area of necrosis and clefting at the chondrosseous junction, with expansion of the underlying marrow spaces by granulation tissue and resorption of subchondral bone by osteoclasts, indicative of some degree of chronicity (Figure 3-3). In contrast, the OCM lesion at the distal femur in the 12-week-old pig lacked bone resorption and fibrosis (Figure 3-4). This lesion was characterized by a focal delay of endochondral ossification accompanied by vascular necrosis affecting a central vascular profile within the region of delayed endochondral ossification and several regional vascular profiles within the epiphyseal cartilage that were arranged in an arboriform pattern.

The maximum extent of the OCL lesions, measured in histological sections, were 2.5 mm and 3.3 mm in the 4-week and 8-week specimens, respectively. The OCM lesion in the 12-week humeral and femoral specimens both had a maximum extent of 6.5 mm (Table 3-2).

Table 3-2. **Histological characteristics of lesions identified by 10.5T MRI.**

Specimen	Joint affected	Site	Maximum width* (mm)	Maximum thickness** (mm)	Histologic features	Diagnosis
4-week	Elbow	Humerus - trochlea	2.5 mm	1.5 mm	*Epiphyseal chondronecrosis* *Necrotic vascular profiles*	OCL
8-week	Elbow	Humerus - trochlea	3.3 mm	1.5 mm	*Epiphyseal chondronecrosis* *Necrotic vascular profiles*	OCL
12-week	Elbow	Humerus - trochlea	6.5 mm	2 mm	*Epiphyseal chondronecrosis* *Necrotic vascular profiles* *Delay of endochondral ossification* Cleft formation without displacement Bone resorption, Myelofibrosis	OCL, OCM
12-week	Knee/stifle	Femur – medial condyle	6.5 mm	5.4 mm	*Epiphyseal chondronecrosis* *Necrotic vascular profiles* *Delay of endochondral ossification*	OCM

OCL = osteochondrosis latens. OCM = osteochondrosis manifesta. *Italics* = diagnostic features.

* Width of lesions were measured in the serial histological section that captured the lesions at their largest point and refers to the greatest extent of the lesion as measured in the plane approximately parallel to the underlying chondrosseous junction.

** Thickness refers to the maximum thickness of affected cartilage as measured in the plane perpendicular to the chondrosseous junction.

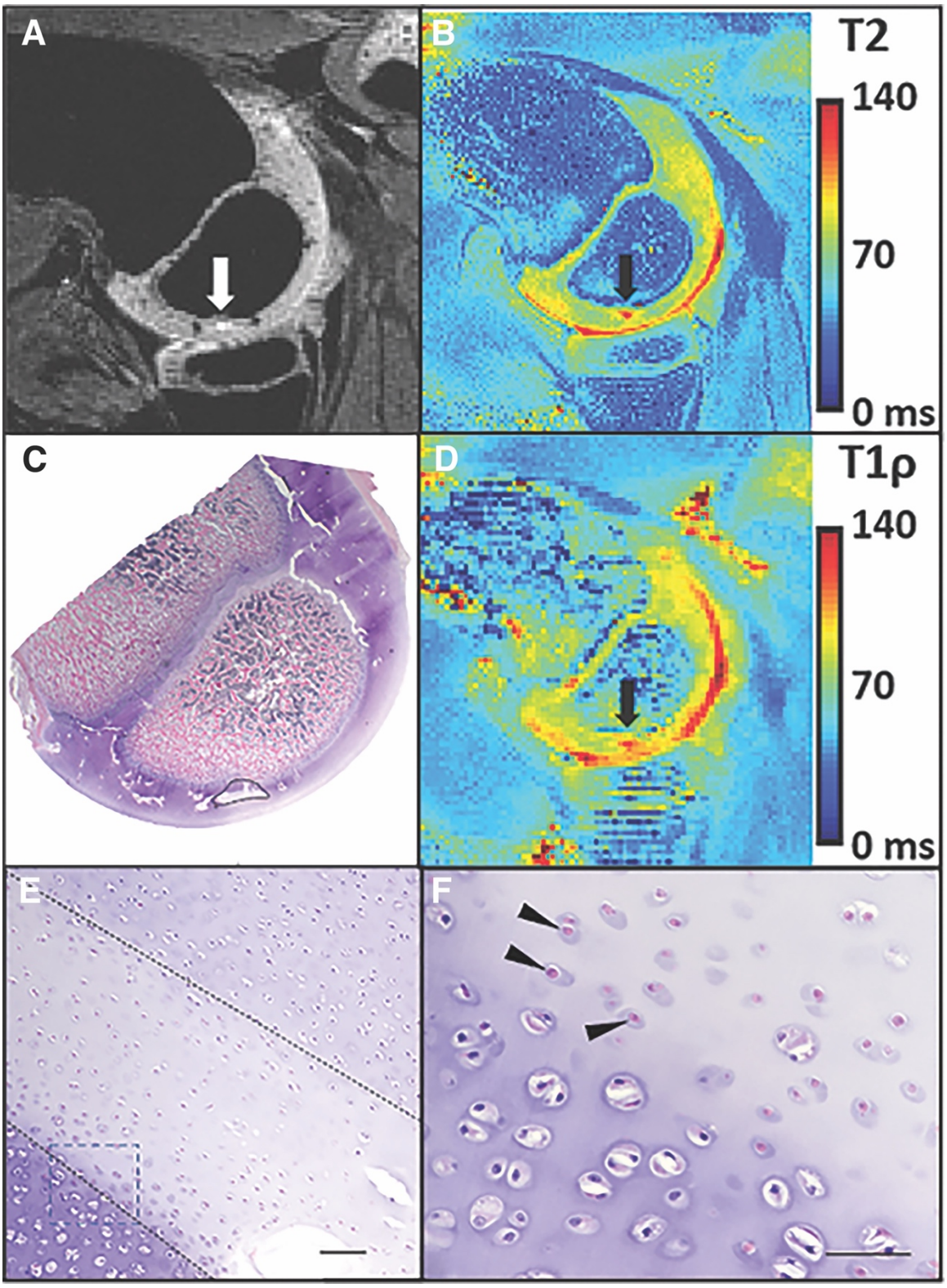

Figure 3-1. OCL lesion at the distal humerus of a 4-week-old pig. A) *A hyperintense region within the cartilage in the 3D DESS image (indicated by*

*white arrow) that corresponds to **B)** an area with increased T2 values (orange and yellow) within the articular epiphyseal cartilage complex (black arrow) in the T2 map with **C)** corresponding histological section showing associated region of chondrocyte necrosis with matrix pallor (outlined in black), consistent with an OCL lesion in the distal humerus of a 4-week-old pig. White clefts between the cartilage (purple) and marrow and bone of the epiphysis and metaphysis are artifactual. Hematoxyliᑎ & eosin (H&E), 0.5× magnification. **D)** Corresponding T1ρ map with increased T1ρ values in the OCL lesion (black arrow). **E)** Higher magnification image (20x) showing localized area of chondronecrosis centrally (bordered by dotted lines) characterized by matrix pallor and chondrocytes that are pyknotic and eosinophilic with loss of detail (chondrocyte cell death). H&E. 10× magnification; scale bar = 100 µm. **F)** Higher magnification image (40x) of the area indicated by the box bordered by dashed lines in E) demonstrating necrotic chondrocytes (black arrowheads) with diffuse eosinophilia and condensed morphology as compared to unaffected neighboring chondrocytes (lower left). H&E. 40× magnification; scale bar = 20 µm.*

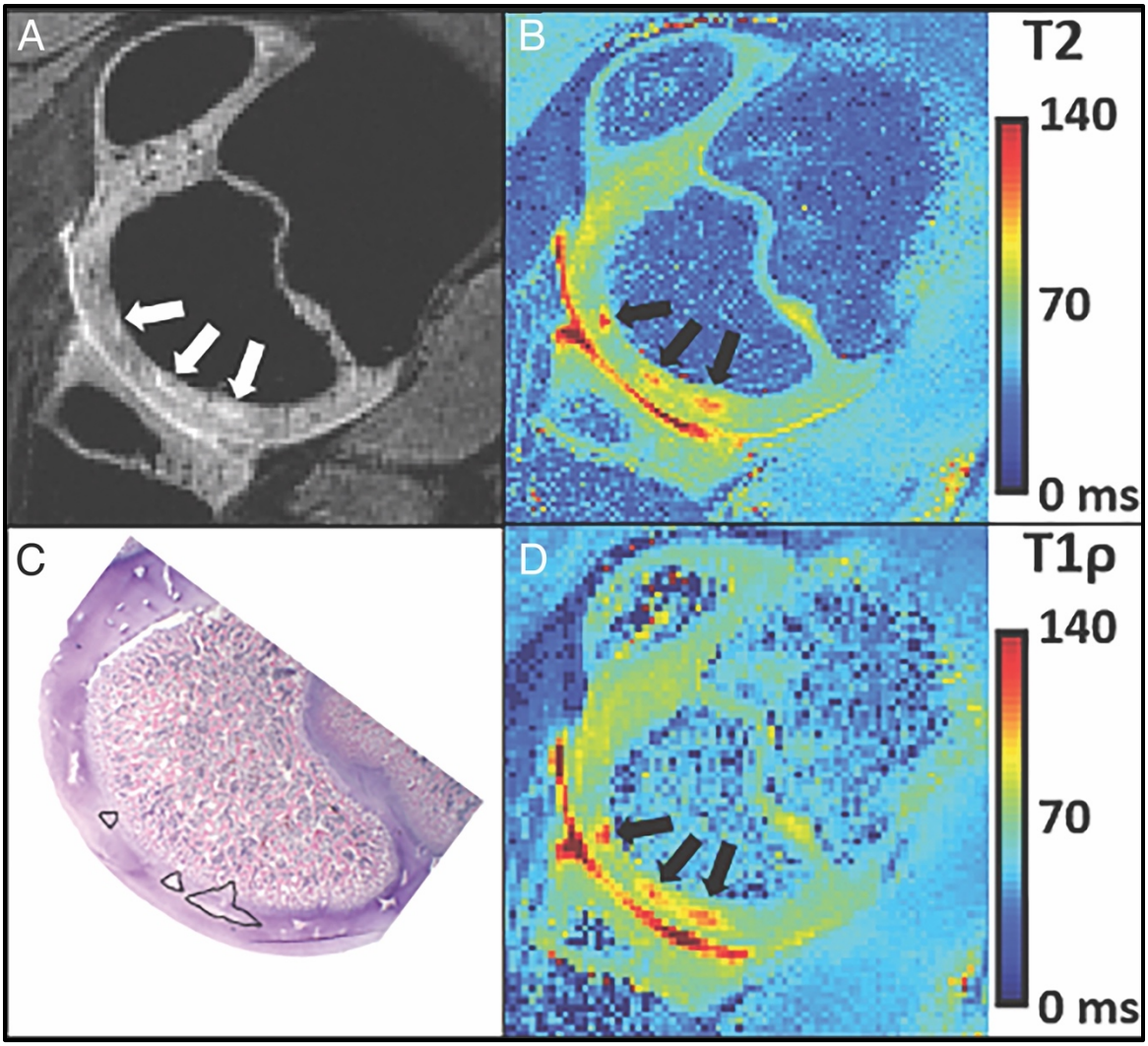

Figure 3-2. OCL lesions at the distal humerus of an 8-week-old pig. A) Three distinct neighboring hyperintense (white to pale gray) regions within the cartilage on 3D DESS (white arrows) that corresponds to B) areas with increased T2 values (orange and yellow) within the articular epiphyseal cartilage complex (black arrows) in the T2 map with C) corresponding histological section showing associated regions of chondrocyte necrosis with matrix pallor (outlined in black), consistent with OCL lesions in the distal humerus of an 8-week-old pig. H&E. 0.5× magnification. D) Corresponding T1ρ map with increased T1ρ relaxation times (orange and yellow) in the OCL lesions (black arrows).

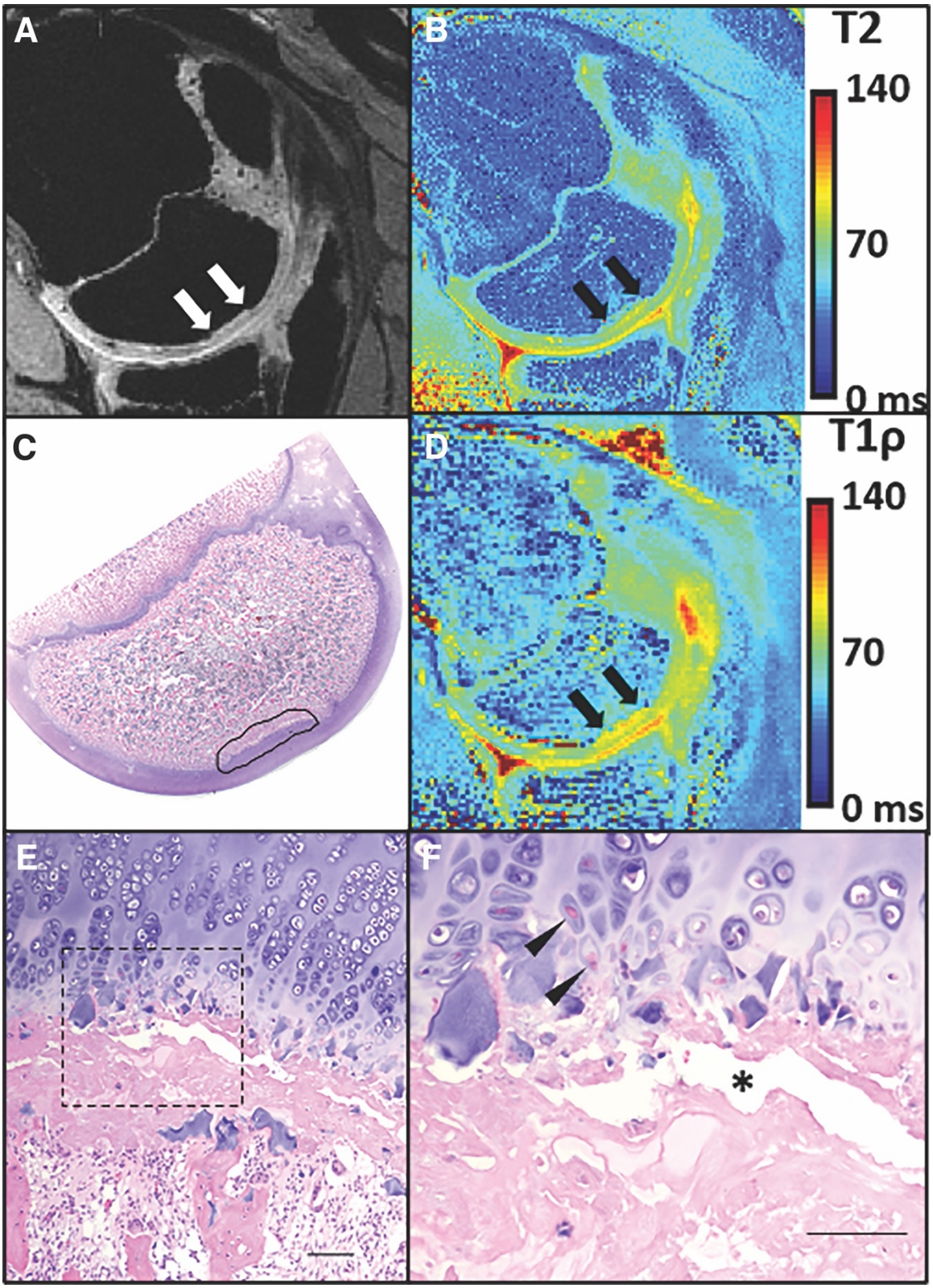
A
B
T2
140
70
0 ms
C
D
T1ρ
140
70
0 ms
E
F
*

Figure 3-3. OCM lesion at the distal humerus of a 12-week-old pig. A) *A hyperintense region within the cartilage in the 3D DESS image (white arrows) that corresponds to* ***B)*** *an area with increased T2 values (yellow to green) within the articular epiphyseal cartilage complex (black arrows) in the T2 map with* ***C)*** *corresponding histological section showing associated region of thickened articular-epiphyseal cartilage complex with delay of endochondral ossification and locally extensive subjacent chondroid matrix necrosis (outlined in black), consistent with OCM in the distal humerus of a 12-week-old pig. H&E. 0.5× magnification.* ***D)*** *Corresponding T1ρ map with increased T1ρ values (orange and yellow) in the OCM lesion (black arrows).* ***E)*** *High magnification image oriented with the articular surface towards the top of the panel (not pictured) showing clefting between the thickened articular-epiphyseal cartilage complex and the subjacent area of necrosis, with fibrosis extending into the subchondral bone (bright pink). H&E. 10× magnification; scale bar = 100 µm.* ***F)*** *High magnification image (40x) from the box in E) demonstrating necrotic chondrocytes (black arrowheads), overlying a cleft (*) and accumulation of eosinophilic necrotic debris. H&E. 40× magnification; scale bar = 50 µm.*

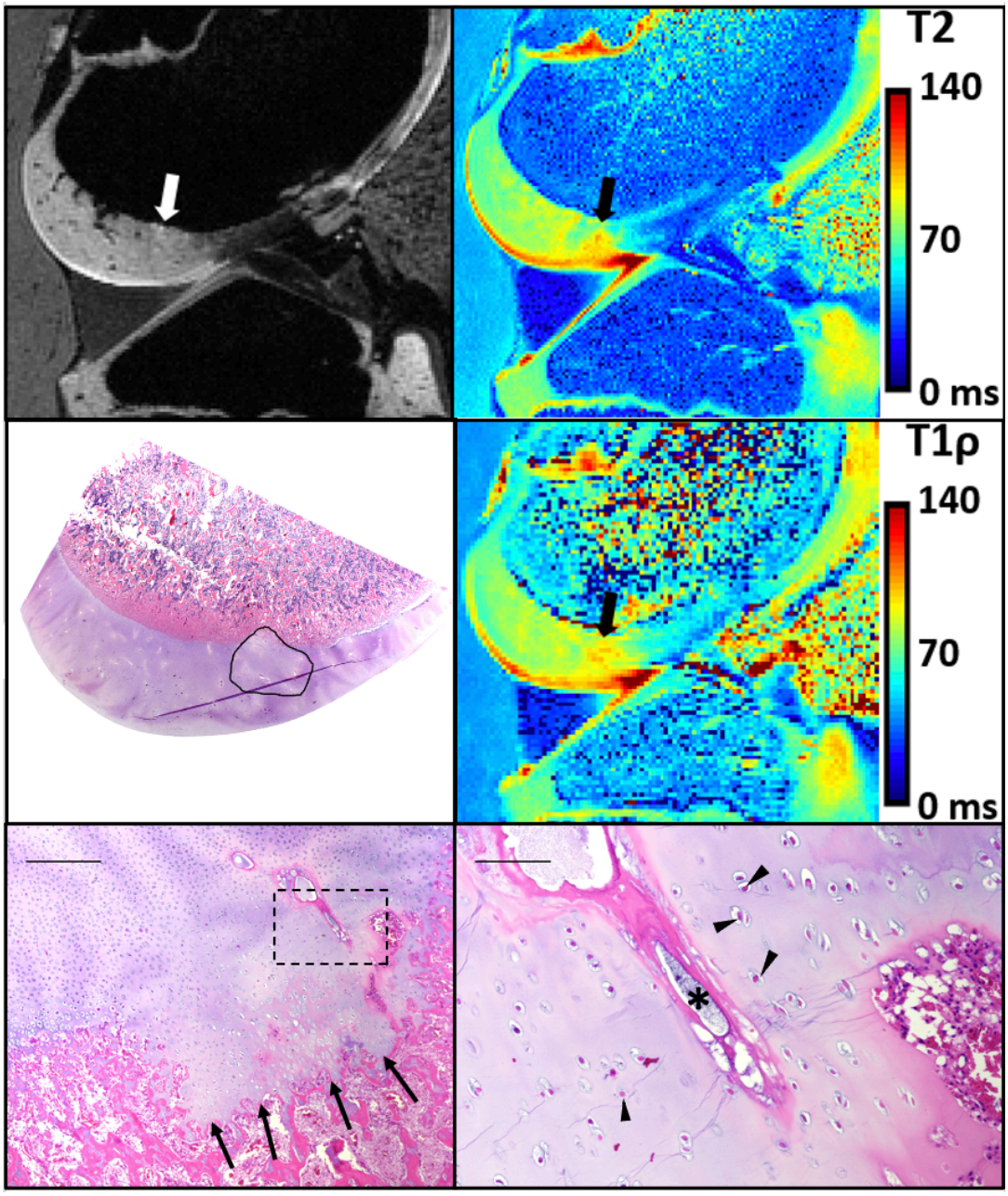

*Figure 3-4. OCM lesion at the distal femur of a 12-week-old pig. A) A hyperintense region (white arrow) within the cartilage in the 3D DESS image (white to pale gray) that corresponds to **B)** an area with increased T2 values (orange to yellow) in a wedge shape within the articular epiphyseal cartilage complex (black arrow) in the T2 map with **C)** corresponding histological section showing a region of focal delay of endochondral ossification and chondrocyte necrosis with matrix pallor (black circle), consistent with OCM in the distal femur*

of a 12-week-old pig. H&E. 0.5× magnification; scale bar = 5 mm. ***D)*** *Corresponding T1ρ map with increased T1ρ values (orange and yellow) in the OCM lesion (black arrow).* ***E)*** *High magnification image oriented with articular surface towards the top of the panel (not pictured) showing focal delay of endochondral ossification (black arrows) and pale matrix and necrotic chondrocytes. H&E. 4× magnification; scale bar = 500 µm.* ***F)*** *High magnification image of the area indicated by the box in E) demonstrating necrotic chondrocytes (black arrowheads) with diffuse eosinophilia and pallor of the associated matrix surrounding a necrotic vascular profile (*). H&E. 20× magnification; scale bar = 50 µm.*

Morphological and Quantitative MRI Assessment

The mean T1ρ and T2 relaxation time values were increased by 20% and 26.9% in the 4-week-old humeral OCL ROI and by 43.9% and 33.7% in the 8-week-old humeral OCL ROI compared to their respective control ROIs (Table 3-3). Values in the 12-week-old specimens were increased by 10.3% (T1ρ) and 5.9% (T2) in the humeral OCM ROI and 15.4% (T1ρ) and 12.6% (T2) in the femoral OCM ROI compared to their respective control ROIs (Table 3). The comparison of all lesion ROIs (OCL and OCM) to their paired control ROIs showed a statistically significant increase in both the mean T2 (n=4, p=0.047) and mean T1ρ (n=4, p=0.035) relaxation times. The magnitude of this increase was similar for both the T1ρ and T2 values (Table 3-3). The OCM lesion in the 12-week-old humerus had increased T2 and T1ρ values within the AECC, coupled with small increases in signal extending into the subjacent epiphysis within the area of focal thickening of the epiphyseal cartilage (Figure 3-3).

Additionally, qualitative visual assessment of 3D DESS images showed increased signal intensities in the locations corresponding to in OCL and OCM lesions and no increased signal was detected in the control regions as demonstrated in Figures 3-1, 3-2, 3-3, and 3-4 (A in panels).

Table 3-3. **Comparison of T2 and T1ρ relaxation times between lesion ROIs and control ROIs.**

Specimen	Control T2 (ms)	Lesion T2 (ms)	T2 % Increase	Control T1ρ (ms)	Lesion T1ρ (ms)	T1ρ % Increase
4-week Humerus	70.65	89.65	26.9%	78.75	94.81	20.0%
8-week Humerus	65.21	87.22	33.7%	64.45	92.78	43.9%
12-week Humerus	67.49	71.49	5.9%	76.45	84.44	10.3%
12-week Femur	74.56	83.96	12.6%	77.39	89.34	15.4%
Mean ± SD	*69.5 ± 4.1*	*83.1± 8.1*	*19.8 ± 12.8%*	*74.3 ± 6.6*	*90.3 ± 4.5*	*22.4 ± 14.9%*

SD = standard deviation.

3.4 Discussion

Our results demonstrate that quantitative MRI methods detect both naturally occurring OCL and OCM lesions at the distal humeral and femoral predilections sites *ex vivo* in intact joints of juvenile pigs. Blinded, qualitative evaluation of the 3D DESS, T2- and T1ρ-weighted images identified each OCL and OCM lesion present in the specimens with no false positive or false negative findings, as validated by histology. Quantitative evaluation of the relaxation time maps confirmed the initial findings by demonstrating significantly increased T2 and T1ρ relaxation times within the lesion ROIs compared to adjacent control ROIs. These findings suggest that T2 and T1ρ cartilage maps have strong potential as diagnostic tools to identify naturally occurring OCL and OCM lesions, warranting their further evaluation *in vivo* at a clinically relevant field strength (≤7T).

The mean T2 and T1ρ relaxation times across all measured OCL (n=2) and OCM (n=2) lesions were significantly increased when compared to their respective control regions. The difference in T2 and T1ρ relaxation times when averaged for the four- and eight-week-old specimens between areas of chondronecrosis (OCL) and controls were 30.3±4.8% and 32±16.9%, respectively. The differences in the present study were somewhat smaller in magnitude than those observed in regions of induced chondronecrosis in a goat model of OC, which had a mean percent difference of 58.4±16.7% and 54.4±30.4% for T2 and T1ρ, respectively.[153] The variation in magnitude of the

difference between the relaxation times in lesions and normal regions may be related to surgical induction causing a complete disruption of local blood supply vs. a less extensive vascular failure occurring in natural lesions. Another possible cause may be the stage of development in the respective animal models, with the goats undergoing surgery to induce ischemia at 4 days of age while the pigs assessed in this manuscript likely developed ischemia and subsequent lesions at a later timepoint.[153] The different tissue composition of OCM lesions, including retention of necrotic, and in some cases non-necrotic, cartilage accompanied by remodeling of the adjacent subchondral bone and marrow, coupled with the greater duration of the lesions, is likely responsible for the smaller differences in T2 and T1ρ in the 12-week-old specimens (humeral ΔT2 = 5.9% and ΔT1ρ = 10.3%, femoral ΔT2 = 12.6% and ΔT1ρ = 15.4%) as compared to the differences in OCL lesions in the 4 and 8-week-old specimens. Comparing the magnitude of change in T1ρ and T2 relaxation times across all lesions and their respective controls demonstrated that both indices increased by a similar degree, with both techniques identifying increased relaxation times associated with lesions in each specimen.

All humeral lesions were located at the trochlea of the distal humerus, one of the most frequent predilection sites for OC in pigs.[158, 159] Interestingly, a lesion was identified in the 4-week-old humeral specimen, at an earlier age than OCL lesions have been previously reported to develop.[20] This may suggest that vascular vulnerability at the elbow joint occurs earlier than at the more frequently

affected femoral sites, the area examined in the vast majority of JOCD-OC studies. Importantly, the 12-week-old humeral lesion exhibited resorption of subchondral bone and replacement of marrow spaces by granulation tissue, suggesting ongoing reparative processes. This is consistent with our previous findings that the majority of OCL and OCM lesions undergo repair, with only a small subset progressing to clinical disease in pigs.[101] Taken together, our findings suggest that it is possible that humeral lesions occur at younger ages in pigs than femoral lesions and develop chronic changes earlier than femoral lesions. Unsurprisingly, the femoral lesion was found in the medial femoral condyle, the primary predilection site of JOCD/OC in the pelvic limb both in children and piglets.[152, 160]

Our study marks the first time that naturally occurring OCL lesions were identified non-invasively in any species and at any location. In pigs, osteochondrosis is initially characterized by a focal area of chondronecrosis within the growth cartilage (OCL) at regions of vascular vulnerability, which correspond to anatomically similar regions in people.[97] In a subset of cases, these regions of chondronecrosis are large enough that they interfere with progression of the ossification front, leading to a focal failure of endochondral ossification (OCM). OCL lesions in humans are also suspected to progress to OCM, which may undergo stages of osseous repair, including peripheral mineralization, progressive ossification, and osseous bridging between the lesion and the parent bone in the course of healing.[32, 96, 161] This process may fail in

some cases, requiring surgical intervention in the hopes of preventing articular cartilage clefting and formation of an osteochondral fragment or “loose body” within the joint.[162] Similarly, studies investigating the pathophysiology of osteochondrosis in growing pigs successfully implemented sequential CT scans to monitor the progression and/or resolution of OCM lesions.[33, 90] These studies demonstrated the utility of this technique in screening pigs for early lesions of osteochondrosis and established a 51-69% spontaneous healing rate for OCM lesions depending on the joint affected.[33] The MRI methods outlined here improve upon these previously reported diagnostic and monitoring methods by not only providing a sensitive and specific means of detecting both OCM and OCL lesions, but by having greater translational potential for pediatric populations due to the absence of ionizing radiation or contrast material. MRI methods such as T2 and T1ρ may provide additional benefits given their quantitative nature and sensitivity to biochemical changes, with studies having shown a correlation of T2 and T1ρ relaxation times to collagen, proteoglycan, and water content as well as to age-related changes in tissue composition and structure.[163-165] 3D-DESS allows evaluation of the cartilage morphology and detection of structural defects in the cartilage by providing excellent contrast between the synovial fluid and cartilage.[166] While 3D-DESS was used only for the morphological evaluation in the present study, this technique was also capable of identifying regions of chondronecrosis without communication with the synovial fluid, confirming its sensitivity to areas with increased T2 relaxation times within

OCL lesions. 3D-DESS is a readily available clinical sequence that does not need extensive postprocessing, making this technique particularly useful for screening pediatric patients.[50, 167] While human studies have been performed at 10.5T under an investigational device exemption and local IRB approval [168, 169], it is currently not approved for pediatric or patient studies. Clinical translation of these sequences for the diagnosis of elbow OCD in human patients will necessitate their further evaluation at lower field strengths (<=7T) which have the additional benefit of being clinically approved. Prolonged scan times, another important factor in pediatric patients, will also have to be addressed before these methods are implemented in clinical practice.[50]

The clinical relevance of our findings is underscored by the recent description of lesions at JOCD predilection sites in randomly sampled pediatric cadavers that were morphologically identical to OCL and OCM lesions seen in animal species.[87] Given the observed propensity for healing of OCL and OCM lesions in pigs, it is reasonable to assume that the prevalence of early asymptomatic lesions in children is higher than the prevalence of symptomatic JOCD lesions.[33] This is supported by the findings of a recent *in vivo* 3T study of 25 patients with 34 JOCD-affected knees that found JOCD lesions in five asymptomatic knees.[161] Furthermore, this 3T study used T2* relaxation time mapping as a measure of the degree of lesion ossification and was able to distinguish between the different stages of disease progression - from the early, predominantly cartilaginous, to the late and almost entirely ossified JOCD

lesions.[161] Noninvasive methods for detecting and monitoring these early lesions may provide insight into factors that contribute to either healing or progression to clinical disease, which could ultimately impact clinical recommendations. Based on our findings, reasonable next investigative steps include the application of 3D-DESS, T2, and T1ρ techniques to pediatric cadaveric specimens to identify *ex vivo* OCL and OCM lesions with a clinical (≤7T) MR system, followed by targeted histological assessment to confirm their presence.

The small sample size may be considered a limitation of this study; however, the high prevalence of OCL and OCM lesions in growing pigs (present in 4 out of 6 specimens in the present study) and the confirmation of all lesions by exhaustive histological evaluations (4/4), considered the gold standard for identification of early-stage JOCD lesions, supports the ability of these MRI methods for the detection of OCL and OCM lesions. Although our study was completed using a 10.5T whole body research magnet and optimized RF coil to maximize both signal to noise ratio and resolution, there is reason to believe that these techniques would also be effective in identifying OCL and OCM lesions at clinical field strengths, as demonstrated in a previous study that successfully used T2 cartilage maps at 3T to identify surgically-induced lesions of chondronecrosis *in vivo* in a goat model.[81] Indeed, during the past 10 years, novel MRI methods have been extensively applied to shed light on the pathogenesis of JOCD/OC and to describe the evolution of JOCD lesions in children.[96, 97, 105, 161, 162, 170]

In conclusion, our results demonstrate that T2 and T1ρ relaxation time mapping methods are highly sensitive and specific to OCL lesions (characterized by chondronecrosis) and OCM lesions (characterized by chondronecrosis accompanied by delayed endochondral ossification). Future clinical implementation of these sequences may allow non-invasive identification and monitoring of early JOCD lesions and determination of risk factors that contribute to their progression in children.

3.5 Acknowledgements

We thank Paula Overn from the University of Minnesota Masonic Cancer Center Comparative Pathology Shared Resource Laboratory for assistance with the preparation of the histological sections. We also thank Drs. Essa Yacoub and Jan Zimmermann from the University of Minnesota Center for Magnetic Resonance Research for allowing us to use the 10.5T head coil hardware and Dr. Casey Johnson from the University of Minnesota Department of Veterinary Clinical Sciences for providing the T1ρ sequence.

3.6 Role of the Funding Source

Funding for this study was provided by grants from several institutes at the NIH, including the National Institute for Arthritis and Musculoskeletal and Skin Diseases (R01AR070020, T32 AR050938), National Institute of Biomedical Imaging and Bioengineering (P41 EB027061) and Office of the Director (T32 OD010993, K01 OD021293). The study sponsors had no role in the study design, collection, analysis and interpretation of data, the writing of the

manuscript, or the decision to submit the manuscript for publication. The content is solely the responsibility of the authors and does not necessarily represent the official views of the National Institutes of Health.

Chapter 4: Optimization of histologic grading schemes in spontaneous and surgically induced murine models of osteoarthritis

This work was also included in the following publication and is reproduced here with permission:

Armstrong AR, Carlson CS, Rendahl AK, Loeser RF. Optimization of histologic grading schemes in spontaneous and surgically-induced murine models of osteoarthritis. *Osteoarthritis and Cartilage.* 2021;29(4):536-546.

4.1 Introduction

Mouse models of osteoarthritis (OA) are commonly used to study the role of specific genes that can be manipulated in genetically engineered mice or for pre-clinical studies of new therapeutics. OA severity in these studies is commonly determined histologically using a variety of grading schemes.[114, 121, 171-174] However, the results of murine OA studies are often difficult or impossible to reproduce.[53, 175-177] As a result, preclinical efficacy of therapeutics for osteoarthritis often fails to translate to clinically effective treatments.[53, 175, 178] One reason for this failure of translation may be the inconsistency with which grading schemes are applied and reported in murine OA studies.

The Osteoarthritis Research Society International (OARSI) published a grading scheme for human OA in 2006 and an updated species-specific set of schemes in 2010 as a part of the OARSI histopathology initiative special

issue.[172, 173, 179] The OARSI grading schemes represent more reproducible and species-specific systems than the Mankin score or the Histologic/Histochemical Grading System (HHGS), both of which were designed for humans but were adapted to animal models.[172, 173, 180-182] However, evidence is limited regarding which scheme(s) to use for a particular study and how to apply them to various OA models in order to provide the best and most consistent determination of OA severity.

The widely used OARSI grading scheme for mice focuses on lesions involving articular cartilage and uses a scale of severity ranging from 0-6.[173] This method was developed based on a surgically-induced model of OA and was validated with a set of 10 static images of the medial tibial plateau (MTP) and the medial femoral condyle (MFC). The authors suggested scoring of the entire articular surface using up to 13-16 coronal sections per joint, harvested at 80 um intervals and stained with either safranin-O/fast-green or toluidine blue to identify loss of proteoglycans from the cartilage matrix.[173]

The articular cartilage structure (ACS) grading scheme provides a similar method of assessment of the articular cartilage, except that it uses hematoxylin and eosin (H&E) stained sections, with grades ranging from 0-12 depending on the width and depth of the lesions.[17, 121, 183] Notably, the ACS scheme was developed based on assessment of stifle joints with either naturally occurring (aged) or surgically-induced OA using the destabilized medial meniscus (DMM) model.[120, 121] A goal of the ACS scheme is to use it in conjunction with scoring of

osteophytes, synovium, and histomorphometric measures of cartilage and subchondral bone to provide a comprehensive assessment of the joint as a whole.[17] In order to limit expense and time in processing multiple sections, a representative mid-coronal section is used (identified based on specific tissue landmarks), rather than the 13 or more sections suggested for the OARSI scheme.[53] Importantly, a direct comparison of the OARSI and ACS schemes has not previously been reported.

The primary objective of the present study was to determine the ramifications of applying the ACS or OARSI grading schemes to either single mid-coronal or multiple sections to determine the outcome of a murine OA study using two models: younger mice with OA induced using DMM surgery and older mice with naturally occurring OA. The secondary objective was to compare the performance of the OARSI and ACS grading schemes in their ability to determine murine OA severity. Because the ACS scheme was developed for H&E stained sections, our third objective was to determine the relative importance of a specific stain on the ability to evaluate OA severity, evaluated by applying a modified OARSI scheme to H&E sections. In addition to ACS and OARSI scores applied to the articular cartilage, and in recognition of the fact that OA is a disease of the entire joint, other features of murine OA were also assessed, including osteophyte and synovial hyperplasia grading and histomorphometry of the cartilage and subchondral bone. A principal components analysis (PCA) was performed to assess the contribution of these semi-quantitative and quantitative

measures to the OA severity and the association of the included features with one another (OARSI and ACS grades, osteophyte and synovial grades, histomorphometry features).

4.2 Methods

Animals

This work was approved by the Institutional Animal Care and Use committee at the University of North Carolina, Chapel Hill, NC, USA. Mouse colonies were maintained in a standard specific pathogen-free facility. Animals were housed in cages holding an average of 3-5 mice per cage with access to water and food ad libitum. The cohort for this study of 40 C57BL/6J background wild-type male mice included aged controls (~18 months of age; n=15) and young (12-week-old) mice that either underwent DMM surgery (n=15) or a sham surgery (n=10) and were sacrificed 8 weeks later (20 weeks of age). Group sizes were powered to detect a significant difference between sham and DMM mice in mean mid-coronal OARSI and ACS grades, using a mean difference of 2 with an estimated standard deviation of 2 for the OARSI scheme and a mean difference of 3 with an estimated standard deviation of 2.9 for the ACS scheme (power=0.8, α=0.05, 2-sided T-test). The DMM and sham surgeries were performed on the right knee in separate groups of mice as previously described.[117, 118]

Histology

Joints were collected and prepared for histology as previously described (see Appendix - Supplementary Methods).[120] Joints were serially sectioned with collection of six representative 4-μm-thick sections at approximately 100 μm intervals throughout the joint, based on the size of the joints and the ability of six total sections taken at 80-120 μm intervals to span the extent of the joint where landmarks for orientation are evident (span of approximately 700 μm) and to include the mid-coronal region (see Appendix - Figure S1). Sections were stained with hematoxylin and eosin (H&E). One additional mid-coronal section was stained with toluidine blue.

Grading of cartilage

Historically, lesions in aging and DMM murine models of OA have been most severe at the tibial plateaus [18]. Because the mid-coronal grades in the tibial plateaus were equal to or higher than those for the femoral condyles in the majority of individuals (Appendix - Table S1), further evaluation focused on the tibial plateaus. The ACS grading scheme was applied as previously described, except that it was applied to all 6 representative coronal H&E-stained sections through each joint (Figure 4-1). A modified OARSI grading scheme, using the presence of an area composed of chondrocyte cell death (CCD) within the articular cartilage without other structural changes to determine the grade of 0.5 as a substitute for loss of toluidine blue staining, was applied to the same 6

representative coronal H&E-stained sections (Figure 4-1). The OARSI grading scheme of 0-6 was also applied as previously published[173] to a single toluidine blue stained mid-coronal section from all mice (toluidine blue section not available for one aged mouse). Grading of the MTP and LTP in each section was performed by both an inexperienced grader (trained veterinary student) and an experienced grader (AA; boarded veterinary anatomic pathologist). The interobserver variation is reported in the Supplementary Results. Toluidine-blue sections were also scored from 0-12 based on the extent of loss of staining as described.[121]

The grading methods were defined as follows: sum grade – summed scores generated from six total sections; average grade – average score generated from six sections; highest grade – highest score selected from six sections; and mid-coronal grade – single score generated from a mid-coronal section chosen based on known landmarks.[53]

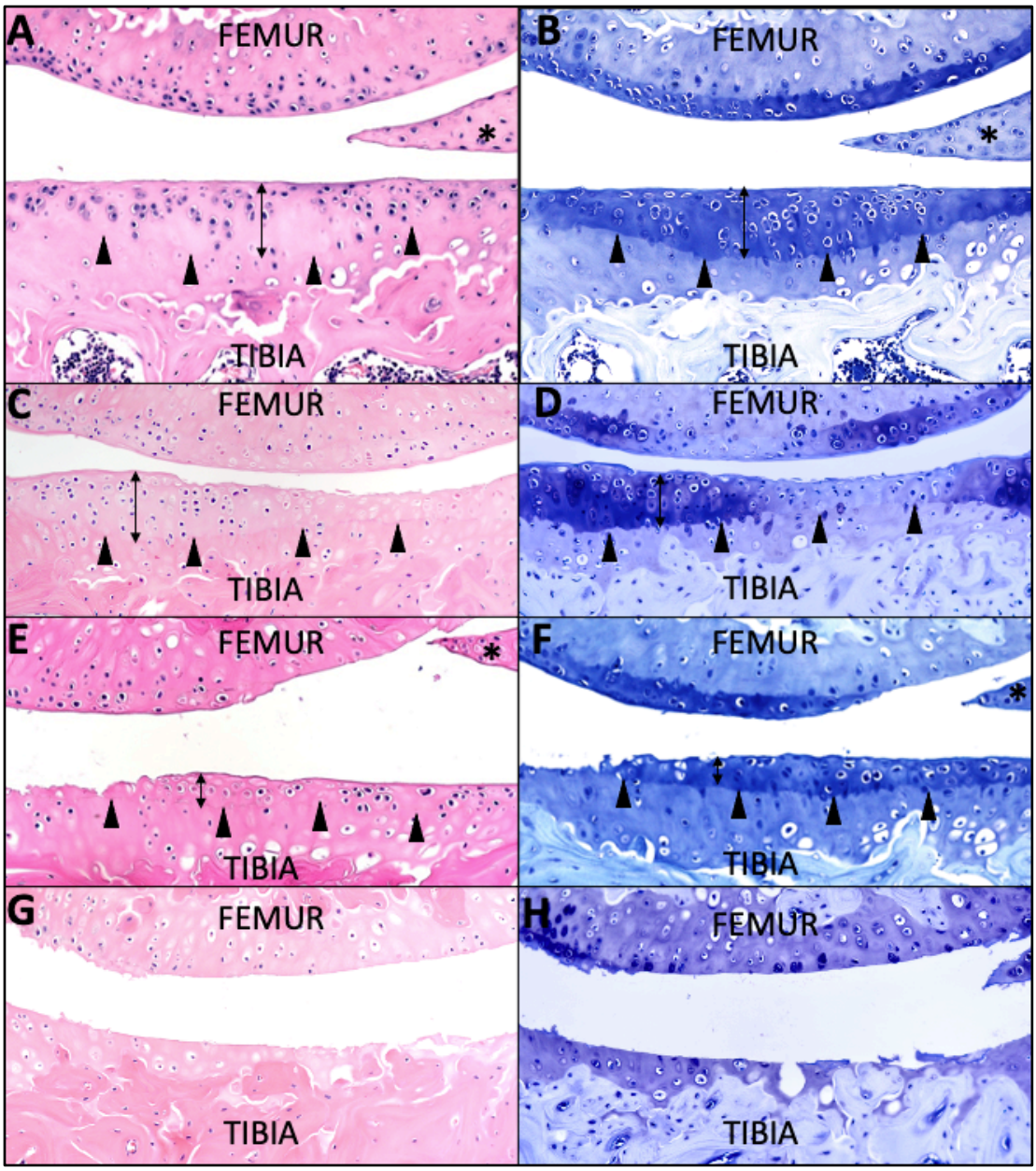

Figure 4-1. Histologic comparison of hematoxylin & eosin (H&E) staining and Toluidine blue staining of the articular cartilage with different grades of osteoarthritis. ***(A)*** *and* ***(B)*** *The medial tibial plateau of a sham mouse with intact articular cartilage and grades based on the ACS scheme and modified OARSI schemes = 0 (A; H&E) and standard OARSI scheme = 0 (B; Toluidine blue).* ***(C)*** *and* ***(D)*** *The medial tibial plateau of a DMM mouse with an ACS grade = 2 (C; H&E), modified OARSI grade = 2 (C; H&E), and standard OARSI grade = 2 (D;*

Toluidine blue). ***(E)*** *and* ***(F)*** *The medial tibial plateau of a mouse after DMM with an ACS grade = 10 (E; H&E), modified OARSI grade = 4 (E; H&E), and standard OARSI grade = 4 (F; Toluidine blue).* ***(G)*** *and* ***(H)*** *The medial tibial plateau of an aged mouse with complete loss of the articular cartilage across the full width of the plateau with an ACS grade = 12 (G; H&E), modified OARSI grade = 6 (G; H&E), and standard OARSI grade = 6 (H; Toluidine blue). Connected arrows = articular cartilage, arrowheads = tidemark, * = meniscus.*

Additional histologic and histomorphometric analysis

Abaxial osteophytes (0-3) and synovial hyperplasia (0-3) were graded as previously described (see Appendix - Supplementary Methods, Figure S2).[118, 121] The details of the histomorphometry have been previously published and are included in the Appendix - Supplementary Methods.[121]

Statistical analysis

All statistical tests were performed in R (R version 3.5.1, 2018, Boston, MA) unless noted otherwise, with figures generated in Prism (Prism version 8.3.0, La Jolla, CA). A bimodal distribution was observed in both the OARSI and ACS grades when assessed for normality visually using a QQ plot and statistically with the Shapiro-Wilk test of normality, indicating that the grades were not normally distributed, with the exception of the sum OARSI grades and the MTP+LTP mid-coronal OARSI grades (used for linear regression). Simple linear regression and determination of the Pearson (OARSI) and Spearman (ACS) correlation coefficients to determine the effect of the grading method (single mid-coronal section vs. sum of multiple sections) on the determination of OA severity were used to compare the relationship of a summed score to the mid-coronal score for all mice. Additional comparisons within each grading scheme were made by comparing the grading methods (average vs. mid-coronal, highest vs. mid-coronal) against another using a Wilcoxon matched pairs signed rank test (non-parametric test), which was also used to compare between the

OARSI (Toluidine blue) and modified OARSI (H&E) grades. The histomorphometry data were continuously and normally distributed and were compared using Students T-tests between the two OA models (DMM and naturally occurring age-related OA) and between the sham-operated and aged mice.

Details of the PCA and interobserver variation analysis are included within the Appendix - Supplementary Methods.

4.3 Results

Comparison of Grading Results Using Single Versus Multiple Histologic Sections

A key point of interest in this study was determination of the effect of evaluating multiple (six) equally spaced coronal sections compared to a single mid-coronal section. In the mice from all experimental groups (n=40), simple linear regression indicated a strong linear correlation between the sum grades from multiple sections and the individual mid-coronal grades, regardless of grading scheme used (OARSI $R^2 = 0.8413$, $p<0.0001$; ACS $R^2 = 0.8455$, $p<0.0001$) with a strong positive correlation based on Pearson correlation coefficients (OARSI r = 0.917, 95% CI: 0.848, 0.956; ACS r = 0.919, 95% CI: 0.852, 0.957; Figure 4-2). Given the lack of normality of the sum ACS grades and MTP+LTP ACS mid-coronal grades, the Spearman correlation was also calculated and was 0.917. This indicates that the mid-coronal grade from a single section per joint consistently generated a similar result for cartilage lesion severity to that determined by a sum grade from multiple sections.

The location of the most severe grade was mid-coronal or within one section of mid-coronal (within 120 um) in 77.5% of OARSI-graded MTP sections and 80% of ACS-graded MTP sections (Appendix - Table S2). For both grading schemes, the average grade of six sections (average MTP + average LTP grade) produced a lower mean grade compared to the MTP+LTP mid-coronal grade (Table 4-1, Figure 4-3). As expected, the highest MTP grade from six sections produced a significantly higher mean grade compared to a single mid-coronal grade (OARSI $p<0.0001$, ACS $p<0.0001$), given that the highest grade will always be equal to or greater than the mid-coronal grade. The grades from young sham mice were compared with those of aged animals. Both grading schemes detected a significant difference in mean OA severity, regardless of the number of sections evaluated or the method of calculating the overall grade (Table 4-1). Overall, the OARSI and ACS grading schemes performed similarly across the variety of grading methods that were applied (highest grade, average grade, mid-coronal grade), with small but statistically significant differences between the means generated from the various methods. A bimodal distribution of grades was particularly apparent in ACS grading; OARSI grades tended to group in the lower range of the 0-6 scale (Figure 4-3).

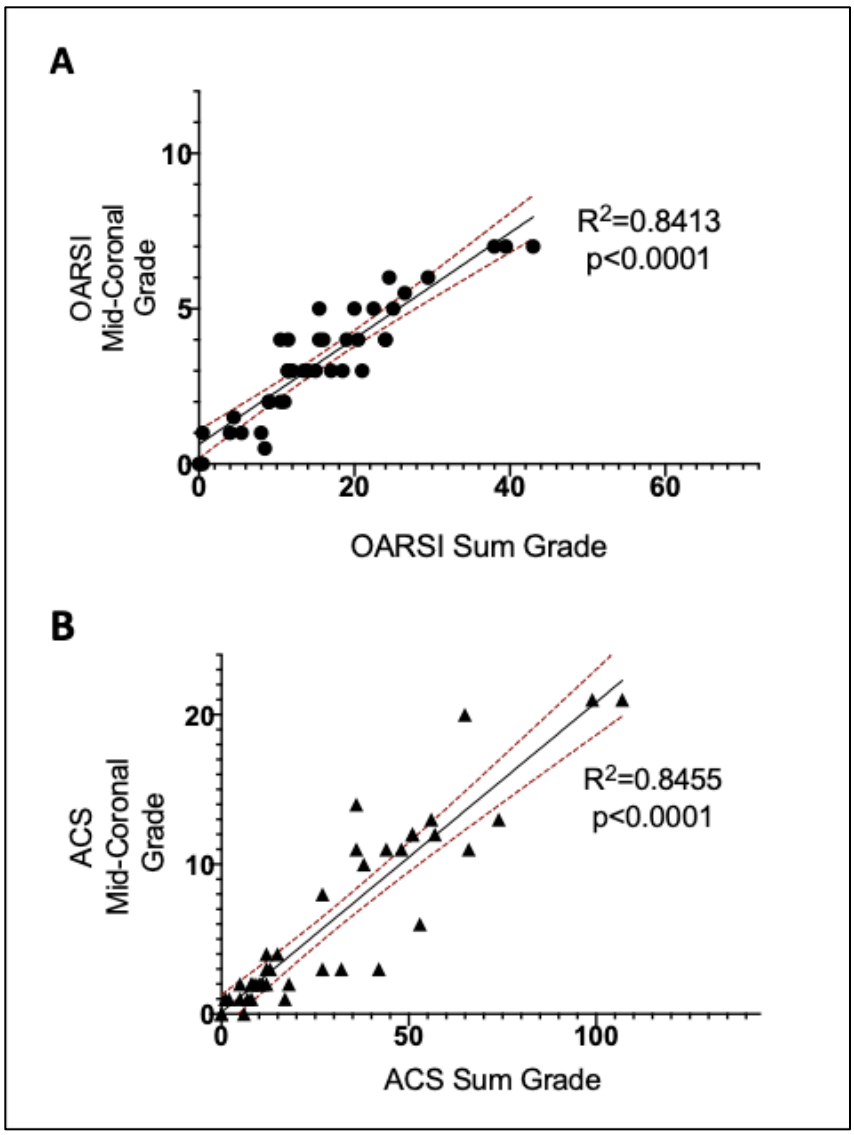

Figure 4-2. Comparison of OARSI and ACS grades from multiple sections (summed) to those from a single section. Simple linear regression showing the strong positive correlation between the summed grade (sum of MTP + LTP grades from six total coronal sections) to the mid-coronal grades from a single section (MTP+LTP) for n=40 mice (n=10 sham mice, n=15 young DMM mice, and n=15 aged mice). (A) The OARSI sum grades were strongly positively correlated to the OARSI mid-coronal grades; R^2=0.8413, linear regression, slope p <0.0001. (B) The ACS sum grades were strongly positively correlated to the

ACS mid-coronal grades; R^2=0.8455; linear regression, slope p <0.0001. Dotted lines = 95%CI.

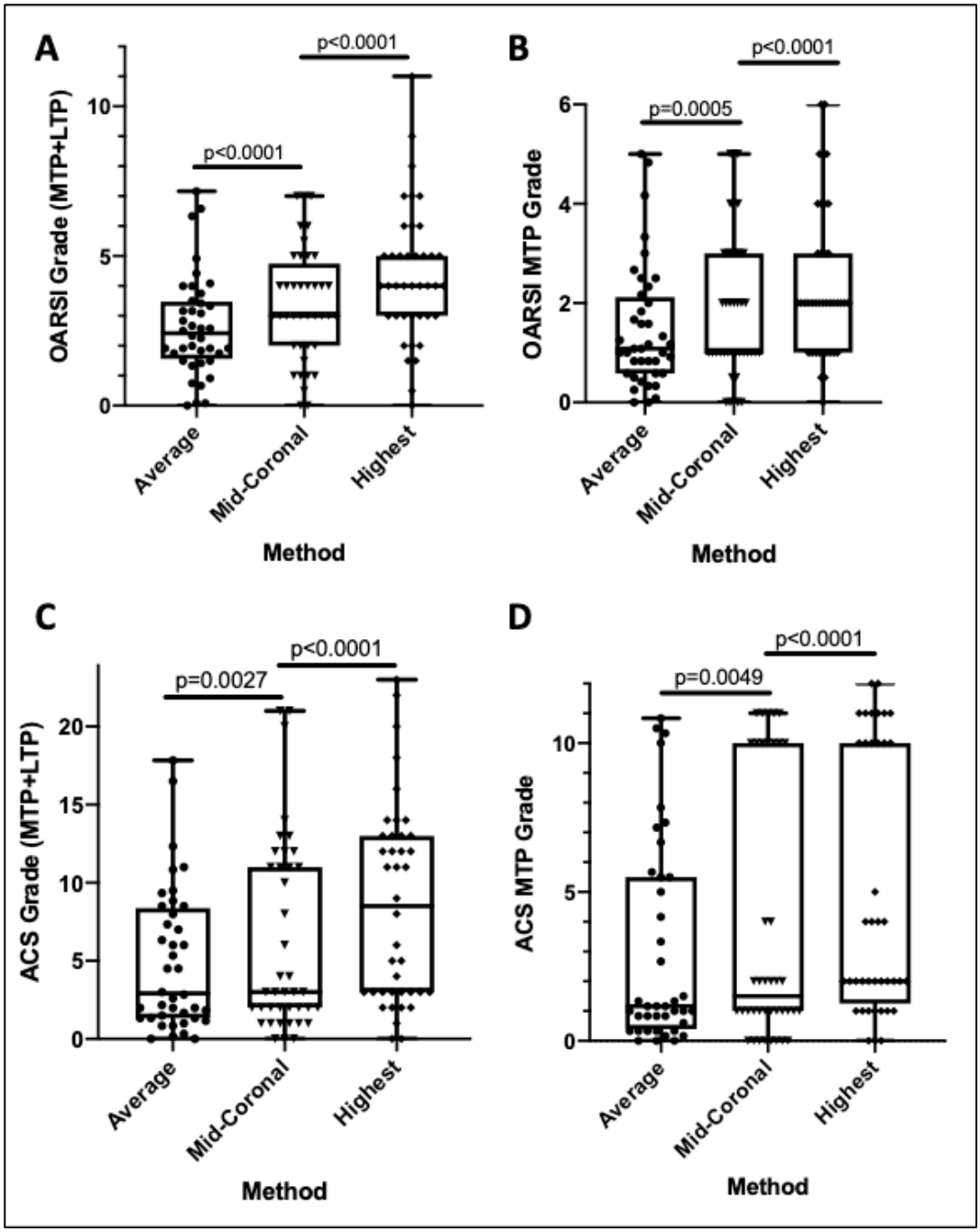

Figure 4-3. Comparison of different ways to present the results for OARSI and ACS scores. **(A)** *Comparison of the OARSI grade by method (average, mid-coronal, highest grade) for the MTP+LTP (n=40). The OARSI grades tend to cluster lower on the scale, with fewer high-scoring individuals relative to the ACS grades.* **(B)** *Comparison of the OARSI grade by method (average, mid-coronal,*

highest grade) for the MTP only (n=40). ***(C)*** *Comparison of the ACS grade by method (average, mid-coronal, highest grade) for the MTP+LTP (n=40). The frequently bimodal distribution of ACS grades is particularly evident when assessing the mid-coronal and highest grade.* ***(D)*** *Comparison of the ACS grade by method (average, mid-coronal, highest grade) for the MTP alone (n=40). The bimodal distribution of ACS grades is particularly evident when assessing the mid-coronal and highest grade within this group of 40 mice. Wilcoxon signed rank test, paired. Boxplot with whiskers = minimum, maximum values.*

Table 4-1. **Summary statistics for the ACS and OARSI grades by group.**

			p-value for difference between aged and DMM mice (Wilcoxon test)		p-value for difference between aged and sham mice (Wilcoxon test)	
Sum Grade (MTP+LTP)	**ACS±SD**	**OARSI±SD**	**ACS**	**OARSI**	**ACS**	**OARSI**
Aged mice	39.1±27.3	21.2±9.6	0.6629	0.3294	<0.0001*	<0.0001*
DMM mice	36.7±27.2	17.5±9.1				
Sham mice	5.1±3.1	6.2±4.0				
Sum Grade (MTP)						
Aged mice	16.1±20.0	9.7±8.4	0.0707	0.0439*	0.0003*	0.0001*
DMM mice	30.5±20.5	12.7±6.5				
Sham mice	2.1±2.0	2.5±1.7				
Sum Grade (LTP)						
Aged mice	22.9±16.5	11.5±4.4	<0.0001*	<0.0001*	<0.0001*	<0.0001*
DMM mice	6.3±10.9	4.7±4.6				
Sham mice	3.0±2.0	3.7±2.5				
Average Grade (MTP+LTP)						
Aged mice	6.5±4.5	3.5±1.6	0.6782	0.2671	<0.0001*	<0.0001*
DMM mice	6.1±4.5	2.8±1.5				
Sham mice	0.9±0.5	1.0±0.7				
Average Grade (MTP)						
Aged mice	2.7±3.3	1.6±1.4	0.0646	0.05358	0.0004*	0.0001*
DMM mice	5.1±3.4	2.1±1.1				
Sham mice	0.4±0.3	0.4±0.3				
Average Grade (LTP)						
Aged mice	3.8±2.8	1.9±0.7	<0.0001*	<0.0001*	<0.0001*	<0.0001*
DMM mice	1.0±1.8	0.8±0.8				
Sham mice	0.5±0.3	0.6±0.4				
Highest Grade (MTP+LTP)						
Aged mice	11.9±6.1	5.5±2.1	0.1695	0.2123	0.0001*	0.0001*
DMM mice	9.6±5.7	4.6±1.9				
Sham mice	2.2±1.0	2.2±1.3				
Highest Grade (MTP)						
Aged mice	4.9±4.1	2.6±1.7	0.203	0.178	0.0002*	0.0019*
DMM mice	7.7±4.2	3.1±1.2				
Sham mice	1.0±0.7	1.0±0.6				
Highest Grade (LTP)						
Aged mice	6.9±3.9	2.9±1.0	<0.0001*	0.0002*	0.0005*	0.0002*

DMM mice	1.9±2.7	1.5±1.1				
Sham mice	1.2±0.6	1.2±0.8				
Mid-Coronal Grade (MTP+LTP)						
Aged mice	7.8±6.5	4.2±1.5	0.7861	0.5375	<0.0001*	0.0013*
DMM mice	8.2±6.1	3.8±1.7				
Sham mice	1.1±0.7	1.5±1.5				
Mid-Coronal Grade (MTP)						
Aged mice	3.7±3.8	1.9±1.4	0.3598	0.0704	0.0001*	0.0046*
DMM mice	6.6±4.8	2.7±1.3				
Sham mice	0.3±0.5	0.6±0.8				
Mid-Coronal Grade (LTP)						
Aged mice	4.1±3.9	2.3±0.9	0.0024*	0.0006*	0.0002*	0.0003*
DMM mice	1.6±2.5	1.1±0.9				
Sham mice	0.8±0.4	0.9±0.7				

Sham n=10, DMM n=15, aged n=15. * indicates $p<0.05$. Average and sum grades were generated from 6 scored sections (MTP or LTP) or from 12 total scores (MTP+LTP).

Comparison of Hematoxylin & Eosin Staining and Toluidine Blue Staining

Both safranin O and toluidine blue stains allow quantification of proteoglycan content within articular cartilage. Although widely used, safranin O staining is prone to variability and is affected by fixation method, length of decalcification, and staining time.[184-186] Toluidine blue staining is often suggested as an alternative stain, although it can also vary in intensity based on the application methods.[187] A comparison of the standard OARSI scheme applied to toluidine blue-stained sections revealed similar results to the modified OARSI scheme using the presence of CCD on H&E to assign a 0.5 score (Figure 4-4). The modified OARSI grading scheme resulted in the same score in all mice except one, which was graded 0 with the modified OARSI scheme and 0.5 with the standard OARSI scheme.

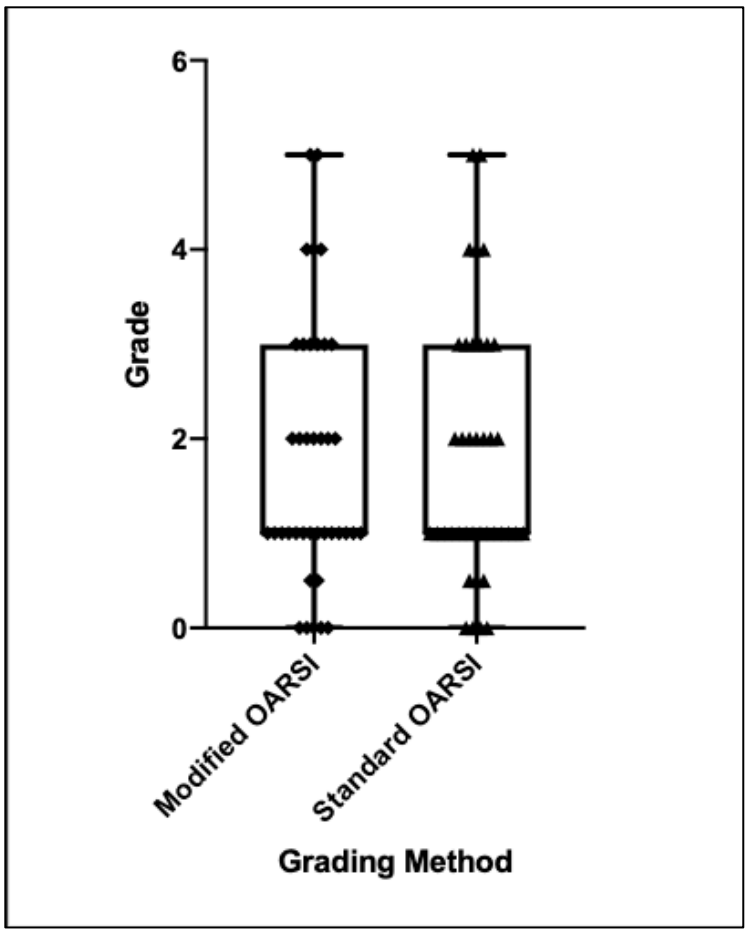

Figure 4-4. Comparison of modified OARSI grading to standard OARSI grading. *The modified OARSI scheme uses presence of articular chondrocyte cell death (CCD) on H&E as a substitute for loss of Toluidine blue staining (proteoglycan loss; n=40) to assign a grade of 0.5. Boxplot with whiskers = minimum, maximum values.*

Comparing the DMM Model and the Aging Model

The ACS and OARSI schemes identified a similar severity of MTP disease for the aged mice (18 months old) and DMM mice (evaluated 8 weeks after surgery), with the exception of a significant difference in the MTP OARSI sum score, with the DMM mice having a mean sum OARSI grade of 12.73 (95%CI = 9.165, 16.30) and the aged group having a mean sum OARSI grade of 9.67 (95%CI = 5.017, 14.32) (Mann Whitney U test, $p=0.044$; Table 4-1). Given that the DMM procedure is performed on the medial side of the joint, this model is expected to induce more severe cartilage lesions at the MTP. Both schemes detected an increased severity of LTP cartilage lesions in the aged mice as compared to the LTP lesions in DMM mice using the sum grade (OARSI and ACS $p<0.0001$; data not shown), the average grade (OARSI and ACS $p<0.0001$), the mid-coronal grade (OARSI $p=0.0006$; ACS $p=0.0024$), and the highest grade (OARSI $p=0.0002$, ACS $p=0.0006$).

Based on histomorphometry, the aged mice had significantly increased area and average thickness of subchondral bone compared with DMM mice (area $p=0.0016$; thickness $p=0.0023$; Table 4-2) but had a similar area and thickness of articular and calcified cartilage. The percentage of CCD was much higher in aged mice compared to the DMM mice (aged mean = 56.2% vs. DMM mean = 12.58%; $p<0.0001$). There was no significant difference in the MTP osteophyte or synovial hyperplasia grades (Figure 4-5; Wilcoxon signed rank test; osteophytes $p=0.1838$, synovial hyperplasia $p=0.0792$).

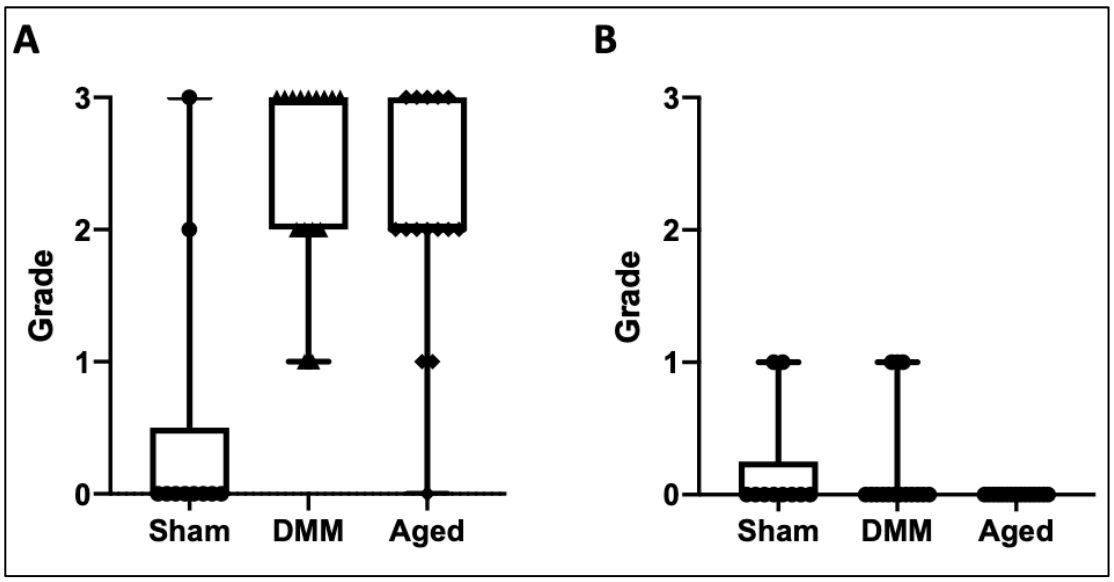

Figure 4-5. Osteophyte and synovial hyperplasia grades by group. (A) Osteophyte grades included the full range from 0 to 3 for all groups, with no significant difference between DMM and aged mice. (B) Synovial hyperplasia grades were limited to either 0 or 1 in all groups. Box plots with whiskers indicating minimum and maximum values.

Table 4-2. **Histomorphometry values by group.**

PARAMETER	*SHAM* MEAN (SD)	*DMM* MEAN (SD)	*AGED* MEAN (SD)	*SHAM* VS *DMM* P VAL	*SHAM* VS *AGED* P VAL	*DMM* VS *AGED* P VAL
Art Cart Area (μm^2)	38,880 (8,011)	29,466 (10,855)	30,030 (8,585)	**0.0215***	**0.0168***	0.876
Art Cart Thickness (μm)	48.43 (8.7)	36.93 (10.5)	40.45 (7.2)	**0.0074***	**0.0281***	0.304
Subchondral Bone Area (μm^2)	65,600 (20,892)	85,067 (21,409)	149,283 (63,334)	**0.0353***	**0.0001***	**0.0016***
Subchondral Bone Thickness (μm)	64.76 (21.7)	84.85 (23.3)	138.4 (54.5)	**0.0391***	**0.0001***	**0.0023***
Calcified cartilage area (μm^2)	51,300 (8,642)	46,200 (7,757)	42,283 (7,469)	0.1497	**0.0151***	0.169
Calcified cartilage thickness (μm)	49.87 (9.5)	46.67 (9.0)	42.11 (7.0)	0.4111	**0.0427***	0.132
% Chondrocyte cell death (area cell death/art cart area*100)	1.66 (1.5)	12.58 (6.3)	56.2 (28.4)	**<0.0001***	**<0.0001***	**<0.0001***

Articular cartilage (Art Cart), subchondral bone, and calcified cartilage measurements were collected from a mid-coronal section from the medial tibial plateau with analysis performed by Osteomeasure Histomorphometry System (OsteoMetrics®). Sham: n=10, DMM: n=15, aged: n=15. **Bold*** indicates p-values <0.05 based on a Student's T-test (unpaired).

Principal Components Analysis (PCA) of Histologic Features of Murine Osteoarthritis

PCA resulted in retention of four factors (principal components) that together accounted for 78.4% of the total variance of the data (Factor 1, 36.4%; Factor 2, 20.8%: Factor 3, 11.3%; Factor 4, 9.9%) (Table 4-3). Factor 1 was driven predominantly by measures of the articular cartilage damage, which included the OARSI grade, ACS grade, Toluidine blue grade, articular cartilage area, and articular cartilage thickness, with the osteophyte grade also contributing significantly to this factor. The second factor was largely driven by the loss of calcified cartilage area and thickness, despite these variables not playing a significant role in distinguishing between the groups (sham, DMM, aged) based on histomorphometry results alone (Table 4-2). The subchondral bone thickness also contributed significantly to variation in Factor 2, with synovial hyperplasia being inversely related to subchondral bone thickness. Variation explained by Factor 3 was largely driven by %CCD, followed by subchondral bone thickness, ACS grade, articular cartilage thickness, and OARSI grade.

***Table 4-3*. Principal components analysis.**

Factor 1: Responsible for 36.4% of variation	**Factor 2: Responsible for 20.8% of variation**	**Factor 3: Responsible for 11.3% of variation**	**Factor 4: Responsible for 9.9% of variation**
ACS grade (0.41)	**CC thickness (-0.50)**	**%CCD (0.55)**	**SCB area (0.62)**
Tblue grade (0.40)	**CC area (-0.50)**	**SCB thickness (0.38)**	**CC thickness (0.41)**
OARSI grade (0.40)	**SCB thickness (0.36)**	**ACS grade (-0.33)**	**AC area (0.34)**
Osteophytes (0.36)	**Synovial hyperplasia (-0.33)**	**AC thickness (-0.31)**	**SCB thickness (0.33)**
AC area (-0.35)	%CCD (0.28)	**OARSI grade (-0.31)**	AC thickness (0.28)
AC thickness (-0.34)	AC thickness (0.26)	AC area (-0.29)	CC area (0.25)
%CCD (0.21)	AC area (0.19)	CC area (0.25)	Osteophytes (0.23)
SCB thickness (0.18)	SCB area (0.17)	Tblue grade (-0.23)	Synovial hyperplasia (-0.09)
CC area (-0.15)	Tblue grade (-0.16)	CC thickness (0.20)	%CCD (-0.08)
SCB area (0.14)	OARSI grade (-0.09)	Osteophytes (0.07)	ACS grade (0.08)
CC thickness (-0.09)	ACS grade (-0.08)	Synovial hyperplasia (0.06)	Tblue grade (0.08)
Synovial hyperplasia (-0.09)	Osteophytes (-0.05)	SCB area (0.00)	OARSI grade (0.02)

The first four factors accounted for 78.4% of the variation within the data set (n=40). Features with a factor loading of > 0.3 or <-0.3 are highlighted in bold. Articular cartilage (AC), calcified cartilage (CC), and subchondral bone (SCB) area and average thickness. %CCD indicates chondrocyte cell death within the articular cartilage (area of articular cartilage chondrocyte cell death/total area of articular cartilage *100).

4.4. Discussion

The ACS and OARSI grading schemes showed a strong correlation between grades generated from multiple sections (sum grade) and the mid-coronal grade from a single section. This suggests that a single mid-coronal section is sufficient for producing a representative cartilage lesion severity grade across a wide range of OA severities, regardless of whether the OARSI or ACS grading scheme is used or whether the model was an aging or surgical model. This contradicts the original recommendation that the mouse OARSI scheme be applied to multiple sections per mouse.[173] Use of a single mid-coronal section reduces the time and expense of preparing and grading multiple slides, while allowing time for more detailed assessment, such as histomorphometry, to complement cartilage grading data.

While the mid-coronal section represented the most severe lesions in a majority of mice, there was variation in the location of the most severe lesions by model, with some aged mice having more severe lesions posterior to the mid-coronal point and a portion of DMM mice having more severe lesions anterior to the mid-coronal point (Appendix - Table S2). Additional caveats to focusing on the mid-coronal region are that the individual doing the sectioning should be well trained in the appropriate landmarks that allow identification of a truly mid-coronal plane of section and the model used does not have a propensity for developing lesions at a location that is not mid-coronal, as in the ACL tear model that develops posterior compartment lesions.[53, 188, 189]

Both the OARSI and the ACS scheme produced different mean grades for the overall OA severity when analyzed using the average or highest grade from multiple sections as compared to the grade from a single mid-coronal section. This indicates that the method of reporting cartilage lesions (average, mid-coronal, highest) may impact the overall severity of cartilage lesions that in some cases might explain differences in cartilage lesion severity within or between studies that use different reporting methods. The use of an average grade from multiple sections may lead to a decreased standard deviation, affecting the power calculation and potentially reducing the necessary group size. However, the use of an average grade may also reduce the overall effect size (difference between group means), reducing or eliminating any perceived advantage in using an average grade based on a power calculation. An additional point of interest is that the variation in these mean grades on the ACS and OARSI scales was small (ACS average = 3.0, mid-coronal = 3.9, highest = 5.0; OARSI average = 1.5, mid-coronal = 1.9, highest = 2.4). The biological significance of such small differences is not clear, suggesting any of these reporting measures would lead to similar conclusions about the results. Importantly, murine OA studies should be appropriately powered to detect biologically significant differences between groups (chosen by the investigator when designing the study), with experimental design fully taking into consideration the range of the chosen histologic grading scheme.[190]

The observed bimodal distribution of the ACS grades is attributed to the tendency for murine articular cartilage to form tidemark clefts, with subsequent full-thickness loss of the articular cartilage across the tibial articular surface rather than loss of articular cartilage from the surface down, leading to a higher (10-12) ACS grade in severely affected animals.[120, 121] The addition of evaluation of articular chondrocyte cell death (CCD) may provide a useful parameter that is more sensitive to early pathologic changes preceding articular cartilage loss.

The presence of focal chondrocyte cell death on H&E to give a score of 0.5 was an effective alternative for the standard 0.5 OARSI score measured by loss of Toluidine blue staining. The standard OARSI scores did not generate a significantly different mean OA severity compared to the modified OARSI grades using sham mice, young DMM mice, or aged mice. Toluidine blue or safranin O staining have commonly been utilized in murine OA studies due to their ability to detect loss of proteoglycans from the articular cartilage, thought to represent an early change in the progression of OA.[173, 186] However, staining intensity can vary significantly between individuals, between staining batches, and between laboratories, necessitating internal positive controls and careful assessment of sections to validate the success of the staining procedure.[186, 191] Decalcification can affect the proteoglycan content of tissue, and loss of proteoglycan content during processing can be significant.[176, 192, 193] H&E staining is the gold standard for evaluation of cell and tissue morphology, is widely used by laboratories performing routine histopathologic assessment, and produces highly consistent

results. An added advantage of H&E staining is the ability to evaluate viability of articular cartilage chondrocytes, allowing determination of the %CCD. Interestingly, the grading scheme outlined by Pritzker et al. incorporated chondrocyte cell death, but the OARSI scheme for murine OA studies dropped this feature.[172, 173] Given our findings, H&E is considered a reasonable and effective method for evaluation of murine OA using either the OARSI or ACS grading scheme. Toluidine blue or safranin O stains may be used to provide supplementary information, as both the OARSI and ACS publications include supplemental schemes using these techniques. This allows more detailed evaluation of the articular cartilage when a significant portion of samples lack articular cartilage structure changes (e.g., fibrillation or cartilage loss) to distinguish severity of OA using the OARSI or ACS scheme.

DMM mice and aged mice had a similar severity of OA in the MTP by the majority of the methods used, while aged mice had significantly greater severity of OA at the LTP regardless of the grading scheme (ACS or OARSI) or method of analyzing the data (sum, average, mid-coronal, highest grade). These results indicate the importance of scoring the LTP in addition to the MTP when evaluating age-related OA. While the OARSI recommendations advocate for evaluation of all four quadrants (MTP, LTP, MFC, and LFC), the femoral condylar articular cartilage is thinner and can be more difficult to evaluate than that of the tibial plateau. In our study and past work, the femoral lesions have been less severe than those of the medial tibial plateau.[120, 121] However, given the fact that

40% of the aged mice in this study had more severe LFC OA than LTP OA, with differences greater than 2 grades (ACS) and greater than 1 grade (OARSI) in 2 mice (13.3%), evaluation of the LFC in addition to the LTP may be informative in aging studies. Embedding and sectioning with the focus on alignment of the tibia to obtain optimal mid-coronal sections with maximal consistency also favors evaluation of the tibial compartment.[176] While these recommendations are based on assessment of established models (aging and DMM), new models may require a separate assessment to determine the location of greatest OA severity. While this study was limited to one time-point for the DMM model (eight weeks post-surgery), we would not expect the location of the lesions to vary at other time points.

Several additional histological features showed variation between the models, including the subchondral bone area and width (increased in aged mice) and the % CCD (increased in aged mice). Evaluation of these features in murine OA studies could be useful in capturing the effects of successful interventions and in aligning murine OA findings more closely with those of human OA phenotypes. For example, subchondral bone has been recognized as having an important role in some subsets of human OA and using a model such as the aging model that recapitulates these changes and reporting histomorphometry findings regarding these features are important.[172, 194] Other commonly used murine models, such as the ACL tear model, may have similar subtle changes in

disease measures that may be missed if histomorphometry is not included as a study endpoint.

PCA allows for the combination of semiquantitative assessments (grades) with continuous measurements (histomorphometry) into a single assessment that simplifies complex data while correlating features that behave similarly in terms of outcome (OA severity) with one another. Four factors were retained by PCA, accounting for 78% of the variance in the MTP data. Both OARSI and ACS grades grouped together in Factor 1, along with the articular cartilage area and width and Toluidine blue staining. Interestingly, calcified cartilage area and thickness were responsible for much of the variation explained by Factor 2. CCD has been reported in past murine OA studies, with limited studies suggesting apoptosis as the causative mechanism, but remains to be investigated in detail [18]. The % CCD was the primary driver of Factor 3, along with subchondral bone width, ACS grade, articular cartilage with, and the OARSI grade. The % CCD was significantly higher in aged mice compared to DMM and sham mice, differentiating these models.

Overall, this study establishes that the OARSI and ACS schemes perform similarly when applied to a murine aging or DMM model and suggests a single H&E-stained mid-coronal section is effective in determination of OA severity in these models. The results also demonstrate the utility of H&E-stained sections with evaluation of cell death as a reliable replacement for proteoglycan-based special stains such as toluidine blue in early disease. The use of

histomorphometry to supplement either grading scheme may be useful in capturing morphologic changes beyond fibrillation/loss of articular cartilage, such as changes to the subchondral bone and %CCD, that may contribute substantially to variation in severity between treatment groups or models.

4.5 Acknowledgements

We would like to acknowledge Katalin Kovacs and Paula Overn from the University of Minnesota Masonic Cancer Center Comparative Pathology Shared Resources Laboratory for their meticulous preparations of the histologic sections utilized in this study, as well as the veterinary students including Katie McDermott, Lindsey Harper, and Sery Johnson who were involved in grading and collection of histomorphometry data for this study.

4.6 Role of the funding source

This project was supported by grants from the National Institute of Arthritis, Musculoskeletal, and Skin Disease (R37-AR049003 and T32-AR050938) and the National Institute on Aging (R01-AG044034). The study sponsors had no role in the study design, collection, analysis and interpretation of data; the writing of the manuscript; or the decision to submit the manuscript for publication.

Chapter 5: Future Directions

Each of these diseases and research areas offer a wealth of opportunities for future investigations with potential for important research and clinical impacts. This section will focus on the specific areas that I find of greatest interest and highest impact, along with the greatest relevance to where I envision my future work leading.

5.1 Legg-Calvé-Perthes Disease

While LCPD is considered an uncommon to rare disease, the limited understanding of etiology, risk factors, prognostic indicators, and ideal treatment regimen support the need for ongoing preclinical research to guide clinical care. Refinement of the animal model and applications of novel molecular techniques to further understand the pathophysiology provide two avenues for advancing our work in this area.

Model Refinement

While the piglet model of LCPD utilized in this work represents a significant improvement over models in mice, rats, or rabbits, it utilizes an open approach and requires dislocation of the hip, which may cause significant local inflammation and tissue damage that does not reflect the natural disease course, in which effects are limited largely to the epiphysis. A less invasive approach, such as an intravascular administration of embolic agents to obstruct the vessels

supplying the femoral head, has the advantage of causing minimal trauma to the tissues of the hip and may also allow modulation of the extent of induced ischemia. This would represent a significant improvement over the current model, which is only able to demonstrate global femoral head ischemia. Studies of perfusion in patients with LCPD have shown that the extent of ischemic injury to the femoral epiphysis varies, with initial percent perfusion averaging 35%,[195] drawing into question the translational relevance of the current global femoral head ischemia model (initial induction of ~0% perfusion) in modeling the human disease. It is possible that the severity of the lesions described in Chapter 2 and their consistency between animals is related to either the global extent of induced femoral head ischemia or the extent of local trauma that occurs secondary to the surgical procedure.[69] A study of the lateral epiphyseal artery supply to the femoral head in LCPD found interruption in the blood supply by these vessels in 68% of hips, which suggests an intravascular model would recapitulate the pathophysiology observed in LCPD in human patients.[196] Given recent studies demonstrating a role for the ligamentum teres in revascularization of LCPD, a model that avoids transection of the ligamentum teres and associated vessels may also improve on the currently accepted porcine model.[197, 198] Histological assessment will be an important first step in validating new preclinical models of LCPD and will allow assessment of the epiphyseal structures, including the growth plate, for direct comparison to studies utilizing the ligature method of ischemia induction.

Spatial genomics

Bone and cartilage present some unique challenges for diagnostic techniques that are complementary to histological assessment, particularly immunohistochemistry, which is useful both for diagnostic purposes and for adding mechanistic information to that which can be gleaned from routine tissue sections.[199] Thorough fixation and decalcification with an appropriate agent is necessary for paraffin embedding, along with adequate processing.[200] Charged or coated slides may be necessary to achieve adequate tissue adherence, and protocols for immunohistochemistry may need to be altered to ensure that the tissue of interest is present in treated sections for evaluation. A long postmortem interval can result in loss of epitopes (targets of antibodies) used in immunohistochemistry and can be a confounding factor due to overlap in some pathways associated with both autolysis and ischemic injury, including several pathways/mechanisms of apoptosis.[199, 201] Given variation between laboratories, suppliers, and protocols, many techniques require laboratory-specific validation even in commonly utilized species. This evaluation can be time-consuming and expensive when it involves novel species without previously established protocols and validation.

Additional challenges are presented by utilization of uncommon animal species; although pigs are widely used in biomedical research, the validation of various antibodies for immunohistochemical assessment in this species is limited. Even with the wide incorporation of pigs into preclinical research over the

past several decades, laboratory technology has lagged in providing validated reagents and techniques for evaluating cells/tissues from this species.[202] A small number of publications exist documenting validation of reagents or techniques between pigs and humans, particularly for neurofibromatosis-1 modeling and certain lung disease models.[202, 203] When in situ hybridization and immunohistochemistry are available, they are typically limited to the evaluation of a small number of genes or proteins.[204] While there also are interesting and unique staining opportunities for non-decalcified bone samples, these techniques are often expensive and limited in availability and may require prolonged processing for resin-embedding and staining. Other methods of characterizing cartilage, such as RNA sequencing, also present challenges in extraction of high-quality RNA given the low cellularity of cartilage and its high proteoglycan content, along with the requirement of removing cells from their native architecture and thus disrupting their relationships with the extracellular matrix.[205-207]

New techniques may provide an opportunity to streamline these processes and generate more comprehensive sets of data. Spatial genomics represents an exciting and novel technique that may be well-suited to accelerating what we can learn from animal models of orthopedic diseases. The spatial genomics or 'spatialomics' technology builds on the methods utilized for single-cell genomics by adding spatial registration of genomic activity in the context of tissue architecture.[208] Instead of limiting assessment to a small

number of genes, the full genome, transcriptome, or proteome of cells can be assessed (currently several thousand to tens of thousands of transcripts available for assessment). From a technical standpoint, techniques may be applied to formalin-fixed paraffin-embedded tissue, which represents the majority of tissue analyzed histologically.[149] Combining these techniques with histopathology provides unique context to the molecular data through retention of tissue organization, which is often disrupted in response to pathological insults ranging from developmental abnormalities to inflammation and infection or neoplasia.

There are several platforms available, including the Visium spatial gene expression platform (https://www.10xgenomics.com/products/spatial-gene-expression) from 10xGenomics and Nanostring's GeoMx digital spatial profiler (DSP) system (https://nanostring.com/products/geomx-digital-spatial-profiler/geomx-dsp-overview/). Visium relies on a kit-based assay that uses a combination of H&E staining and RNA capture based on oligo-dT overhangs combined with RNA-sequencing of fresh-frozen samples.[209] GeoMx DSP is also kit-based and starts with tissue incubation with antibodies or RNA probes conjugated to UV-cleavable oligonucleotides, followed by scanning with the use of fluorescence markers to help define regions of interest, selection of ROIs, UV cleavage of the oligonucleotides for collection from the ROIs, and probe counting by nCounter or other next-generation sequencing techniques.[209] It can be applied to formalin-fixed paraffin-embedded sections, tissue microarrays, or fresh-frozen

samples. Importantly, several studies have found strong conservation of gene expression within the same organs across species, suggesting findings using these techniques would provide insight to human disease even if performed in tissue from animal models.[210]

These methods also have tremendous potential for adding insight to the processes occurring in developing embryos and young animals. Defining the developmental programs at work in various tissues and species can add important context to information gained from diseased samples. The application of single-cell RNA sequencing in combination with spatialomics to developing chicken hearts allowed identification of spatiotemporal interactions between cells during cardiogenesis, allowing the characterization of unique progenitor and differentiated cell types by location and in context with various regulatory factors.[211] While this technology is still in its infancy, its rapid development will likely lead to profiling of most tissues across species and to application to many disease states, quickly advancing our knowledge and providing interesting opportunities to better understand disease pathogenesis in a spatial context.[212]

Spatialomics has already led to significant advances in knowledge. Observations of similar gene expression across cell types has helped show that characterizing cells based on just a few morphologic features or surface markers is likely insufficient to fully characterize cell types and activity in the tissue or organism context.[213] The central nervous system has provided a rich opportunity for better understanding degenerative nervous system diseases. Spatialomics

demonstrated spatial dysregulation of expression of genes (*GRM3* and *USP47)* across the cerebral cortex that were not appreciated using previous techniques in patients with amyotrophic lateral sclerosis.[214] The growth cartilage is well-suited for spatialomics, given the unique morphology of chondrocytes within the different tissue zones that would preclude the need for specific markers to define the target cell populations for assessment of differential gene expression.[31, 39] Regions of interest (ROIs) can be defined, at least initially, based on morphologic characteristics. Expression could be compared between subpopulations of chondrocytes, between control and ischemic samples in the context of LCPD models, and across species to determine the mechanisms underlying the observed histological changes. In the context of LCPD, we may be able to define the response of different subtypes of chondrocytes to hypoxia and ischemic injury comprehensively within the growth cartilage, elucidating new biological pathways and treatment targets.

5.2 Osteochondrosis

Our work identifying early lesions of OC in pigs using quantitative MRI provides a foundation for both future studies of OC in the pig to further elucidate the pathogenesis of this disease and to noninvasively evaluate the efficacy of treatments. While logical next steps include applications of these techniques at lower clinical field strengths (≤7T) and to additional predilection sites to demonstrate the shared pathogenesis across articular surfaces, these

techniques are also well-suited for application to other poorly understood developmental orthopaedic diseases affecting humans and animals.

Advanced Imaging

Imaging of the cartilage continues to present unique challenges due to the variation in zonal structure and composition that changes across very small areas.[46, 49] While histology continues to be the gold standard for diagnosis of many diseases, the increasing resolution of MRI systems combined with development of new morphological and quantitative MRI methods, especially when used in combination, has the potential to provide additional detailed information about the health of the bone and cartilage noninvasively that would not otherwise be obtainable. There are several advanced quantitative MRI techniques in development or currently being applied to orthopaedic disorders that represent significant advancements over historically favored radiographs and contrast-based techniques.[49] These are particularly useful during development, given that radiographs fail to provide detailed information about cartilage and the associated vascular networks intimately involved in diseases like OC and LCPD.[50, 51] They also provide a quantitative means for evaluating structures in the joint that may be followed temporally or compared across disease states in a more objective manner than typical clinical MRI techniques that are qualitative in nature.

T2 relaxation time mapping of cartilage is used to assess degeneration or biochemical alteration to the cartilage without structural damage, producing a color-scaled map through post-processing that demonstrates regional variation within hyaline cartilage.[50] T2 mapping captures the interaction of extracellular matrix and water molecules, with relaxation times increasing with increased water mobility secondary to collagen damage.[50] T2 mapping applied to the *in vivo* monitoring of growth plates in a rabbit model of premature growth plate closure detected variation in values in the adjacent, uninjured growth plate following drilling through the growth plate, though the underlying cause of T2 variation was not determined.[215] T2* mapping is the transverse relaxation time constant that characterizes how quickly the MR signal declines in the tissue due to variability within the local static magnetic field.[161] T2* mapping is used to assess cartilage integrity and microstructure, and has been shown to increase in early OC lesions.[162, 216] T2* values have been shown to vary related to underlying disorders, with variation across stages of disease in human JOCD patients reflecting the degree of ossification of lesions.[161] Advantages of T2* include the faster rates of acquistion, which are particularly useful in pediatric patients, and the reflection of microscopic field gradients in the values that may have clinical or structural significance.[162] T1 in the rotating frame (T1ρ) is an MRI parameter that has been hypothesized to reflect the proteoglycan content within the cartilage matrix, with variation in several conditions associated with proteoglycan loss including osteoarthritis.[50, 51] T2 and T1ρ are sensitive to ischemic injury in the

described piglet model of LCPD as early as 48 hours following induction of ischemia.[76, 79] While several of these techniques are already being utilized in a research context, they have not been widely introduced in a clinical context pending sufficient preclinical research to demonstrate safety, efficacy, and clinical relevance of changes in signal *in vivo* and at clinical field strengths.

While these techniques are already being applied to the study of LCPD and OC, they provide an opportunity to shed light on other important developmental orthopaedic diseases. A particular disease of interest is developmental dysplasia of the hip. By applying a combination of advanced imaging, gross, and histological assessments to this disorder, there are opportunities to investigate the role of the acetabular vascularity in development of DDH. Many of the same imaging techniques and histological techniques would be useful in evaluating the vascularity of the hip both as a possible inciting factor in development of DDH and as a relevant biomarker of the condition that could be useful in screening infants and children noninvasively.

5.3 Osteoarthritis

Major hurdles in the translation of preclinical work to clinical impact in osteoarthritis include the widespread use of small animal models, primarily mice, with a relatively limited utilization of large animal models. The high volume of preclinical small animal studies also producing tissue for evaluation that can be time-consuming, require specialty expertise, and be expensive.[2] By incorporating

large animal models into OA studies in larger numbers, there is greater potential to translate effective interventions to human patients in a timely manner, while streamlining data collection through technological advances like artificial intelligence could increase both the thoroughness of evaluation and the consistency and efficiency of data generation.

Large Animal Models of Osteoarthritis

Large animal studies are considered expensive and time-consuming and are constrained by available research space. Researchers may be biased against these studies due to perceived differences in physiology or pathophysiology between these species and humans.[2] There is a critical need to address these biases and highlight the value and necessity of large animal research in the orthopedic research field. While genetic engineering is now available for pigs, with examples including novel pig models of Duchenne muscular dystrophy and cystic fibrosis, the complexity of OA and absence of a model of spontaneously occurring OA in pigs limits the usefulness of this advance for OA research.[217] More promising future directions include expansion of the use of canine, small ruminant, and equine models to help bridge the gap from rodent studies to clinically meaningful human advances in the treatment of disease.[2] Client-owned animals may provide a means to address this gap, given the high prevalence of naturally occurring osteoarthritis in dogs and horses.[218, 219]

Using client-owned animals for clinical studies presents some unique challenges, including a potentially high proportion of animals being lost to follow-up, the need for unbiased evaluations of the response to treatment (e.g. veterinary assessment rather than self-reported owner assessment), and the added risk of owner distress in the case of adverse events.[220] However, if the early stages of evaluation of interventions can be completed with confidence in the safety profile prior to introduction in client-owned animals, these populations can provide a large patient base and may enhance successful translatability of results to human patients. While use of client-owned animals could address a significant gap in preclinical research, concerns exist regarding the ethics of this research. Additional regulation to limit bias in these studies and ensure consistency among institutions may be necessary to ensure the scientific integrity of these studies.[220] A recent review of studies assessing the efficacy of intra-articular mesenchymal stem cell administration at the hip joint for treatment osteoarthritis in dogs demonstrated the challenges in comparing multicenter studies among institutions due to lack of standardized techniques for evaluation along with a moderate to high risk of bias based on study design.[219] These issues are complex but addressable, with a focus on rigor and reproducibility going forward.

Artificial intelligence

An ongoing challenge in preclinical research is developing consistent, easily applied, and widely accepted methods for histopathologic evaluation of lesions. While our work regarding murine models of osteoarthritis represents a small step in addressing this critical gap, much work remains to be done across systems and models to improve the consistency and validity of histopathologic evaluations. It can be hard or impossible to find pathologists with expertise in this area, and many published studies depend on researchers with other backgrounds and variable training to analyze histopathologic results.[221] One emerging area that will likely help address these issues is expansion of digital pathology (generating, managing, and interpreting pathology information from digitized glass slides) and expansion of the application of artificial intelligence (AI) to histological assessment.[222] While whole-slide imaging and the use of digital slides for diagnostic and research purposes has existed for quite some time, these technologies have recently become more efficient, less expensive, and more widely available, making expansion of the applications of AI more realistic. Several large veterinary diagnostic companies adopted fully digital workflows in 2014, while clearance by the FDA for digital pathology systems for diagnostic purposes in human specimens were not approved until 2017.[222]

Histopathologic scoring is typically a means for producing semi-quantitative data from tissue samples. Histologic scoring systems may include various features of the tissue of interest and ideally are validated through

evaluation of both the repeatability and validity of the tissue pathobiological processes and their representation in the system.[223, 224] Certain features of cartilage, bone, and joints that are amenable to quantitative analysis through histomorphometry assessment (e.g. articular cartilage area and thickness) may be amenable to semi-automated or automated assessment. Advantages to adoption of AI include gathering more quantitative data from tissues with large numbers of samples, sections, or large tissue areas, reduction in bias, and often the creation of a permanent record of results (imaging and data) that can be referred to as needed.[224] Studies of osteoarthritis utilizing histomorphometry provide an excellent opportunity to apply AI technology, allowing rapid evaluation of multiple sections per individual and detailed quantitative assessment of the varied structures that compose the joint and that may be altered in disease. However, studies applying these techniques to osteoarthritis are fairly limited, particularly when it comes to histological assessment. For example, strategies are still being developed to accurately distinguish the medial and lateral compartments of the stifle, which may differ in disease severity.[224-226] Major effort will be needed to advance the current technology to the point of utility and time and cost-savings for investigators.

Hurdles to adoption include the initial cost of equipment and the need for adequate storage space and bandwidth for the large data files produced, a method for backup of data, and access to an appropriate program for reading and analyzing slides.[222, 224] Open-source software like ImageJ (FIJI), a Java

program based on NIH Image for Macintosh, and QuPath (specific for digital tissue image analysis) have increased accessibility to appropriate tools for many applications and provide options for customizability, with many options for analysis of still photomicroscopic images.[222, 227] Several tools have been developed for assessment of the musculoskeletal system in ImageJ, including: Myosoft, which analyzes muscle fiber type and size; ZFBONE, which provides semi-automatic analysis of zebrafish bony structures; and BoneJ, which can be used to assess various skeletal features from CT and microCT images.[228, 229] While these methods can provide valuable savings in time, they often still require oversight by a trained specialist such as a pathologist to ensure that the input is high-quality and that the selected parameters are appropriate to the question at hand, to ensure consistency in analysis and interpretation.[222, 230]

5.4 Conclusion

To better understand the effects of epiphyseal ischemia on the growth plate, we used a piglet model of LCPD to characterize the histologic, histomorphometric, and immunohistochemical alterations in the 28 days following ischemia and demonstrated significant acute effects on the growth plate zones and associated disruption of endochondral ossification. We demonstrated in a piglet model of OC that quantitative MRI methods can identify the earliest lesions in development of disease *ex vivo* at predilection sites. Finally, we compared the utility of two widely accepted grading schemes for determination of murine OA

severity, finding the schemes perform comparably, that evaluation of chondrocyte cell death may complement grading in the determination of severity, and highlighting differences between the destabilization of the medial meniscus model and spontaneously developing disease. Collectively, these findings support the ongoing use and refinement of the pig as a model of LCPD and OC and provide guidance in utilizing mice to study OA. Preclinical research in orthopaedics is not a new concept, but the advent of new technologies including paradigm-shifting molecular techniques like spatialomics, novel advanced imaging methods, and advances in artificial intelligence have poised the field for rapid advancement in the coming decades and have direct applications to the continuation and expansion of this work.

Funding Acknowledgements

These studies were supported by several grants from various institutes at the NIH (study-specific information included at the end of each chapter):

National Institute of Arthritis, Musculoskeletal, and Skin Disease
- R01AR070020
- R37-AR049003
- T32-AR050938
- R56AR078315
- K01AR070894

National Institute on Aging
- R01-AG044034

National Institute of Biomedical Imaging and Bioengineering
- P41EB027061

Office of the Director
- K01OD021293
- T32OD010993

National Center for Advancing Translational Sciences
- UL1TR002494

Bibliography

References

1. Cardiff RD, Ward JM, Barthold SW. 'One medicine---one pathology': are veterinary and human pathology prepared? Lab Invest 2008; 88(1):18-26.

2. Ribitsch I, Baptista PM, Lange-Consiglio A, Melotti L, Patruno M, Jenner F, et al. Large Animal Models in Regenerative Medicine and Tissue Engineering: To Do or Not to Do. Front Bioeng Biotechnol 2020; 8972.

3. Schomberg DT, Tellez A, Meudt JJ, Brady DA, Dillon KN, Arowolo FK, et al. Miniature Swine for Preclinical Modeling of Complexities of Human Disease for Translational Scientific Discovery and Accelerated Development of Therapies and Medical Devices. Toxicol Pathol 2016; 44(3):299-314.

4. Go AS, Mozaffarian D, Roger VL, Benjamin EJ, Berry JD, Blaha MJ, et al. Heart Disease and Stroke Statistics—2014 Update. Circulation 2014; 129(3):e28-e292.

5. Percy DH, Barthold SW: Pathology of Laboratory Rodents and Rabbits. 3rd ed. Ames, Iowa: Blackwell Pub, 2007.

6. Hukkanen RR, Dybdal N, Tripathi N, Turner PV, Troth SP. Scientific and Regulatory Policy Committee Points to Consider*: The Toxicologic Pathologist's Role in the 3Rs. Toxicologic Pathology 2019; 47(7):789-98.

7. Törnqvist E, Annas A, Granath B, Jalkesten E, Cotgreave I, Öberg M. Strategic Focus on 3R Principles Reveals Major Reductions in the Use of Animals in Pharmaceutical Toxicity Testing. PLoS ONE 2014; 9(7):e101638.

8. Knoblaugh SE, Hohl TM, La Perle KMD. Pathology Principles and Practices for Analysis of Animal Models. ILAR Journal 2018; 59(1):40-50.

9. Allen MR. Preclinical Models for Skeletal Research: How Commonly Used Species Mimic (or Don't) Aspects of Human Bone. Toxicol Pathol 2017; 45(7):851-4.

10. Bahney CS, Zondervan RL, Allison P, Theologis A, Ashley JW, Ahn J, et al. Cellular biology of fracture healing. Journal of Orthopaedic Research 2019; 37(1):35-50.

11. Takarada T, Nakazato R, Tsuchikane A, Fujikawa K, Iezaki T, Yoneda Y, et al. Genetic analysis of Runx2 function during intramembranous ossification. Development 2015; 143(2):211-8.

12. Mackie EJ, Ahmed YA, Tatarczuch L, Chen KS, Mirams M. Endochondral ossification: how cartilage is converted into bone in the developing skeleton. Int J Biochem Cell Biol 2008; 40(1):46-62.

13. Blumer MJF. Bone tissue and histological and molecular events during development of the long bones. Ann Anat 2021; 235151704.

14. Yang G, Zhu L, Hou N, Lan Y, Wu X-M, Zhou B, et al. Osteogenic fate of hypertrophic chondrocytes. Cell Research 2014; 24(10):1266-9.

15. Rux D, Decker RS, Koyama E, Pacifici M: Joints in the appendicular skeleton: Developmental mechanisms and evolutionary influences. Elsevier, 2019. pp. 119-51.

16. Khan IM, Redman SN, Williams R, Dowthwaite GP, Oldfield SF, Archer CW: The Development of Synovial Joints. Elsevier, 2007. pp. 1-36.

17. Loeser RF, Goldring SR, Scanzello CR, Goldring MB. Osteoarthritis: a disease of the joint as an organ. Arthritis Rheum 2012; 64(6):1697-707.

18. Wancket LM. Animal Models for Evaluation of Bone Implants and Devices: Comparative Bone Structure and Common Model Uses. Vet Pathol 2015; 52(5):842-50.

19. Garnero P. The Role of Collagen Organization on the Properties of Bone. Calcified Tissue International 2015; 97(3):229-40.

20. McCoy AM, Tóth F, Dolvik NI, Ekman S, Ellermann J, Olstad K, et al. Articular osteochondrosis: a comparison of naturally-occurring human and animal disease. Osteoarthritis Cartilage 2013; 21(11):1638-47.

21. Bullough PG: Atlas of Orthopedic Pathology with Clinical and Radiologic Correlations. 2nd ed. New York: Gower Medical Publishing, 1992.

22. Jansson N, Ducharme NG. Angular limb deformities in foals: treatment and prognosis. Comp Cont Educ Pract 2005; 27134.

23. Reiland S. Growth and skeletal development of the pig. Acta Radiol Suppl 1978; 35815-22.

24. Blumer MJF, Longato S, Fritsch H. Structure, formation and role of cartilage canals in the developing bone. Annals of Anatomy - Anatomischer Anzeiger 2008; 190(4):305-15.

25. Blumer MJF, Longato S, Richter E, Perez MT, Konakci KZ, Fritsch H. The role of cartilage canals in endochondral and perichondral bone formation: are there similarities between these two processes? Journal of Anatomy 2005; 206(4):359-72.

26. Tóth F, Nissi MJ, Zhang J, Benson M, Schmitter S, Ellermann JM, et al. Histological confirmation and biological significance of cartilage canals demonstrated using high field MRI in swine at predilection sites of osteochondrosis. J Orthop Res 2013; 31(12):2006-12.

27. Olstad K, Ytrehus B, Ekman S, Carlson CS, Dolvik NI. Epiphyseal cartilage canal blood supply to the tarsus of foals and relationship to osteochondrosis. Equine Veterinary Journal 2008; 40(1):30-9.

28. Ytrehus B, Ekman S, Carlson CS, Teige J, Reinholt FP. Focal changes in blood supply during normal epiphyseal growth are central in the pathogenesis of osteochondrosis in pigs. Bone 2004; 35(6):1294-306.

29. Nguyen JC, Markhardt BK, Merrow AC, Dwek JR. Imaging of Pediatric Growth Plate Disturbances. Radiographics 2017; 37(6):1791-812.

30. Byers PD, Brown RA. Cell columns in articular cartilage physes questioned: a review. Osteoarthritis and Cartilage 2006; 14(1):3-12.

31. Buckwalter JA, Mower D, Schafer J, Ungar R, Ginsberg B, Moore K. Growth-plate-chondrocyte profiles and their orientation. Journal of Bone and Joint Surgery 1985; 67-A(6):942-55.

32. Ytrehus BC, C.S.; Ekman, S. Etiology and pathogenesis of osteochondrosis. Vet Pathol 2007; 44429-48.

33. Olstad K, Kongsro J, Grindflek E, Dolvik NI. Consequences of the natural course of articular osteochondrosis in pigs for the suitability of computed tomography as a screening tool. BMC Veterinary Research 2014; 10(1).

34. Bi W, Deng JM, Zhang Z, Behringer RR, De Crombrugghe B. Sox9 is required for cartilage formation. Nature Genetics 1999; 22(1):85-9.

35. Han Y, Lefebvre VR. L-Sox5 and Sox6 Drive Expression of the Aggrecan Gene in Cartilage by Securing Binding of Sox9 to a Far-Upstream Enhancer. Molecular and Cellular Biology 2008; 28(16):4999-5013.

36. Buckwalter JA, Mankin HJ, Grodzinsky AJ. Articular cartilage and osteoarthritis. AAOS Instructional Course Lectures 2005; 54465-80.

37. Kronenberg HM. Developmental regulation of the growth plate. Nature 2003; 423(6937):332-6.

38. Chagin AS, Newton PT. Postnatal skeletal growth is driven by the epiphyseal stem cell niche: potential implications to pediatrics. Pediatric Research 2020; 87(6):986-90.

39. Byers S, Moore AJ, Byard RW, Fazzalari NL. Quantitative histomorphometric analysis of the human growth plate from birth to adolescence. Bone 2000; 27(4).

40. Decker RS, Koyama E, Pacifici M. Articular Cartilage: Structural and Developmental Intricacies and Questions. Current Osteoporosis Reports 2015; 13(6):407-14.

41. Hunziker EB, Kapfinger E, Geiss J. The structural architecture of adult mammalian articular cartilage evolves by a synchronized process of tissue resorption and neoformation during postnatal development. Osteoarthritis Cartilage 2007; 15(4):403-13.

42. van Weeren PR, Jeffcott LB. Problems and pointers in osteochondrosis: Twenty years on. Vet J 2013; 197(1):96-102.

43. Shea KG, Jacobs JC, Jr., Carey JL, Anderson AF, Oxford JT. Osteochondritis dissecans knee histology studies have variable findings and theories of etiology. Clin Orthop Relat Res 2013; 471(4):1127-36.

44. Kim HK, Stephenson N, Garces A, Aya-ay J, Bian H. Effects of disruption of epiphyseal vasculature on the proximal femoral growth plate. J Bone Joint Surg Am 2009; 91(5):1149-58.

45. Kim HKW, Skelton DN, Quigley EJ. Pathogenesis of metaphyseal radiolucent changes following ischemic necrosis of the capital femoral epiphysis in immature pigs. JBJS 2004; 86-A(1):129-35.

46. Sophia Fox AJ, Bedi A, Rodeo SA. The Basic Science of Articular Cartilage: Structure, Composition, and Function. Sports Health: A Multidisciplinary Approach 2009; 1(6):461-8.

47. Jayasuriya CT, Chen Q. Potential benefits and limitations of utilizing chondroprogenitors in cell-based cartilage therapy. Connective Tissue Research 2015; 56(4):265-71.

48. Loeser RF. Aging and osteoarthritis: the role of chondrocyte senescence and aging changes in the cartilage matrix. Osteoarthritis Cartilage 2009; 17(8):971-9.

49. Li X, Majumdar S. Quantitative MRI of articular cartilage and its clinical applications. Journal of Magnetic Resonance Imaging 2013; 38(5):991-1008.

50. Chauvin NA. Pediatric Cartilage Imaging. Semin Roentgenol 2021; 56(3):266-76.

51. Barendregt AM, Mazzoli V, van den Berg JM, Kuijpers TW, Maas M, Nederveen AJ, et al. T1rho-mapping for assessing knee joint cartilage in children with juvenile idiopathic arthritis - feasibility and repeatability. Pediatr Radiol 2020; 50(3):371-9.

52. Lerisson H, Tillaux C, Boutry N. Radiographic/MR Imaging Correlation of the Pediatric Knee Growth. Magn Reson Imaging Clin N Am 2019; 27(4):737-51.

53. McCoy AM. Animal Models of Osteoarthritis: Comparisons and Key Considerations. Vet Pathol 2015; 52(5):803-18.

54. Denayer T, Stöhr T, Roy MV. Animal models in translational medicine: Validation and prediction. European Journal of Molecular & Clinical Medicine 2014; 2(1):5.

55. Kim HK. Pathophysiology and new strategies for the treatment of Legg-Calve-Perthes disease. J Bone Joint Surg Am 2012; 94(7):659-69.

56. Kim HK, Herring JA. Pathophysiology, classifications, and natural history of Perthes disease. Orthop Clin North Am 2011; 42(3):285-95, v.

57. Kim HKW. Legg-Calve-Perthes Disease: etiology, pathogenesis, and biology. J Pediatr Orthop 2011; 31S141-S6.

58. Joseph B, Varghese G, Mulpuri K, Rao N, Nair NS. Natural evolution of Perthes disease: a study of 610 children under 12 years of age at disease onset. J Pediatr Orthop 2003; 23590-600.

59. Herring JA, Kim HT, Browne R. Legg-Calve-Perthes disease. Part II: Prospective multicenter study of the effect of treatment on outcome. J Bone Joint Surg Am 2004; 862121-34.

60. Newton B, Crawford CJ, Powers DL, Allen BL, Jr. The immature goat as an animal model for Legg-Calve-Perthes disease. J Invest Surg 1994; 7(5):417-30.

61. Fan M, Peng J, Qin L, Lu S. Experimental animal models of osteonecrosis. Rheumatol Int 2011; 31(8):983-94.

62. Nishino M, Matsumoto T, Nakamura T, Tomita K. Pathological and hemodynamic study in a new model of femoral head necrosis following traumatic dislocation. Archives of Orthopaedic and Trauma Surgery 1997; 116(5):259-62.

63. Levin D, Norman D, Zinman C, Rubinstein L, Sabo E, Misselevich I, et al. Treatment of experimental avascular necrosis of the femoral head with hyperbaric oxygen in rats: histological evaluation of the femoral heads during the early phase of the reparative process. Experimental and Molecular Pathology 1999(67):99-108.

64. Hwang Y, Park J, Choi SH, Kim G. Traumatic and Non-traumatic Osteonecrosis in the Femoral Head of a Rabbit Model. Lab Anim Res 2011; 27(2):127-31.

65. Motomura G, Yamamoto T, Irisa T, Miyanishi K, Nishida K, Iwamoto Y. Dose effects of corticosteroids on the development of osteonecrosis in rabbits. J Rheumatol 2008; 35(12):2395-9.

66. Iwakiri K, Oda Y, Kaneshiro Y, Iwaki H, Masada T, Kobayashi A, et al. Effect of simvastatin on steroid-induced osteonecrosis evidenced by the serum lipid level and hepatic cytochrome P4503A in a rabbit model. Journal of Orthopaedic Science 2008; 13(5):463-8.

67. Janke LJ, Liu C, Vogel P, Kawedia J, Boyd KL, Funk AJ, et al. Primary epiphyseal arteriopathy in a mouse model of steroid-induced osteonecrosis. Am J Pathol 2013; 183(1):19-25.

68. D'Andrea CR, Alfraihat A, Singh A, Anari JB, Cahill PJ, Schaer T, et al. Part 2. Review and meta-analysis of studies on modulation of longitudinal bone growth and growth plate activity: A micro-scale perspective. J Orthop Res 2021; 39(5):919-28.

69. Kim HKW, Su P-H, Qiu Y-S. Histopathologic changes in growth-plate cartilage following ischemic necrosis of the capital femoral epiphysis. JBJS 2001; 83-A(5):688-97.

70. Kim HKW, Su P-H. Development of flattening and apparent fragmentation following ischemic necrosis of the capital femoral epiphysis in a piglet model. Journal of Bone and Joint Surgery 2002; 84-A(8):1329-33.

71. Kim HK, Bian H, Aya-ay J, Garces A, Morgan EF, Gilbert SR. Hypoxia and HIF-1alpha expression in the epiphyseal cartilage following ischemic injury to the immature femoral head. Bone 2009; 45(2):280-8.

72. Kim HK, Aruwajoye O, Stetler J, Stall A. Effects of non-weight-bearing on the immature femoral head following ischemic osteonecrosis: an experimental investigation in immature pigs. J Bone Joint Surg Am 2012; 94(24):2228-37.

73. Kim HK, Aruwajoye O, Du J, Kamiya N. Local administration of bone morphogenetic protein-2 and bisphosphonate during non-weight-bearing treatment of ischemic osteonecrosis of the femoral head: an experimental investigation in immature pigs. J Bone Joint Surg Am 2014; 96(18):1515-24.

74. Aruwajoye OO, Monte F, Kim A, Kim HKW. A Comparison of Transphyseal Neck-Head Tunneling and Multiple Epiphyseal Drilling on Femoral Head Healing Following Ischemic Osteonecrosis: An Experimental Investigation in Immature Pigs. J Pediatr Orthop 2020; 40(4):168-75.

75. Adapala NS, Yamaguchi R, Phipps M, Aruwajoye O, Kim HKW. Necrotic Bone Stimulates Proinflammatory Responses in Macrophages through the Activation of Toll-Like Receptor 4. The American Journal of Pathology 2016; 186(11):2987-99.

76. Johnson CP, Tóth F, Carlson CS, Armstrong AR, Zbyn S, Wu B, et al. T1ρ and T2 Mapping Detect Acute Ischemic Injury in a Piglet Model of Legg-Calve-Perthes Disease. J Orthop Res 2022; 40(2):484-94.
77. Kim HKW, Park MS, Alves do Monte F, Gokani V, Aruwajoye OO, Ren Y. Minimally Invasive Necrotic Bone Washing Improves Bone Healing After Femoral Head Ischemic Osteonecrosis: An Experimental Investigation in Immature Pigs. J Bone Joint Surg Am 2021.
78. Johnson CP, Wang L, Tóth F, Aruwajoye O, Kirkham B, Carlson CS, et al. Quantitative susceptibility mapping detects neovascularization of the epiphyseal cartilage after ischemic injury in a piglet model of legg-calvé-perthes disease. Journal of Magnetic Resonance Imaging 2019; 50(1):106-13.
79. Johnson CP, Wang L, Tóth F, Aruwajoye O, Carlson CS, Kim HKW, et al. Quantitative MRI Helps to Detect Hip Ischemia: Preclinical Model of Legg-Calve-Perthes Disease. Radiology 2018; 289(2):386-95.
80. Tóth F, Nissi MJ, Wang L, Ellermann JM, Carlson CS. Surgical induction, histological evaluation, and MRI identification of cartilage necrosis in the distal femur in goats to model early lesions of osteochondrosis. Osteoarthritis Cartilage 2015; 23(2):300-7.
81. Tóth F, David FH, LaFond E, Wang L, Ellermann JM, Carlson CS. In vivo visualization using MRI T2 mapping of induced osteochondrosis and osteochondritis dissecans lesions in goats undergoing controlled exercise. J Orthop Res 2017; 35(4):868-75.

82. Tóth F, Johnson CP, Mills B, Nissi MJ, Nykanen O, Ellermann J, et al. Evaluation of the Suitability of Miniature Pigs as an Animal Model of Juvenile Osteochondritis Dissecans. J Orthop Res 2019; 37(10):2130-7.

83. Olstad K, Hendrickson EH, Carlson CS, Ekman S, Dolvik NI. Transection of vessels in epiphyseal cartilage canals leads to osteochondrosis and osteochondrosis dissecans in the femoro-patellar joint of foals; a potential model of juvenile osteochondritis dissecans. Osteoarthritis Cartilage 2013; 21(5):730-8.

84. Ekman S, Carlson CS. The Pathophysiology of Osteochondrosis. Veterinary Clinics of North America: Small Animal Practice 1998; 28(1):17-32.

85. Olstad K, Shea KG, Cannamela PC, Polousky JD, Ekman S, Ytrehus B, et al. Juvenile osteochondritis dissecans of the knee is a result of failure of the blood supply to growth cartilage and osteochondrosis. Osteoarthritis Cartilage 2018; 26(12):1691-8.

86. Bruns J, Werner M, Habermann C. Osteochondritis dissecans: etiology, pathology, and imaging with a special focus on the knee joint. Cartilage 2018; 9(4):346-62.

87. Tóth F, Tompkins MA, Shea KG, Ellermann JM, Carlson CS. Identification of Areas of Epiphyseal Cartilage Necrosis at Predilection Sites of Juvenile Osteochondritis Dissecans in Pediatric Cadavers. J Bone Joint Surg Am 2018; 100(24):2132-9.

88. Laverty S, Girard C. Pathogenesis of epiphyseal osteochondrosis. Vet J 2013; 197(1):3-12.

89. Olstad K, Ytrehus B, Ekman S, Carlson CS, Dolvik NI. Early lesions of osteochondrosis in the distal tibia of foals. J Orthop Res 2007; 25(8):1094-105.
90. Olstad K, Kongsro J, Grindflek E, Dolvik NI. Ossification defects detected in CT scans represent early osteochondrosis in the distal femur of piglets. J Orthop Res 2014; 32(8):1014-23.
91. Etterlin PE, Morrison DA, Österberg J, Ytrehus B, Heldmer E, Ekman S. Osteochondrosis, but not lameness, is more frequent among free-range pigs than confined herd-mates. Acta Veterinaria Scandinavica 2015; 57(1).
92. Bertholle CP, Meijer E, Back W, Stegeman A, Van Weeren PR, Van Nes A. A longitudinal study on the performance of in vivo methods to determine the osteochondrotic status of young pigs. BMC Veterinary Research 2016; 12(1).
93. Ytrehus BH, H.A.; Mellum, C.N.; Mathisen, L.; Carlson, C.S.; Ekman, S.; Teige, J.; Reinholt, F.P. Experimental ischemia of porcine growth cartilage produces lesiosn of osteochondrosis. J Orthop Res 2004; 221201-9.
94. Carlson CSC, L.D.; Meuten, D.J. Osteochondrosis of the articular-epiphyseal cartilage complex in young horses: evidence for a defect in cartilage canal blood supply. Vet Pathol 1995; 32641-7.
95. Takahara M, Maruyama M, Uno T, Harada M, Satake H, Takahara D, et al. Progression of Epiphyseal Cartilage and Bone Pathology in Surgically Treated Cases of Osteochondritis Dissecans of the Elbow. Am J Sports Med 2021; 49(1):162-71.

96. Ellermann J, Johnson CP, Wang L, Macalena JA, Nelson BJ, Laprade RF. Insights into the Epiphyseal Cartilage Origin and Subsequent Osseous Manifestation of Juvenile Osteochondritis Dissecans with a Modified Clinical MR Imaging Protocol: A Pilot Study. Radiology 2017; 282(3):798-806.

97. Tóth F, Nissi MJ, Ellermann JM, Wang L, Shea KG, Polousky J, et al. Novel Application of Magnetic Resonance Imaging Demonstrates Characteristic Differences in Vasculature at Predilection Sites of Osteochondritis Dissecans. Am J Sports Med 2015; 43(10):2522-7.

98. Štembírek J, Kyllar M, Putnová I, Stehlík L, Buchtová M. The pig as an experimental model for clinical craniofacial research. Laboratory Animals 2012; 46(4):269-79.

99. Mosekilde L, Weisbrode SE, Safron JA, Stills HF, Jankowsky ML, Ebert DC, et al. Calcium-restricted ovariectomized sinclair S-1 minipigs: an animal model of osteopenia and trabecular plate perforation. Bone 1993; 14379-82.

100. Laiblin C, Jaeschke G. Clinical chemistry examinations of bone and muscle metabolism under stress in the Gottingen miniature pig - an experimental study. Berl Munch Tierarztl Wochenschr 1979; 92(6):124-8.

101. Tóth FT, J.L.; Harper, L.; Bussieres, D.; Wilson, M.E.; Crenshaw, T.D.; Carlson, C.S. Osteochondrosis prevalence and severity at 12 and 24 weeks of age in commerical pigs with and without organic-complexed trace mineral supplementation. Journal of Animal Science 2016; 943817-25.

102. van Grevenhof EM, Schurink A, Ducro BJ, van Weeren PR, van Tartwijk JM, Bijma P, et al. Genetic variables of various manifestations of osteochondrosis and their correlations between and within joints in Dutch warmblood horses. J Anim Sci 2009; 87(6):1906-12.

103. Grondahl AM, Dolvik NI. Heritability estimations of osteochondrosis in the tibiotarsal joint and of bony fragments in the palmar/plantar portion of the metacarpo- and metatarsophalangeal joints of horses. J Am Vet Med Assoc 1993; 203101-4.

104. Nissi MJ, Tóth F, Zhang J, Schmitter S, Benson M, Carlson CS, et al. Susceptibility weighted imaging of cartilage canals in porcine epiphyseal growth cartilage ex vivo and in vivo. Magn Reson Med 2014; 71(6):2197-205.

105. Nissi MJ, Tóth F, Wang L, Carlson CS, Ellermann JM. Improved Visualization of Cartilage Canals Using Quantitative Susceptibility Mapping. PLoS One 2015; 10(7):e0132167.

106. Blagojevic M, Jinks C, Jeffery A, Jordan KP. Risk factors for onset of osteoarthritis of the knee in older adults: a systematic review and meta-analysis. Osteoarthritis and Cartilage 2010; 18(1):24-33.

107. Zaki S, Blaker CL, Little CB. OA foundations - experimental models of osteoarthritis. Osteoarthritis Cartilage 2022; 30357-80.

108. Driban JB, Sitler MR, Barbe MF, Balasubramanian E. Is osteoarthritis a heterogeneous disease that can be stratified into subsets? Clinical Rheumatology 2010; 29(2):123-31.

109. Jimenez PA, Glasson SS, Trubetskoy OV, Haimes HB. Spontaneous osteoarthritis in Dunkin Hartley guinea pigs: histologic, radiologic, and biochemical changes. Lab Anim Sci 1997; 47(6):598-601.

110. Bendele A, McComb J, Gould T, McAbee T, Sennello G, Chlipala E, et al. Animal models of arthritis: relevance to human disease. Toxicol Pathol 1999; 27(1):134-42.

111. Shimada M, Mizokami N, Ichinohe T, Kanno N, Suzuki S, Yogo T, et al. Long-term outcome and progression of osteoarthritis in uncomplicated cases of cranial cruciate ligament rupture treated by tibial plateau leveling osteotomy in dogs. Journal of Veterinary Medical Science 2020; 82(7):908-16.

112. Kimmel DB, Jee WSS. A quantitative histologic study of bone turnover in young adult beagles. The Anatomical Record 1982; 203(1):31-45.

113. Recker RR, Kimmel DB, Dempster D, Weinstein RS, Wronski TJ, Burr DB. Issues in modern bone histomorphometry. Bone 2011; 49(5):955-64.

114. Glasson SS, Blanchet TJ, Morris EA. The surgical destabilization of the medial meniscus (DMM) model of osteoarthritis in the 129/SvEv mouse. Osteoarthritis Cartilage 2007; 15(9):1061-9.

115. Deveza LAN, A.E.; Loeser, R.F. Phenotypes of osteoarthritis - current state and future implications. Clin Exp Rheumatol 2019; 3764-72.

116. Blaker CL, Clarke EC, Little CB. Using mouse models to investigate the pathophysiology, treatment, and prevention of post-traumatic osteoarthritis. Journal of Orthopaedic Research 2017; 35(3):424-39.

117. Loeser RF, Olex AL, McNulty MA, Carlson CS, Callahan MF, Ferguson CM, et al. Microarray analysis reveals age-related differences in gene expression during the development of osteoarthritis in mice. Arthritis Rheum 2012; 64(3):705-17.

118. Rowe MA, Harper LR, McNulty MA, Lau AG, Carlson CS, Leng L, et al. Reduced Osteoarthritis Severity in Aged Mice With Deletion of Macrophage Migration Inhibitory Factor. Arthritis Rheumatol 2017; 69(2):352-61.

119. Loeser RF, Olex AL, McNulty MA, Carlson CS, Callahan M, Ferguson C, et al. Disease progression and phasic changes in gene expression in a mouse model of osteoarthritis. PLoS One 2013; 8(1):e54633.

120. McNulty MA, Loeser RF, Davey C, Callahan MF, Ferguson CM, Carlson CS. Histopathology of naturally occurring and surgically induced osteoarthritis in mice. Osteoarthritis Cartilage 2012; 20(8):949-56.

121. McNulty MA, Loeser RF, Davey C, Callahan MF, Ferguson CM, Carlson CS. A Comprehensive Histological Assessment of Osteoarthritis Lesions in Mice. Cartilage 2011; 2(4):354-63.

122. Mason RM, Chambers MG, Flannelly J, Gaffen JD, Dudhia J, Bayliss MT. The STR/ort mouse and its use as a model of osteoarthritis. Osteoarthritis Cartilage 2001; 9(2):85-91.

123. van der Kraan PM, Stoop R, Meijers TH, Poole AR, van den Berg WB. Expression of type X collagen in young and old C57Bl/6 and Balb/c mice.

Relation with articular cartilage degeneration. Osteoarthritis Cartilage 2001; 9(2):92-100.

124. Staines KA, Poulet B, Wentworth DN, Pitsillides AA. The STR/ort mouse model of spontaneous osteoarthritis - an update. Osteoarthritis Cartilage 2017; 25(6):802-8.

125. Zucker EJ, Lee EY, Restrepo R, Eisenberg RL. Hip disorders in children. AJR Am J Roentgenol 2013; 201(6):W776-96.

126. Leroux J, Abu Amara S, Lechevallier J. Legg-Calvé-Perthes disease. Orthopaedics & Traumatology: Surgery & Research 2018; 104(1):S107-S12.

127. Catterall AP, J.; Byers, P.D.; Fulford, G.E. A review of the morphology of Perthes Disease. Journal of Bone and Joint Surgery 1982; 64-B(3):269-76.

128. Kitakoji T, Hattori T, Kitoh H, Katoh M, Ishiguro N. Which is a better method for Perthes' disease: femoral varus or Salter osteotomy? Clin Orthop Relat Res 2005(430):163-70.

129. Wiig O, Terjesen T, Svenningsen S. Prognostic factors and outcome of treatment in Perthes' disease: a prospective study of 368 patients with five-year follow-up. J Bone Joint Surg Br 2008; 90(10):1364-71.

130. Sponsellar PD, Desai SS, Millis MB. Abnormalities of proximal femoral growth after severe Perthes disease. Journal of Bone and Joint Surgery Br 1989; 71-B610-4.

131. Bowen JR, Schreiber FC, Foster BK, Wein BK. Premature femoral neck physeal closure in Perthes' Disease. Clin Orthop Relat Res 1982(171):24-9.

132. Ponseti IVM, J.A.; Weinstein, S.L.; Ippolito, E.G.; Pous, J.G. Legg-Calve-Perthes Disease: histochemical and ultrastructural observations of the epiphyseal cartilage and physis. Journal of Bone and Joint Surgery 1983; 65-A(6):797-808.

133. Smith SR, Ions GK, Gregg PJ. The radiological features of the metaphysis in Perthes disease. J Pediatr Orthop 1982; 2401-4.

134. Gracia G, Baunin C, Vial J, Accadbled F, Sales De Gauzy J. Diffusion-weighted MRI for outcome prediction in early Legg-Calvé-Perthes disease: Medium-term radiographic correlations. Orthopaedics & Traumatology: Surgery & Research 2019; 105(3):547-50.

135. Yoo WJ, Choi IH, Cho T-J, Jang W, Chung CY, Park MS, et al. Risk factors for femoral head deformity in the early stage of Legg-Calve-Perthes disease: MR contrast enhancement and diffusion indexes. Radiology 2016; 279(2):562-70.

136. De Rosa V, Laurent M, Canavese F, Merlini L. A simple, precocious, and reliable way to assess future clinical outcome in children with Perthes disease and mild femoral head involvement: correlation between MRI with diffusion-weighted and dynamic gadolinium-enhanced subtraction and Catterall and Herr. European Journal of Orthopaedic Surgery & Traumatology 2018; 28(7):1283-90.

137. Kim HKW, Su P-H, Qiu Y-S. Histopathologic changes in growth-plate cartilage following ischemic necrosis of the capital femoral epiphysis. Journal of Bone and Joint Surgery 2001; 83-A(5):688-98.

138. Armstrong AR, Bhave S, Buko EO, Chase KL, Tóth F, Carlson CS, et al. Quantitative T2 and T1ρ mapping are sensitive to ischemic injury to the epiphyseal cartilage in an in vivo piglet model of Legg-Calvé-Perthes disease. Osteoarthritis and Cartilage 2022.

139. Schneider CA, Rasband WS, Eliceiri KW. NIH Image to ImageJ: 25 years of image analysis. Nat Methods 2012; 9(7):671-5.

140. Beier F, Ali Z, Mok D, Taylor AC, Leask T, Albanese C, et al. TGFβ and PTHrP Control Chondrocyte Proliferation by Activating Cyclin D1 Expression. Molecular Biology of the Cell 2001; 12(12):3852-63.

141. Mak KK, Kronenberg HM, Chuang P-T, Mackem S, Yang Y. Indian hedgehog signals independently of PTHrP to promote chondrocyte hypertrophy. Development 2008; 135(11):1947-56.

142. Hunziker EB. Mechanism of longitudinal bone growth and its regulation by growth plate chondrocytes. Microscopy Research and Technique 1994; 28(6):505-19.

143. Beier F. Cell-cycle control and the cartilage growth plate. Journal of Cellular Physiology 2005; 202(1):1-8.

144. Young MH. Epiphysial infarction in a growing long bone. Journal of Bone and Joint Surgery Br 1966; 48-B(4):826-40.

145. Hajdu S, Schwendenwein E, Kaltenecker G, László I, Lang S, Vécsei V, et al. Growth potential of different zones of the growth plate-an experimental study in rabbits. Journal of Orthopaedic Research 2012; 30(1):162-8.

146. Rosado E, Schwartz Z, Sylvia VL, Dean DD, Boyan BD. Transforming growth factor-β1 regulation of growth zone chondrocytes is mediated by multiple interacting pathways. Biochimica et Biophysica Acta (BBA) - Molecular Cell Research 2002; 1590(1-3):1-15.

147. Wang W, Song B, Anbarchian T, Shirazyan A, Sadik JE, Lyons KM. Smad2 and Smad3 Regulate Chondrocyte Proliferation and Differentiation in the Growth Plate. PLOS Genetics 2016; 12(10):e1006352.

148. Brouwers JE, van Donkelaar CC, Sengers BG, Huiskes R. Can the growth factors PTHrP, Ihh and VEGF, together regulate the development of a long bone? J Biomech 2006; 39(15):2774-82.

149. Dries R, Chen J, Del Rossi N, Khan MM, Sistig A, Yuan G-C. Advances in spatial transcriptomic data analysis. Genome Research 2021; 31(10):1706-18.

150. Olstad K, Ytrehus B, Ekman S, Carlson CS, Dolvik NI. Early lesions of articular osteochondrosis in the distal femur of foals. Vet Pathol 2011; 48(6):1165-75.

151. Ytrehus B, Carlson CS, Lundeheim N, Mathisen L, Reinholt FP, Teige J, et al. Vascularisation and osteochondrosis of the epiphyseal growth cartilage of the distal femur in pigs—development with age, growth rate, weight and joint shape. Bone 2004; 34(3):454-65.

152. Carlson CSM, D.J.; Richardson, D.C. Ischemic necrosis of cartilage in spontaneous and experimental lesions of osteochondrosis. J Orthop Res 1991; 9317-29.

153. Wang L, Nissi MJ, Tóth F, Shaver J, Johnson CP, Zhang J, et al. Multiparametric MRI of Epiphyseal Cartilage Necrosis (Osteochondrosis) with Histological Validation in a Goat Model. PLoS One 2015; 10(10):e0140400.

154. Olstad K, Ekman S, Carlson CS. An Update on the Pathogenesis of Osteochondrosis. Vet Pathol 2015; 52(5):785-802.

155. Ertürk MA, Wu X, Eryaman Y, Moortele PF, Auerbach EJ, Lagore RL, et al. Toward imaging the body at 10.5 tesla. Magnetic Resonance in Medicine 2017; 77(1):434-43.

156. Lagore RL, Moeller S, Zimmermann J, Delabarre L, Radder J, Grant A, et al. An 8-dipole transceive and 24-loop receive array for non-human primate head imaging at 10.5 T. NMR in Biomedicine 2021.

157. Yacoub E, Grier MD, Auerbach EJ, Lagore RL, Harel N, Adriany G, et al. Ultra-high field (10.5 T) resting state fMRI in the macaque. NeuroImage 2020; 223117349.

158. Ytrehus B, Grindflek E, Teige J, Stubsjoen E, Grondalen T, Carlson CS, et al. The Effect of Parentage on the Prevalence, Severity and Location of Lesions of Osteochondrosis in Swine. Journal of Veterinary Medicine Series A 2004; 51(4):188-95.

159. Nissen CW, Albright JC, Anderson CN, Busch MT, Carlson C, Carsen S, et al. Descriptive Epidemiology From the Research in Osteochondritis Dissecans of the Knee (ROCK) Prospective Cohort. Am J Sports Med 20213635465211057103.

160. Yonetani Y, Nakamura N, Natsuume T, Shiozaki Y, Tanaka Y, Horibe S. Histological evaluation of juvenile osteochondritis dissecans of the knee: a case series. Knee Surg Sports Traumatol Arthrosc 2010; 18(6):723-30.
161. Zbýň Š, Santiago C, Johnson CP, Ludwig KD, Zhang L, Marette S, et al. Compositional evaluation of lesion and parent bone in patients with juvenile osteochondritis dissecans of the knee using T 2 * mapping. Journal of Orthopaedic Research 2021.
162. Ludwig KD, Johnson CP, Zbýň Š, Nowacki A, Marette S, Takahashi T, et al. MRI evaluation of articular cartilage in patients with juvenile osteochondritis dissecans (JOCD) using T2∗ mapping at 3T. Osteoarthritis and Cartilage 2020; 28(9):1235-44.
163. Ho-Fung VM, Jaramillo D. Cartilage imaging in children: current indications, magnetic resonance imaging techniques, and imaging findings. Radiol Clin North Am 2013; 51(4):689-702.
164. Keenan KE, Besier TF, Pauly JM, Han E, Rosenberg J, Smith RL, et al. Prediction of glycosaminoglycan content in human cartilage by age, T1ρ and T2 MRI. Osteoarthritis and Cartilage 2011; 19(2):171-9.
165. Nguyen JC, Allen H, Liu F, Woo KM, Zhou Z, Kijowski R. Maturation-Related Changes in T2 Relaxation Times of Cartilage and Meniscus of the Pediatric Knee Joint at 3 T. American Journal of Roentgenology 2018; 211(6):1369-75.

166. Moriya S, Miki Y, Yokobayashi T, Ishikawa M. Three-dimensional double-echo steady-state (3D-DESS) magnetic resonance imaging of the knee: contrast optimization by adjusting flip angle. Acta Radiol 2009; 50(5):507-11.
167. Thakkar RSF, A.J.; Chhabra, A.; Padua, A.; Carrino, J.A. 3T MR imaging of cartilage using 3D Dual Echo Steady State (DESS). Orthop Imaging Clinical 2011; 333-6.
168. Sadeghi-Tarakameh A, Delabarre L, Lagore RL, Torrado-Carvajal A, Wu X, Grant A, et al. In vivo human head MRI at 10.5T: A radiofrequency safety study and preliminary imaging results. Magnetic Resonance in Medicine 2020; 84(1):484-96.
169. He X, Ertürk MA, Grant A, Wu X, Lagore RL, Delabarre L, et al. First in-vivo human imaging at 10.5T: Imaging the body at 447 MHz. Magnetic Resonance in Medicine 2020; 84(1):289-303.
170. Martel G, Kiss S, Gilbert G, Anne-Archard N, Richard H, Moser T, et al. Differences in the vascular tree of the femoral trochlear growth cartilage at osteochondrosis-susceptible sites in foals revealed by SWI 3T MRI. J Orthop Res 2016; 34(9):1539-46.
171. Chambers MG, Bayliss MT, Mason RM. Chondrocyte cytokine and growth factor expression in murine osteoarthritis. Osteoarthritis and Cartilage 1997; 5301-8.

172. Pritzker KP, Gay S, Jimenez SA, Ostergaard K, Pelletier JP, Revell PA, et al. Osteoarthritis cartilage histopathology: grading and staging. Osteoarthritis Cartilage 2006; 14(1):13-29.

173. Glasson SS, Chambers MG, Van Den Berg WB, Little CB. The OARSI histopathology initiative - recommendations for histological assessments of osteoarthritis in the mouse. Osteoarthritis Cartilage 2010; 18 Suppl 3S17-23.

174. Nagira K, Ikuta Y, Shinohara M, Sanada Y, Omoto T, Kanaya H, et al. Histological scoring system for subchondral bone changes in murine models of joint aging and osteoarthritis. Scientific Reports 2020; 10(1).

175. Malfait AM, Little CB. On the predictive utility of animal models of osteoarthritis. Arthritis Res Ther 2015; 17225.

176. Pastoureau P, Leduc S, Chomel A, De Ceuninck F. Quantitative assessment of articular cartilage and subchondral bone histology in the meniscectomized guinea pig model of osteoarthritis. Osteoarthritis and Cartilage 2003; 11(6):412-23.

177. Kuyinu EL, Narayanan G, Nair LS, Laurencin CT. Animal models of osteoarthritis: classification, update, and measurement of outcomes. J Orthop Surg Res 2016; 1119.

178. Wendler A, Wehling M. The translatability of animal models for clinical development: biomarkers and disease models. Current Opinion in Pharmacology 2010; 10(5):601-6.

179. Percie du Sert N. Maximising the output of osteoarthritis research: the ARRIVE guidelines. Osteoarthritis Cartilage 2012; 20(4):253-5.

180. Mankin HJD, H.; Lippiello, L.; Zarins, A. . Biochemical and metabolic abnormalities in articular cartilage from oste-arthritic human hips. 1971; 83-A523-37.

181. Ostergaard KA, C.B.; Petersen, J.; Bendtzen, K.; Salter, D.M. Validity of histopathological grading of articular cartilage from osteoarthritic knee joints Ann Rheum Dis 1999; 58208-13.

182. Ostergaard KP, J.; Andersen, C.B.; Bendtzen, K.; Salter, D.M. Histologic/histochemical grading system for osteoarthritis articular cartilage. Arthritis & Rheumatism 1997; 40(10):1766-71.

183. Aigner T, Cook JL, Gerwin N, Glasson SS, Laverty S, Little CB, et al. Histopathology atlas of animal model systems - overview of guiding principles. Osteoarthritis Cartilage 2010; 18 Suppl 3S2-6.

184. Camplejohn KL, Allard SA. Limitations of safranin 'O' staining in proteoglycan-depleted cartilage demonstrated with monoclonal antibodies. Histochemistry 1988; 89185-8.

185. Király K, Lammi M, Arokoski J, Lapveteläinen T, Tammi M, Helminen H, et al. Safranin O reduces loss of glycosaminoglycans from bovine articular cartilage during histological specimen preparation. The Histochemical Journal 1996; 28(2):99-107.

186. Schmitz N, Laverty S, Kraus VB, Aigner T. Basic methods in histopathology of joint tissues. Osteoarthritis Cartilage 2010; 18 Suppl 3S113-6.

187. Bergholt NL, Lysdahl H, Lind M, Foldager CB. A standardised method for toluidine blue metachromatic staining for assessment of chondrogenesis. Cartilage 2019; 10(3):370-4.

188. Kamekura S, Hoshi K, Shimoaka T, Chung U, Chikuda H, Yamada T, et al. Osteoarthritis development in novel experimental mouse models induced by knee joint instability. Osteoarthritis and Cartilage 2005; 13(7):632-41.

189. Rai MF, Duan X, Quirk JD, Holguin N, Schmidt EJ, Chinzei N, et al. Post-Traumatic Osteoarthritis in Mice Following Mechanical Injury to the Synovial Joint. Scientific Reports 2017; 7(1):45223.

190. Pearce GL, Frisbie DD. Statistical evaluation of biomedical studies. Osteoarthritis Cartilage 2010; 18 Suppl 3S117-22.

191. Laverty S, Girard CA, Williams JM, Hunziker EB, Pritzker KP. The OARSI histopathology initiative - recommendations for histological assessments of osteoarthritis in the rabbit. Osteoarthritis Cartilage 2010; 18 Suppl 3S53-65.

192. Hunziker EB, Graber W. Differential extraction of proteoglycans from cartilage tissue matrix compartments in isotonic buffer salt solutions and commercial tissue-culture media. Journal of Histochemistry & Cytochemistry 1986; 34(9):1149-53.

193. Melrose J, Smith S, Ghosh P: Histological and Immunohistological Studies on Cartilage. Humana Press. pp. 039-64.

194. Pelletier J-P, Boileau C, Brunet J, Boily M, Lajeunesse D, Reboul P, et al. The inhibition of subchondral bone resorption in the early phase of experimental dog osteoarthritis by licofelone is associated with a reduction in the synthesis of MMP-13 and cathepsin K. Bone 2004; 34(3):527-38.

195. Kim HK, Burgess J, Thoveson A, Gudmundsson P, Dempsey M, Jo CH. Assessment of Femoral Head Revascularization in Legg-Calve-Perthes Disease Using Serial Perfusion MRI. J Bone Joint Surg Am 2016; 98(22):1897-904.

196. Atsumi T, Yamano K, Muraki M, Yoshihara S, Kajihara T. The blood supply of the lateral epiphyseal arteries in Perthes' disease. JBJS 2000; 82-B392-8.

197. Morris WZ, Valencia AA, McGuire MF, Kim HKW. The Role of the Artery of Ligamentum Teres in Revascularization in Legg-Calve-Perthes Disease. J Pediatr Orthop 2022; 42(4):175-8.

198. Atsumi T, Yoshihara S, Hiranuma Y. Revascularization of the artery of the ligamentum teres in Perthes disease. Clin Orthop Relat Res 2001; 386210-7.

199. Scudamore CL, Hodgson HK, Patterson L, Macdonald A, Brown F, Smith KC. The effect of post-mortem delay on immunohistochemical labelling—a short review. Comparative Clinical Pathology 2010; 20(2):95-101.

200. Gunson DE, Carlson CS, Gropp KE. No Bones About It: The Challenges and Rewards of Osteopathology. Vet Pathol 2015; 52(5):766-9.

201. Janke LJ, Ward JM, Vogel P. Classification, Scoring, and Quantification of Cell Death in Tissue Sections. Vet Pathol 2019; 56(1):33-8.

202. Meyerholz DO-A, GK; Leidinger, MR; Adam Goeken, J; Khanna, R; Sieren, JC; Darbro, BW; Quelle, DE, Weimer, JM. Immunohistochemical markers for prospective studies in pig neurofibromatosis-I porcine models. J Histochem Cytochem 2017; 65(10):607-18.

203. Meyerholz DK, Lambertz AM, Reznikov LR, Ofori-Amanfo GK, Karp PH, McCray PB, Jr., et al. Immunohistochemical Detection of Markers for Translational Studies of Lung Disease in Pigs and Humans. Toxicol Pathol 2016; 44(3):434-41.

204. Rao A, Barkley D, Franca GS, Yanai I. Exploring tissue architecture using spatial transcriptomics. Nature 2021; 596(7871):211-20.

205. Le Bleu HK, Kamal FA, Kelly M, Ketz JP, Zuscik MJ, Elbarbary RA. Extraction of high-quality RNA from human articular cartilage. Anal Biochem 2017; 518134-8.

206. Tanay A, Regev A. Scaling single-cell genomics from phenomenology to mechanism. Nature 2017; 541(7637):331-8.

207. Stahl PL, Salmen F, Vickovic S, Lundmark A, Navaro JF, Magnusson J, et al. Visualization and analysis of gene expression in tissue sections by spatial transcriptomics. Science 2016; 353(6294):78-63.

208. McGuire AL, Gabriel S, Tishkoff SA, Wonkam A, Chakravarti A, Furlong EEM, et al. The road ahead in genetics and genomics. Nature Reviews Genetics 2020; 21(10):581-96.

209. Wang N, Li X, Wang R, Ding Z. Spatial transcriptomics and proteomics technologies for deconvoluting the tumor microenvironment. Biotechnology Journal 20212100041.

210. Sudmant PH, Alexis MS, Burge CB. Meta-analysis of RNA-seq expression data across species, tissues and studies. Genome Biology 2015; 16(1).

211. Mantri M, Scuderi GJ, Abedini-Nassab R, Wang MFZ, McKellar D, Shi H, et al. Spatiotemporal single-cell RNA sequencing of developing chicken hearts identifies interplay between cellular differentiation and morphogenesis. Nature Communications 2021; 12(1).

212. Liu B, Li Y, Zhang L. Analysis and Visualization of Spatial Transcriptomic Data. Frontiers in Genetics 2022; 12.

213. Xia B, Yanai I. A periodic table of cell types. Development 2019; 146(12):dev169854.

214. Gregory JM, McDade K, Livesey MR, Croy I, Marion de Proce S, Aitman T, et al. Spatial transcriptomics identifies spatially dysregulated expression of GRM3 and USP47 in amyotrophic lateral sclerosis. Neuropathol Appl Neurobiol 2020; 46(5):441-57.

215. Wada H, Ikoma K, Oka Y, Nishida A, Onishi O, Kim WC, et al. Status of growth plates can be monitored by MRI. J Magn Reson Imaging 2020; 51(1):133-43.

216. Andreisek G, Weiger M. T2* Mapping of Articular Cartilage. Investigative Radiology 2014; 49(1):57-62.

217. Klymiuk N, Seeliger F, Bohlooly YM, Blutke A, Rudmann DG, Wolf E. Tailored Pig Models for Preclinical Efficacy and Safety Testing of Targeted Therapies. Toxicol Pathol 2016; 44(3):346-57.

218. Oke SL, McIlwraith CW. Review of the economic impact of osteoarthritis and oral joint-health supplements in horses. AAEP Proceedings 2010; 5612-6.

219. Olsson DC, Teixeira BL, Jeremias TDS, Reus JC, De Luca Canto G, Porporatti AL, et al. Administration of mesenchymal stem cells from adipose tissue at the hip joint of dogs with osteoarthritis: A systematic review. Res Vet Sci 2021; 135495-503.

220. Bertout JA, Baneux PJR, Robertson-Plouch CK. Recommendations for Ethical Review of Veterinary Clinical Trials. Front Vet Sci 2021; 8715926.

221. Sharkey LC, Simpson RM, Wellman ML, Craig LE, Birkebak TA, Kock ND, et al. The Value of Biomedical Research Training for Veterinary Anatomic and Clinical Pathologists. Veterinary Pathology 2012; 49(4):581-5.

222. Zuraw A, Aeffner F. Whole-slide imaging, tissue image analysis, and artificial intelligence in veterinary pathology: An updated introduction and review. Vet Pathol 2022; 59(1):6-25.

223. Gibson-Corley KN, Olivier AK, Meyerholz DK. Principles for valid histopathologic scoring in research. Vet Pathol 2013; 50(6):1007-15.

224. Dominguez VM, Agnew AM. The use of ROI overlays and a semi-automated method for measuring cortical area in ImageJ for histological analysis. American Journal of Physical Anthropology 2019; 168(2):378-82.

225. Barck KH, Lee WP, Diehl LJ, Ross J, Gribling P, Zhang Y, et al. Quantification of cortical bone loss and repair for therapeutic evaluation in collagen-induced arthritis, by micro-computed tomography and automated image analysis. Arthritis & Rheumatism 2004; 50(10):3377-86.

226. Mori Y, Oichi T, Enomoto-Iwamoto M, Saito T. Automatic Detection of Medial and Lateral Compartments from Histological Sections of Mouse Knee Joints Using the Single-Shot Multibox Detector Algorithm. CARTILAGE 2022; 13(1):194760352210740.

227. Jensen EC. Quantitative Analysis of Histological Staining and Fluorescence Using ImageJ. The Anatomical Record 2013; 296(3):378-81.

228. Doube M, Klosowski MM, Arganda-Carreras I, Cordelieres FP, Dougherty RP, Jackson JS, et al. BoneJ: Free and extensible bone image analysis in ImageJ. Bone 2010; 47(6):1076-9.

229. Tarasco M, Cordelieres FP, Cancela ML, Laize V. ZFBONE: An ImageJ toolset for semi-automatic analysis of zebrafish bone structures. Bone 2020; 138115480.

230. La Perle KMD. Machine Learning and Veterinary Pathology: Be Not Afraid! Vet Pathol 2019; 56(4):506-7.

Appendix 1. Chapter 2 Supplementary Material

A1. Supplementary Figure

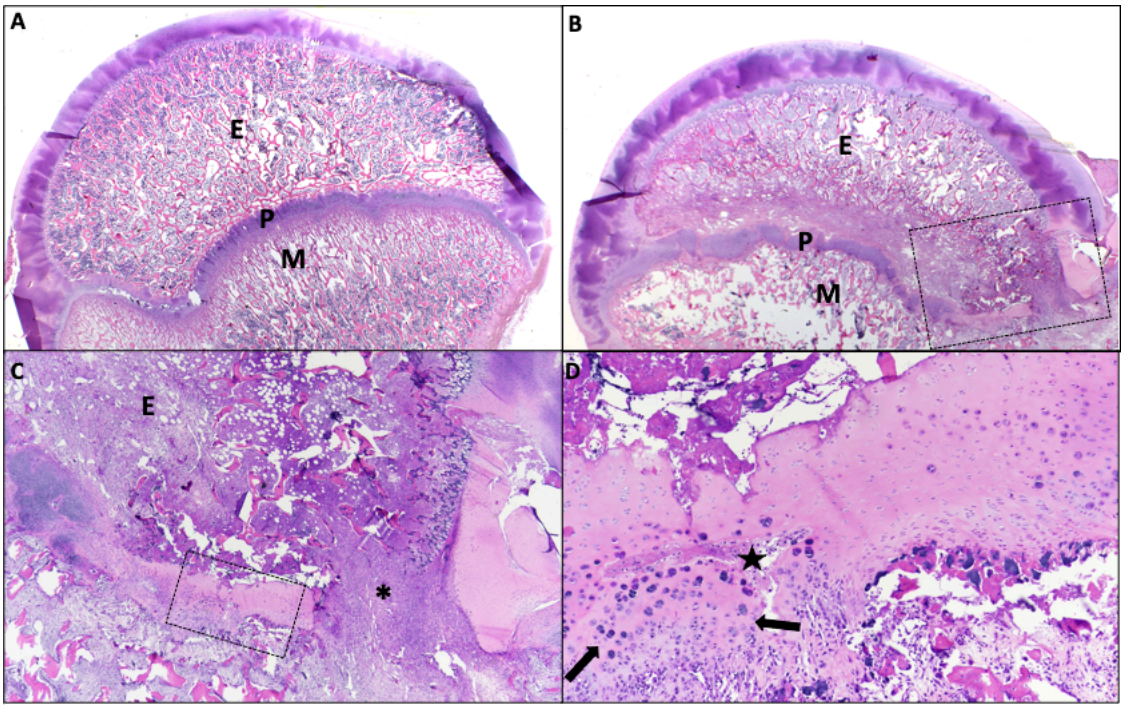

Figure S1. Piglet with extensive disruption of growth plate precluding histomorphometry at 28 days following induction of ischemia. *(A) Normal contralateral control femoral head and* ***(B)*** *ischemic femoral head with focal bridging and replacement of physis by fibrovascular tissue. E = bony epiphysis, M = metaphysis, P = physis. 0.5× magnification, H&E.* ***(C)*** *Higher magnification (4×) of area in box in* ***(B)*** *showing fibrovascular bridging and replacement of physis (*), with adjacent physeal chondrocyte cell death and loss of matrix staining of growth cartilage bordering fibrovascular bridge. E = bony epiphysis. H&E.* ***(D)*** *Higher magnification (10×) of chondrocyte cell death within the remnant of physeal cartilage within box in* ***(C)****, accumulation of cellular debris within the*

epiphysis and metaphysis, and disorganization of remaining viable chondrocytes (arrows). Star = necrotic vascular canal containing cellular debris. H&E.

Appendix 2. Chapter 4 Supplementary Material

A1. Supplementary Methods

Histology

Right knee (stifle) joints were collected from each animal and fixed in 10% neutral buffered formalin with the joint angle at approximately 120 degrees. After fixation, the joints were decalcified in 10% EDTA for approximately two weeks and processed for histology as previously described.[18].The specimens were relabeled and randomized at the time of histologic processing to blind the evaluators to group assignments. The joints were embedded intact in paraffin with the patella down and the femur and tibia forming equal angles to the margins of the embedding cassette to minimize medial or lateral rotation of the joint.

Power Calculations

Group sizes were powered to detect a biologically significant difference between sham mice and DMM mice based on the mean mid-coronal OARSI and ACS grades, using a mean difference of 2 with an estimated standard deviation of 2 for the OARSI scheme and a mean difference of 3 with an estimated standard deviation of 2.9 for the ACS scheme (power=0.8, α=0.05, 2-sided T-test).

Statistical Analysis of Histomorphometry Data

The histomorphometry data were continuously and normally distributed and were compared using Students t-tests between the two OA models (DMM and naturally occurring age-related OA) and between the sham-operated and aged mice.

Statistical Analysis of Interobserver Variation

The correlation (interobserver variation) between graders was determined by generation of non-parametric Spearman correlation values for the experienced and inexperienced grader for the MTP and LTP grades from six sections per specimen for both OARSI and ACS scheme (Prism). A non-parametric test was chosen based on a visual assessment of the Q-Q plots and lack of normality on the Shapiro-Wilk test (OARSI $W=0.8449$, $p<0.0001$; ACS $W=0.6645$, $p<0.0001$).

Grading of Tibial Plateaus

The focus of both OARSI and ACS grading was placed on the medial and lateral tibial plateaus (MTP and LTP), given evaluation of the femoral condyles that indicated the femoral condyles consistently scored the same or less than the coinciding tibial plateau.

Osteophyte and Synovial Hyperplasia Grading

Osteophytes were evaluated as previously published on a scale of 0-3, with 0 = no osteophyte, 1 = small osteophyte (approximately the same thickness as the adjacent cartilage), 2 = medium osteophyte (approximately 1-3 times the thickness of the adjacent cartilage), and 3 = large osteophyte (greater than 3 times the thickness of the adjacent cartilage).[5,20,32] Synovial hyperplasia was evaluated as previously published on a scale of 0-3 with 0 = 1-3 cell layers of synoviocytes, 1 = 4-6 cell layers of synoviocytes, 2 = 7-9 cell layers of synoviocytes, and 3 = 10 or more cell layers of synoviocytes.[5,20]

Histomorphometry

Histomorphometry was performed on a single representative mid-coronal H&E-stained section from each joint (n=40) as previously described [5] and included measurements of the area and average thickness of the articular cartilage (cartilage above the tidemark), area and average thickness of the calcified cartilage (cartilage below the tidemark), and area and average thickness of the subchondral bone (Supplemental Figure 3). Area of articular cartilage containing dead chondrocytes (chondrocyte cell death, CCD; identified by shrunken, eosinophilic chondrocytes lacking identifiable nuclei; Supplemental Figure 4) was also measured and used to generate a percentage of CCD (area of CCD/total articular cartilage area *100). These measurements were collected using an OsteoMeasure bone histomorphometry system (OsteoMetrics, Atlanta, GA) based on a 700-µm wide by 600-µm field of view centered on the tibial

plateau, which included at least 75% of its width (methods described in detail previously) [5].

Principal Components Analysis

PCA included 12 OA parameters measured on a single mid-coronal section for each individual (n=40): OARSI grades, ACS grades, Toluidine blue grades, synovial hyperplasia grades, osteophyte grades, and histomorphometry measurements (articular cartilage area and thickness, calcified cartilage area and thickness, subchondral bone area and thickness, and %CCD). These 12 parameters were reduced to four factors that were responsible for 78% of the variation in the data. Parameters with factor loadings >0.30 were considered to contribute substantially to the factors.

A2. Supplementary Results

Interobserver Variation

An important feature of grading systems is the repeatability and ease of application, particularly when utilized by both experienced and novice graders. ACS and OARSI scores were determined by both an experienced grader and novice grader as described in the methods. The Spearman correlation value for the modified OARSI scheme across all graded H&E sections (6 per mouse; 240 total grades) between the two graders was 0.8418 (95% CI: 0.8217, 0.8668) while the Spearman correlation value for the ACS scheme was 0.776 (95% CI:

0.7383, 0.8116), indicating a somewhat greater correlation between graders when applying the OARSI scheme as compared to the ACS scheme.

A3. Supplementary Figures

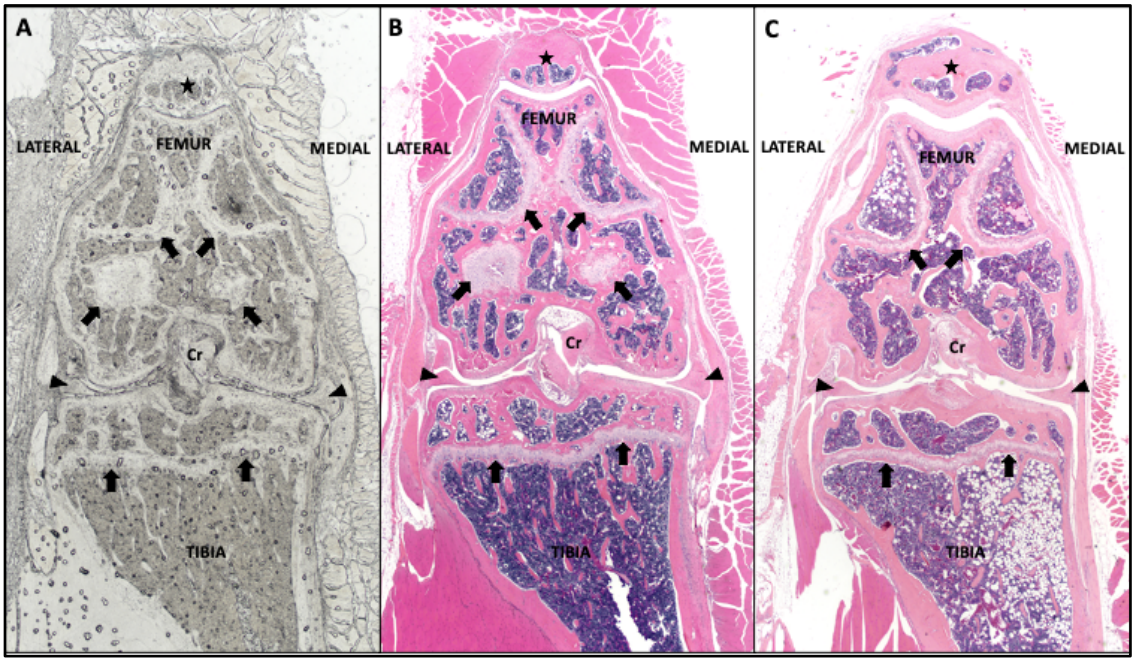

Figure S1. Features of an ideal mid-coronal section. *The alignment of the tibia and menisci are the primary indicators of symmetry, with the femur and patella serving as secondary indicators. (A) Unstained mid-coronal section from a DMM mouse, with landmarks present to indicate a mid-coronal location. The tibial plateau is generally flat within the mid-coronal region, with symmetry of the femoral condyles and the growth plates of the femur and tibia and a central and symmetrical patella. The medial aspect is on the right with the lateral aspect to the left. Menisci are symmetrical and taper sharply. The fibula is not observed (present in coronal sections from the posterior portion of joint). Arrows indicate the cartilage of the physis, which normally remain open in the mouse tibia and*

femur. (A) An unstained section can be used to determine alignment and adjust as coronal sectioning takes place. Sections may be stored unstained long-term for later use, with staining and evaluation reserved for mid-coronal section(s). The section shown unstained in (A) is immediately adjacent to the H&E-stained section shown in (B). (B) and (C) H&E-stained mid-coronal sections with ideal features for assessment of the articular cartilage structure along with histomorphometry. Subtle variation is present in the femur alignment and depth of section, where the growth plate is apparent proximally and distally (arrows) in (B) and only in the proximal portion in (C). Star = patella. Arrow heads = menisci. Cr = cruciate ligament insertions.

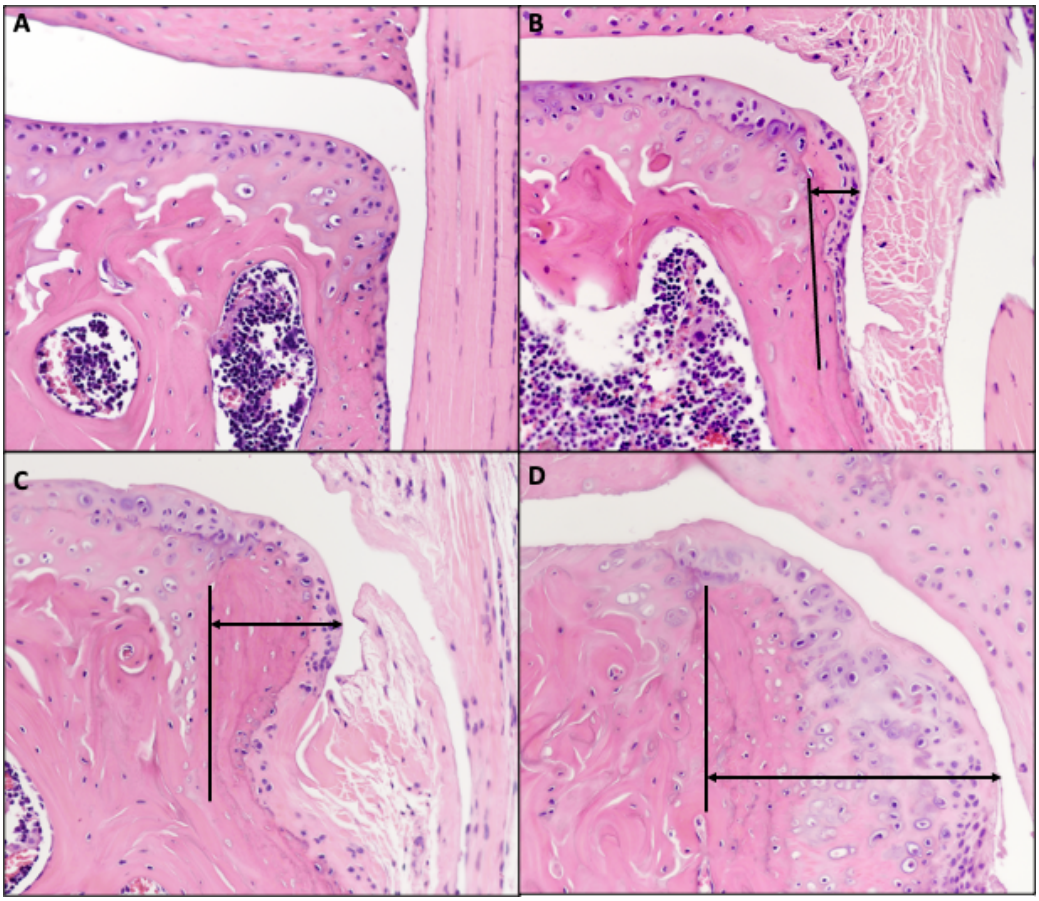

Figure S2. Osteophyte grading. *(A) A normal abaxial joint margin without osteophyte formation (osteophyte grade = 0). A smooth layer of articular cartilage overlies the medial tibial plateau and extends to the margin of the joint. (B) Fibrocartilage and bone forming a small osteophyte at the abaxial margin of the medial tibial plateau. Osteophyte grade = 1 with the thickness approximately equal to the thickness of the adjacent articular cartilage. (C) A medium osteophyte at the abaxial margin of the tibial plateau that is approximately three times the thickness of the articular cartilage (osteophyte grade = 2). (D) A large osteophyte composed of bone and cartilage markedly expands the margin of the joint, with complete loss of the articular cartilage at the tibial plateau (osteophyte*

grade = 3). Vertical line = approximate natural margin of the tibia. Double-sided arrows indicate widest point of the abaxial osteophyte. 200x magnification, H&E staining.

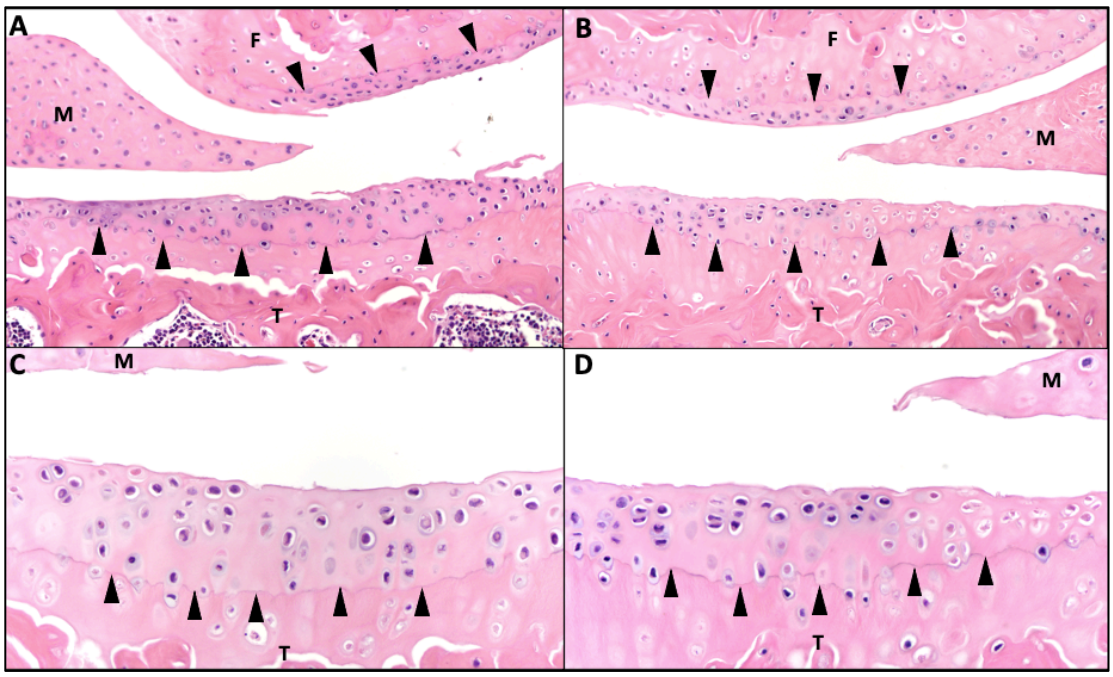

Figure S3. Examples of the tidemark separating articular cartilage from calcified cartilage. *Depending on the balance of hematoxylin and eosin stains, the tidemark varies from deep purple to deep pink and forms a continuous line separating the articular cartilage from the calcified cartilage. (A) (B) 200x magnification. (C) (D) 400x magnification. F = femur, T = tibia, M = meniscus. Hematoxylin and eosin (H&E) stain.*

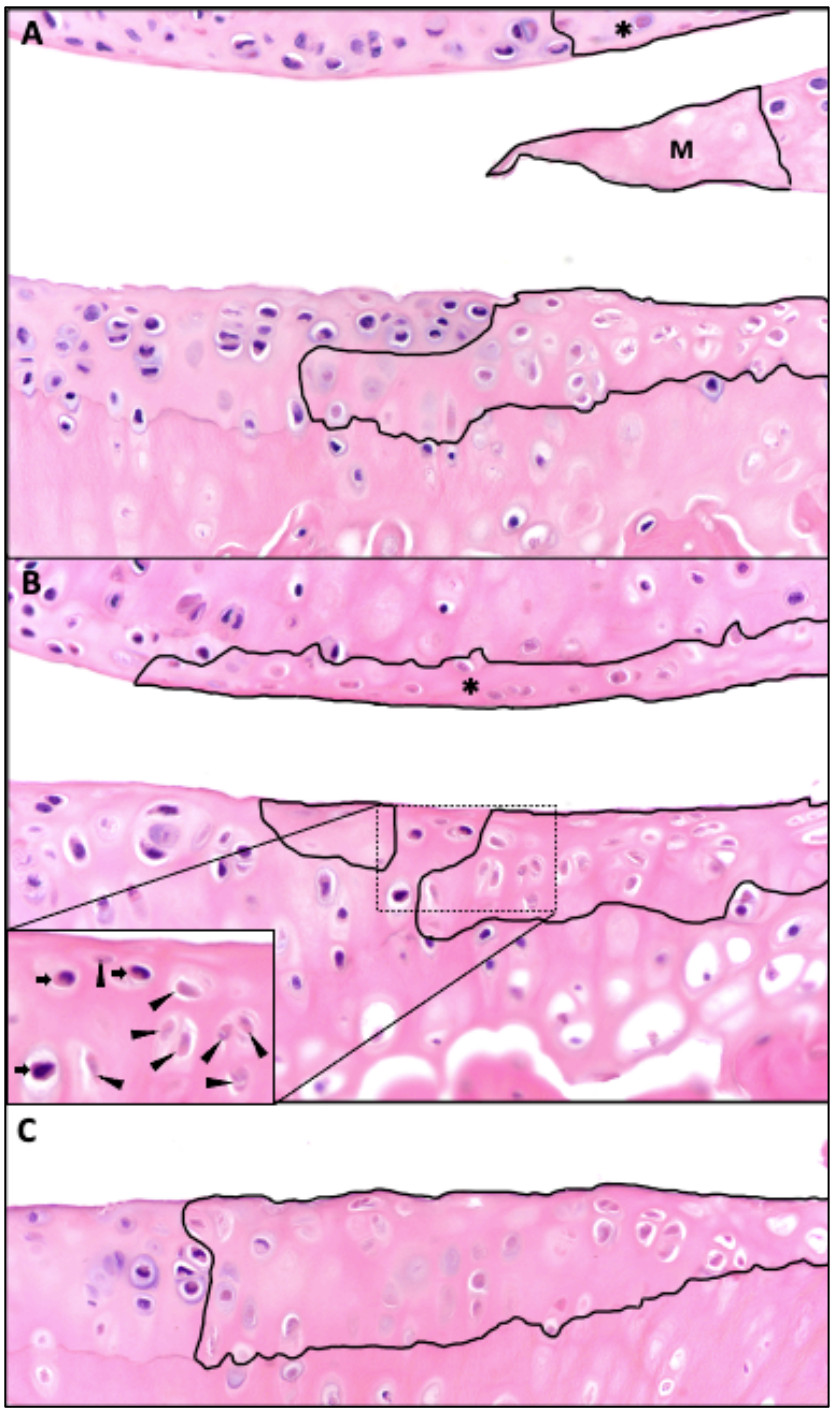

Figure S4. Chondrocyte cell death. *(A), (B), and (C): Three examples highlighting regions of chondrocyte cell death within the articular cartilage. Areas are included if they consist of two or more necrotic chondrocytes, which are*

*characterized by nuclear eosinophilia, loss of nuclear detail, and condensation. Associated matrix is included and may add some subjectivity to the measurement, but this can be addressed by having all graders in a study use consistent guidelines when they make their measurements. Often, there are so-called "kissing" lesions consisting of chondrocyte cell death within the femoral articular cartilage in direct apposition to areas of cell death at the tibial plateau (indicated by *). M = region of chondrocyte cell death in the meniscus in (A). 400x.*

A4. Supplementary Tables

Table S1. **Comparison of the femoral condyle grades to the corresponding tibial plateau grades.**

	MFC≤MTP	LFC≤LTP
OARSI grading		
Total (n=40)	**90%**	**80%**
Sham (n=10)	100%	100%
DMM (n=15)	86.7%	86.7%
Aged (n=15)	86.7%	60%
ACS grading		
Total (n=40)	**90%**	**82.5%**
Sham (n=10)	100%	100%
DMM (n=15)	86.7%	93.3%
Aged (n=15)	86.7%	60%

In the majority of mid-coronal sections, the grade of the femoral condyle was equal to or less than the grade of the corresponding tibial plateau.

Table S2. **Location of most severe lesions.**

Location of Highest Grade	Anterior	Mid-Coronal	Posterior	Highest grade within one section of the mid-coronal section
OARSI MTP				
Total (n=40)	**20%**	**45%**	**35%**	**77.5%**
Sham (n=10)	10%	50%	40%	80%
DMM (n=15)	46.7%	46.7%	6.6%	73.3%
Aged (n=15)	0%	40%	60%	80%
OARSI LTP				
Total (n=40)	**7.5%**	**65%**	**27.5%**	**87.5%**
Sham (n=10)	0%	80%	20%	90%
DMM (n=15)	13.3%	60%	26.7%	80%
Aged (n=15)	6.7%	60%	33.3%	93.3%
ACS MTP				
Total (n=40)	**15%**	**52.5%**	**32.5%**	**80%**
Sham (n=10)	0%	50%	50%	90%
DMM (n=15)	40%	53.3%	6.7%	73.3%
Aged (n=15)	0%	53.3%	46.7%	80%
ACS LTP				
Total (n=40)	**12.5%**	**57.5%**	**30%**	**75%**
Sham (n=10)	0%	70%	30%	70%
DMM (n=15)	6.7%	80%	13.3%	93.3%
Aged (n=15)	26.7%	26.7%	46.6%	60%

Overall, the most severe lesions tended to be mid-coronal for both the medial and lateral tibial plateau regardless of grading scheme used. However, the models showed a significant variation in the location of most severe lesions when they were not located in the mid-coronal section, with DMM mice frequently having most severe lesions anterior to mid-coronal and aged mice more frequently having most severe lesions posterior to the mid-coronal section. Overall, the most severe lesions were frequently either mid-coronal or within one section of mid-coronal, suggesting the mid-coronal region (encompassing a 150-250 μm span of the joint) is still a relevant region for focus in both the DMM and aging model.